California AHMCT Program
University of California at Davis
California Department of Transportation

CONTROL SYSTEM DEVELOPMENT FOR TETHERED MOBILE ROBOT FOR AUTOMATING HIGHWAY MAINTENANCE OPERATION*

Daehie Hong

AHMCT Research Report
UCD-ARR-94-9-12-01

Interim Report of Contract
IA65Q168-MOU 92-9

September 12, 1994

* This work was supported by California Department of Transportation (Caltrans) Contract Number IA65Q168-MOU 92-9 through the Advanced Highway Maintenance and Construction Technology Research Center at the University of California at Davis.

CONTROL SYSTEM DEVELOPMENT FOR TETHERED MOBILE ROBOT FOR AUTOMATING HIGHWAY MAINTENANCE OPERATION

Interim Report

Daehie Hong

Department of Mechanical & Aeronautical Engineering
University of California, Davis

September 12, 1994

Advanced Highway Maintenance and Construction Technology Program

DISCLAIMER/DISCLOSURE

"The research reported herein was performed as part of the Advanced Highway Maintenance and Construction Technology Program (AHMCT), within the Department of Mechanical and Aeronautical Engineering at the University of California, Davis and the Division of New Technology and Materials Research at the California Department of Transportation. It is evolutionary and voluntary. It is a cooperative venture of local, state and federal governments and universities."

"The contents of this report reflect the views of the author(s) who is (are) responsible for the facts and the accuracy of the data presented herein. The contents do not necessarily reflect the official views or policies of the STATE OF CALIFORNIA or the FEDERAL HIGHWAY ADMINISTRATION and the UNIVERSITY OF CALIFORNIA. This report does not constitute a standard, specification, or regulation."

ABSTRACT

A new concept, the use of a self-propelled mobile robot working in close proximity to a support vehicle for purposes of power, materials, etc., has been proposed for highway maintenance operations which require positioning equipment within close proximity to a support vehicle and almost always demand an end-effector to follow a specific path with precise path following requirements. This mobile robot system has been termed the Tethered Mobile Robot (TMR), and such an approach has the potential for use in a wide variety of applications as a positioning module. This report discusses the control system development of the TMR including various tracking control modes and controller hardware for their implementation.

A new non-linear path tracking control algorithm for a 2 DOF differentially steered mobile robot is presented and its exponential stability is proved. There have been no papers that have applied the feedback linearization for non-holonomic mobile robot control problem due to non-square nature of its equations of motion. A new idea is proposed to overcome the inherent problem and an exponentially stable non-linear control law is successfully derived using the feedback linearization.

In the TMR control, the biggest concerns are the non-linear terms due to centrifugal force and routing force that is very hard to estimate. However, the upper and lower bounds of the fluctuating routing force can be determined using an appropriate experimental method. Therefore, the robust control using the sliding mode technique is appropriate to the TMR control problem. The sliding mode control for wheeled mobile robot is formulated and this is a unique control strategy for the TMR and general wheeled mobile robot.

To implement the developed algorithms, a new mobile robot controller is optimally designed using 80486 CPU and the motor controller equipped with the Flexible Servo Controller (FSC). The motor controller board is fabricated with the Printed Circuit Board

CAD. This motor controller is the first application of the FSC chip. The TMR controller has unique feature utilizing the advantages of the developed servo motor controller.

EXECUTIVE SUMMARY

Most of highway maintenance operations such as crack sealing require positioning equipment within close proximity to a support vehicle. Also, these activities almost always demand an end-effector to follow a specific path as opposed to merely moving from one location to another without precise path following requirements as in most manufacturing automation applications. For example, highway crack sealing operations involve the use of robotic positioning equipment dispensing sealant from a wand and following crack path. Another example is roadway sign stenciling operation which also involves paint nozzle following a pre-defined path. The research to automate crack sealing operation has been conducted using conventional SCARA (Selectively Compliant Assembly Robot Arm) type robot as a positioning equipment of applicators such as router, cleaner, heater, or sealer, through the Strategic Highway Research Program's H-107A project at the University of California, Davis. This approach provides accurate and consistent positioning capability. But problems are relatively low heavy load carrying capacity, small workspace and vibratory motion. And commercially available robots are costly and relatively slow.

A new concept, the use of a self-propelled mobile robot working in close proximity to a support vehicle for purposes of power, materials, etc., has been proposed as a natural evolution of the UC-Davis SHRP H107A concept. This mobile robot system has been termed the Tethered Mobile Robot (TMR), and such an approach has the potential for use in a wide variety of applications as a positioning module. This report discusses the control system development of the TMR including various tracking control modes and controller hardware for their implementation.

In order to cope with all possible situations that the TMR would meet for highway maintenance operations, three different modules are proposed for the TMR control system in this paper. The first is *Manual Control with Joystick* performed by human operator with joystick. This control mode can be used for the cases when operator needs to manually

place the TMR at a specific position or to make the TMR trace a path manually. The second is *Automatic Trajectory Tracking Control.* Using this mode, the TMR can automatically track a specific path without any manual operations. The reference path for this mode can be a pre-defined curve in a disk file form. The roadway sign stenciling, for example, needs a sequence of pre-defined reference path commands to draw a pre-defined roadway sign. And it can be generated with a real-time sensor, laser range finding sensor for the crack sealing operation for example, which forms a sensor based real time navigation problem. The third one is *Robust TMR Velocity Control.* Many of highway maintenance operations require very robust control system to external force disturbances that are hard to estimate. The routing process for the crack sealing operation is a good example. The routing force is difficult to predict and also severely fluctuating during the process.

A new non-linear path tracking control algorithm for a 2 DOF differentially steered mobile robot is presented and its exponential stability is proved. There have been no papers that have applied the feedback linearization for non-holonomic mobile robot control problem due to non-square nature of its equations of motion. A new idea is proposed to overcome the inherent problem and an exponentially stable non-linear control law is successfully derived using the feedback linearization.

In the TMR control, the biggest concerns are the non-linear terms due to centrifugal force and routing force that is very hard to estimate. However, the upper and lower bounds of the fluctuating routing force can be determined using an appropriate experimental method. Therefore, the robust control using the sliding mode technique is appropriate to the TMR control problem. The sliding mode control for wheeled mobile robot is formulated and this is a unique control strategy for the TMR and general wheeled mobile robot.

To implement the developed algorithms, a new mobile robot controller is optimally designed using 80486 CPU and the motor controller equipped with the Flexible Servo Controller (FSC). The motor controller board is fabricated with the Printed Circuit Board

CAD. This motor controller is the first application of the FSC chip. The TMR controller has unique feature utilizing the advantages of the developed servo motor controller.

TABLE OF CONTENTS

LIST OF FIGURES AND TABLES

LIST OF APPENDICES

Chapter 1. Introduction.

Most of highway maintenance operations such as crack sealing require positioning equipment within close proximity to a support vehicle. Also, these activities almost always demand an end-effector to follow a specific path as opposed to merely moving from one location to another without precise path following requirements as in most manufacturing automation applications. For example, highway crack sealing operations involve the use of robotic positioning equipment dispensing sealant from a wand and following crack path. Another example is roadway sign stenciling operation which also involves paint nozzle following a pre-defined path. The research to automate crack sealing operation has been conducted using conventional SCARA (Selectively Compliant Assembly Robot Arm) type robot as a positioning equipment of applicators such as router, cleaner, heater, or sealer, through the Strategic Highway Research Program's H-107A project at the University of California, Davis (Velinsky, 1993). This approach provides accurate and consistent positioning capability. But problems are relatively low heavy load carrying capacity, small workspace and vibratory motion. And commercially available robots are costly and relatively slow.

A new concept, the use of a self-propelled mobile robot working in close proximity to a support vehicle for purposes of power, materials, etc., has been proposed as a natural evolution of the UC-Davis SHRP H107A concept (Winters, Hong, Velinsky, and Yamazaki, 1994). As such, the support vehicle contains the associated maintenance supplies (sealant, etc.), power supply (hydraulic power supply, electrical generator, etc.), and in many cases the primary maintenance operation sensing devices (e.g., machine vision for crack sealing operations). The mobile robot is supplied with the necessary maintenance materials and power through a tether from the support vehicle, and a passive linkage system accurately determines the location of the robot relative to the support vehicle. This system has been termed the Tethered Mobile Robot (TMR), and such an approach has the

potential for use in a wide variety of applications as a positioning module. The crack sealing operation consists of 2 major tasks, routing and sealing the crack. Those two tasks are performed in sequential manner, so that the whole crack sealing process can be automated by separating the two tasks into two different mobile robot platforms. We can make the first robot carry the routing unit and the second one carry the sealing unit. Consequently, the TMR system consists of multiple mobile robot platforms due to the multiple sequential nature of crack sealing operation like most of other highway maintenance operations. Among the tasks required for the crack sealing operation, the most demanding is routing in which a 0.5-2 in (13 - 51 mm) channel is cut to enlarge the crack reservoir (Velinsky, 1993, Velinsky and Kirschke, 1991). The following two chapters, 2, 3, briefly explain the Automated Crack Sealing Machine configuration developed by the UC-Davis SHRP H107A project and the TMR configuration proposed.

1-1. Literature Review

This paper discusses the control system development of the TMR including tracking control algorithm and controller hardware for its implementation. In order to investigate existing research, a literature review was initially performed. The purpose of this literature review is to identify existing technologies which may be adapted to the TMR control problem for automating highway maintenance operations.

A very tight path tracking control system is required to apply the TMR to highway maintenance operations involving very winding curve, such as pavement crack. But there has been no research to develop a tracking control system of a mobile robot for automating highway maintenance operations. Many studies have however been conducted to develop a tracking control algorithm for a general mobile robot.

Cox and Wilfong (1990) classified autonomous vehicle research into six independent sub-disciplines: guidance, sensors, navigation, cartography, sensing strategies, and motion planning. Since we are concerned with controlling the TMR along a desired trajectory, our problem falls into the guidance control sub-discipline. From this reason, the literature

review is concentrated on the guidance control of a wheeled mobile robot in this thesis. There have been numerous papers about wheeled mobile robots but most have focused on the navigation problem with a real time sensor, typically a vision camera. There was not much mobile robot guidance control papers in the past. Recently, prominent progress has however been made in the guidance control research area. After intensive literature review was performed, very closely related papers to the TMR control problem are cited here.

Kinematic modeling method was well established for a general manipulator type robot but there was little research related to wheeled mobile robots. Muir and Neuman (1987) introduced a systematic way for kinematic modeling of wheeled mobile robot. Alexander and Maddocks (1990) formulated the kinematics of Wheeled Mobile Robot using linear algebra. They introduced a dissipation function whose minimization was equivalent to the quasi-static motions.

There exist three different types of Wheeled Mobile Robots (WMRs) according to wheel arrangement, two degrees of freedom conventionally steered type WMRs, two degrees of freedom (DOF) differentially steered type WMRs, and three degrees of freedom omnidirectional WMRs. The first two types, that is two degrees of freedom, are often called nonholonomic WMRs and the omnidirectional types are also referred as holonomic WMRs. The existing WMRs were well reviewed according to this wheel arrangement by Winters, 1992. The followings are added in this thesis to supplement Winters's review. Gentile and Mangialardi (1992) examined different mobile robot configurations. They considered the architecture, propulsion system, and directional control system of vehicles in order to classify the type of mobile robots. West and Asada (1992) introduced a new design of holonomic omnidirectional vehicle. A fundamental method of obtaining omnidirectional motion with holonomic constraints with the floor was presented using a mechanism with spherical tires. Pin and Killough (1994) presented the concepts for a new family of holonomic wheeled platforms. They used "orthogonal wheel" concepts (this is also called "easy roller") to develop the holonomic cart.

Tsumura, et al. (1981) proposed a path tracking control algorithm using a straight line segments. Petrov (1991) proposed dynamically based tracking control algorithm for tricycle wheeled mobile robot with a front steering wheel. Salichs, et al. (1991) showed some contour following guidance control algorithms for a mobile robot and analyzed system performance. Difference between classical, fuzzy and neural network control techniques were also discussed in their paper. Banta (1988) developed a parameter estimation scheme for correcting modeling errors due to wear, misalignment or calibration degradation. Khoukhi (1989) discussed the optimal navigation problem of an autonomous mobile robot in a crowded environment. Kinematic model and control were presented first and then dynamic model was developed. A mobility estimation function was introduced with the velocity and orientation of the robot. Then the optimal trajectory search was formulated as a nonlinear problem. Kanayama, et al. (1990) proposed a nonlinear control law and proved its stability using Lyapunov function. Kanayama and Krahn (1993) proposed a new 2D transformation group to represent positioning of rigid body vehicles. One of the advantages of this transformation is that the orientation of the vehicle is explicitly given, not by its trigonometric function values.

Recently, many efforts were conducted to establish a mathematical way to prove controllability and stabilizability of wheeled mobile robot control problem. Also, many papers applied advanced modern control theory. Samson and Ait-Abderrahim (1991) discussed controllability and state feedback stabilization for a two wheel driven nonholonomic cart and proposed a nonlinear trajectory control law. Zhao and BeMent (1992) proved the controllability of nonholonomic robot systems for six common wheel and axle configurations that possess two or three degrees of freedom. Borenstein (1994) proposed the design and implementation of a model-reference adaptive motion controller for a differential-drive mobile robot. Reister and Unseren (1993) developed a new approach to the control of a vehicle with multiple steerable drive wheels. They applied the control architecture to the HERMIES-III robot and measured a dramatic reduction in error

compared to motions without constraint force control. Laumond (1993) presented a proof of controllability for a multibody mobile robot (e.g., a car pulling and pushing trailers). This paper proved the controllability of a general n-body vehicle. Sϕrdalen and de Wit (1993) proposed a piecewise smooth feedback control law for path following. They used a kinematic model of a nonholonomic mobile robot. The desired path was supposed to be composed of straight lines and arcs of circles joined at intermediate configurations. Baumgartner and Skaar (1994) described the theoretical development and experimental implementation of a complete navigation procedure for structured environments. Estimates of the vehicle's position and orientation were based on the rapid observation of visual cues located at discrete positions within the environment. The extended Kalman filter was used to combine these visual observations with sensed wheel rotations to produce optimal estimates continuously. The complete estimation procedure, as well as the control algorithm, was developed to be time independent.

Borenstein (1994) presented a new approach to accurate and reliable dead-reckoning for mobile robot. Using one linear and two rotary encoders, the system can measure the relative distance and bearing between two mobile robots. This relative position information and conventional dead-reckonings of both robots are used to correct dead-reckoning errors.

Excessive off-road mobility is required in the fields of military applications, agriculture, particularly forestry, mining and planetary exploration. Kumar and Waldron (1989) proposed the idea of an actively coordinated vehicle system and derived its mathematics. This system used independent actuation of suspension and locomotion degrees of freedom. Sreenivasan, Dutta, and Waldron (1994) described the kinematic configuration, the mechanical systems, and the sensing, control, and actuation sub-systems of the Wheeled Actively Articulated Vehicle (WAAV). They developed an experimental system to demonstrate the use of active coordination in terrain adaptive wheeled vehicle. Actively coordinated vehicle systems such as WAAV are different from road vehicles with

active suspensions. This actively coordinated vehicle concept might be applied to wheeled mobile robot development for highway maintenance operations.

As related to research efforts for this project, Winters (1992) and Winters, et al. (1994) announced the TMR concept. Kochekali and Velinsky (1994) reviewed the past research and development activities in the subject of Wheeled Mobile Robots in order to evaluate their potential use in highway maintenance and construction tasks. This report focused on mobility as an essential feature for highway maintenance and construction application. Boyden and Velinsky (1994) published the paper that examined dynamic modeling of differentially and conventionally steered wheeled mobile robots for high load applications such as highway maintenance and construction. They developed from kinematic models to very detailed dynamic models with complete tire models for both types of WMRs. From the TMR controller side of view, Hong, et al. (1994) presented the development of the TMR controller as a feasibility study for a new generation flexible servo controller. The new type of servo controller was presented in this paper with its application to the TMR controller. Zhang and Velinsky (1994) discussed inherent kinematics and fundamental tracking control algorithms for differentially steered WMR. They developed globally convergent tracking control algorithm. This research is closely related to the development of the Automated Crack Sealing Machine for the UC-Davis SHRP H107A project. The following papers and reports were published related to this project: Velinsky and Kirschke (1991), Kirschke and Velinsky (1992), Velinsky (1993), and Velinsky (1993, SHRP final report).

1-2. Problem Statement and Objectives

Although many algorithms and systems have been developed, these are not appropriate for applying them to the TMR control problem since these are all for controlling the general purpose mobile robot running on clean building floor and tracking very smooth pre-defined path. The TMR should track very complex highway crack in very harsh environment such as pavement surface, severe vibration due to the router, big cutting force,

and very heavy robot platform ranging from around 200 lbs to 500 lbs. In order to cope with these problems, the tracking control algorithm must be exponentially stable and robust to severe disturbances.

This thesis confines the control system development to one mobile robot system although the TMR system consists of multiple robot platforms, since the focus of this thesis is development of the most appropriate tracking control algorithm, optimal controller hardware for the TMR, and its realization.

In order to cope with all possible situations that the TMR would meet for highway maintenance operations, three different modules are proposed for the TMR control system in this paper. The first is *Manual Control with Joystick* performed by human operator with joystick. This control mode can be used for the cases when operator needs to manually place the TMR at a specific position or to make the TMR trace a path manually. The second is *Automatic Trajectory Tracking Control.* Using this mode, the TMR can automatically track a specific path without any manual operations. The reference path for this mode can be a pre-defined curve in a disk file form. The roadway sign stenciling, for example, needs a sequence of pre-defined reference path commands to draw a pre-defined roadway sign. And it can be generated with a real-time sensor, laser range finding sensor for the crack sealing operation for example, which forms a sensor based real time navigation problem. The third one is *Robust TMR Velocity Control.* Many of highway maintenance operations require very robust control system to external force disturbances that are hard to estimate. The routing process for the crack sealing operation is a good example. The routing force is difficult to predict and also severely fluctuating during the process.

A new path tracking control algorithm for a 2 DOF differentially steered mobile robot is presented for the Automatic Trajectory Tracking Control and its exponential stability is proved in this paper. The approach to derive the algorithm is systematic and unique. There have been no papers that have applied the feedback linearization for non-holonomic mobile robot control problem due to non-square nature of its equations of motion. In this paper, a

new idea is proposed to overcome the inherent problem and an exponentially stable non-linear control law is successfully derived using the feedback linearization. The stability for a non-linear system usually does not guarantee its robustness to uncertainties. The robustness of the developed algorithm against parametric uncertainty and unmodeled dynamics is explored through simulation. This stable and robust control algorithm would be more appropriate to the applications to highway maintenance operations than the control algorithms developed for general purpose mobile robots.

Much research has been conducted about wheeled mobile robot control as cited in Section 1-1. But there have not been any papers concerning the sliding mode control issue for wheeled mobile robot. In the TMR control, the biggest concerns are the non-linear terms due to centrifugal forces and the routing force that is very hard to estimate. But we can figure out the upper and lower bounds of the fluctuating routing force using an appropriate experimental method. Therefore, the robust control using the sliding mode technique is very appropriate to the TMR control problem. In this research, the sliding mode control for wheeled mobile robot is formulated and this is a unique control strategy for the TMR and general wheeled mobile robot.

To implement the developed algorithms, a new mobile robot controller is optimally designed using 80486 CPU and the motor controller equipped with the Flexible Servo Controller ASIC (Application Specific Integrated Circuit) chip developed by de Schepper,et al., 1990. The motor controller is the most important part in the TMR controller hardware. The motor controller board is designed with the Flexible Servo Controller (FSC) chip and fabricated using the Printed Circuit Board CAD software (OrCAD). There have been no papers that applied the FSC chip since the chip was developed. This servo motor controller is the first application of the FSC chip. The TMR controller has unique feature utilizing the advantages of the servo motor controller board equipped with the FSC. The details are included in the Chapter 8.

Since the initial intended use of the TMR is for the pavement crack preparation and sealing, the discussion of the TMR control system will be based on the application to this operation. Brief review of the crack sealing operation and the Automated Crack Sealing Machine are presented in the Chapter 2. The Chapter 3 contains the summary of the TMR configurations in mechanical point of view developed by Winters, 1993 and new facts that have been proposed since then. This chapter also contains overall description of the TMR control system in control software point of view. The detail controller hardware design and fabrication is included in the Chapter 8. Chapter 4, 5, and 6 describe the details of three control modules, derivation procedure of the control laws, simulation results, and experimental results. The TMR position tracking system is explained in the Chapter 7 including error analysis due to the uncertainties caused by sensors and mechanical structure. As mentioned earlier, Chapter 8 contains the detail design of the TMR controller hardware including the FSC architecture, the servo motor controller design and fabrication, constitution of the TMR controller, and some experimental results of the motor control with the TMR platform.

Chapter 2. Crack Sealing Operation

The aim of this chapter is to provide the brief reviews of the crack sealing operation, the configuration of the Automated Crack Sealing Machine (ACSM), and the final configuration of the TMR focused on the mechanical system aspects. The detail control system configuration of the TMR will be included in the next chapter. The section 1-3 of the thesis by White (1994) is rewritten in the section 2-1 in order to describe the crack sealing operation. The section of 1-4 of the thesis by White (1994) is also rewritten in the section 2-2 in order to describe the configuration of the Automated Crack Sealing Machine. The TMR configuration is summarized in the section 2-3 based on the thesis by Winters (1992) and the paper by Winters et al. (1994).

2-1. Description of the Crack Sealing Operation

The methods of preparation and sealant application in crack sealing operations vary considerably throughout the state transportation departments but evaluation of the effectiveness of these methods was beyond the scope of the ACSM project. Since it was not feasible to accommodate all different methods in one piece of equipment, a selection of some of the more general methods was made to prove the concepts of automation. Generally the basic steps of crack sealing require some cleaning and preparation of the road surface followed by the application of a sealing compound in a liquid state.

Crack surface cleaning generally includes the removal of contamination that could interfere with proper bonding of the sealant with the roadway base. In some operations the pavement is heated prior to sealant application to improve the bond. In addition, a router is sometimes used to modify the physical dimensions of the crack with the intent of providing a seal geometry that optimizes life and effectiveness of the seal. Removal of contaminants such as dirt, debris, and moisture is typically achieved by blasting with hot or cold air.

Application of heat serves to drive off moisture and raise the temperature of the surface which can allow better penetration of hot applied sealants which then harden upon cooling.

Different sealants are available with various performance characteristics but they are generally applied as hot or cold liquid compounds that harden after application. The most common sealant, and the sealant used in development of the ACSM, is a hot applied thermoplastic compound that is applied in a liquid state at over 350° F (177°C).

Present day sealing operations involve the use of manual equipment to perform the steps of preparation and sealant application described above. Workers are in direct contact with equipment such as hand held hot compressed air lances with exhaust temperatures of 3000° F (1650° C), high temperature sealant applicator wands that dispense the hot tar like materials at 350° F (177° C) and 20 H.P. (15 kw) router units that are maneuvered by hand all within close proximity to fast moving traffic.

2-2. Description of the Automated Crack Sealing Machine

The Automated Crack Sealing Machine senses, prepares and seals cracks and joints in the highway. The primary sensing occurs at the front of the vehicle using two line scan cameras that observes the full lane width. As the vehicle moves along at 1 to 2 mph (1.6 to 3.2 Km/hr), the image is processed and a robot path is planned. The sealing operation occurs at the rear of the vehicle with motion currently provided by the inverted, slide mounted SCARA robot. A laser range finder based sensor is mounted on the robot tooling to verify the presence of cracks and to provide feedback for accurate crack following. Details of the vision based sensing have been described in Kirschke and Velinsky, 1992. The TMR is intended to replace the current SCARA robot.

To meet the project objectives a first generation prototype machine known as the Automated Crack Sealing Machine (ACSM) was designed, fabricated and tested. A complete description is found in Velinsky (1993). This vehicle, shown in Figure 2-1, combines all the systems necessary for a fully automated crack sealing process beginning

with the identification of cracks through a vision recognition system to the final steps of using robotic manipulation of tooling to prepare and seal the cracks. During development, two categories of crack sealing operations were identified and addressed. In the most general case, cracks propagate in random directions across a lane but a significant proportion of cracks, including pavement joints, are the result of the road construction processes and will be oriented in orthogonal directions. Cracks and joints that run parallel to the direction of the roadway typically between highway lanes and between lanes and shoulders, are known as longitudinal cracks. These longitudinal cracks are nearly linear and are much simpler to follow and seal than the general cracks.

This characteristic led to the development of two different subsystems known as the Integrated General Crack Sealing System (IGCSS) and the Integrated Longitudinal Crack Sealing System (ILCSS) both of which have been incorporated into the ACSM. These systems are designed to use common and modular system components when possible.

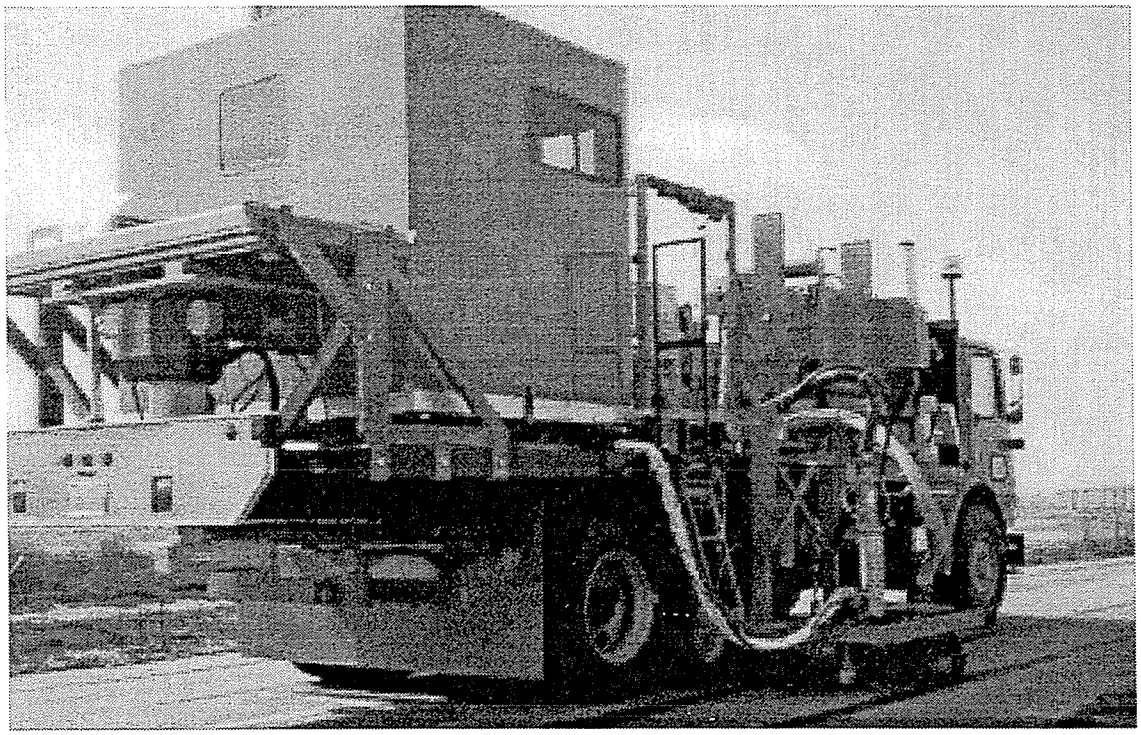

Figure 2-1. *Automated Crack Sealing Machine. (Redrawn from White, 1994.)*

These various subsystems of the ACSM include the following:

• Applicator and Peripherals System (APS) - Components in this system were designed to prepare and seal cracks using a selection of methods most common to present day crack sealing procedures as described in Section 2-1. Included is a router unit, a heating, cleaning, and debris removal system, and a sealant applicator.

• Robot Positioning System (RPS) - The RPS consists of two manipulator systems, the general robotic positioning system (general RPS) for use with the Integrated General Crack Sealing System and the Longitudinal Robotic Positioning System (LRPS) used with the Integrated Longitudinal Crack Sealing System.

• Local Sensing System (LSS) - This system uses a laser vision system sensor at the end effector of both RPS systems to define the location of a crack within close proximity to the crack sealing tools. In the IGCSS the LSS provides feedback that allows the location of the general crack to be verified and defined with greater accuracy than is achieved in the initial crack identification and tracking process but on the ILCSS, the LSS is the sole source of longitudinal crack position feedback.

• Vision Sensing System (VSS) - In the VSS, video imaging of the road in front of the truck is processed to identify the location and orientation of cracks across the full width of the road. Data from this system is further processed in conjunction with input from the LSS to control the operation of the general RPS system.

• Vehicle Orientation and Control System (VOC) - The VOC system uses encoded data from two fifth wheel assemblies to track the motion of the ACSM and provide a local reference system for the VSS and general RPS systems.

• Integration and Control Unit (ICU) - Integration of input to and from most systems and data processing on the ASCM is accomplished through the ICU. It also is the primary interface for the human operator.

To seal the general cracks, the Integrated General Crack Sealing System first identifies and locates cracks in the two dimensional plane of the road and then manipulates APS equipment for the sealing operations. In addition to manipulating tooling with respect to translation in the plane, the system has to process a third degree of freedom, rotation, that is necessary for the operations which use directional tools or combinations of tools and sensors. Router operation, for example, requires the manipulator to orient the router in the direction of the crack and tangent to any curvature of the crack path as it follows the crack. A combination of tooling on the same manipulator, such as blowing followed by sealing would also require control of orientation with respect to the crack. Although the sealant applicator by itself can be operated without regard to orientation, the system requires feedback from the LSS sensor which has to lead the applicator as the crack is followed. Therefore all operations of the Integrated General Crack Sealing System require active control in these three degrees of freedom.

Integrated Longitudinal Crack Sealing System operations are much simpler since control is limited to one degree of freedom. Longitudinal cracks and joints run in the direction of travel and tend to change direction very gradually. Since forward movement on these cracks is provided by motion of the vehicle, following these cracks involves a mechanism that moves the tooling laterally with respect to the truck bed. A complete ILCSS includes the Longitudinal Robotic Positioning System (LRPS), all the APS components and the LSS system for guidance. Although integrated into the ACSM, a primary design objective was that the ILCSS could be operated as a completely independent system.

Chapter 3. TMR Configuration

The aim of this chapter is to provide the brief reviews of the final configuration of the TMR. The first section is focused on the mechanical system aspects. The detail control system configuration of the TMR is included in the next section.

3-1. TMR Configuration - Mechanical System Aspects.

The general configuration of the TMR system is shown in Figure 3-1. The TMR will be connected to the rear side of the support vehicle which is the main body of the Automated Crack Sealing Machine through the mechanical linkage. The details of the configurations have been previously concluded as followings (Winters, 1992, and Winters et al., 1994).

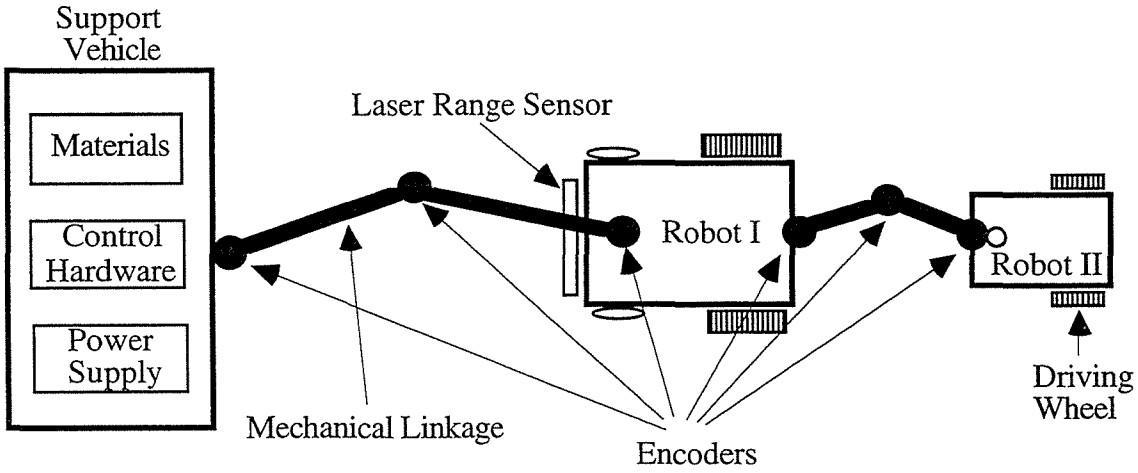

Figure 3-1. *Configuration of the Tethered Mobile Robot.*

3-1-1. Wheel/Cart Configuration

Many different wheel configurations of a general mobile robot were reviewed and investigated for use as the propelling method for the TMR. The plane motion of a rigid body has 3 degree of freedom, namely x, y translation and rotation θ about the vertical axis

to the ground. The existing mobile robots can be classified into 3 big categories according to the number of degree-of-freedom (DOF) that their platforms can have, such as:

- 2 DOF differential drive type which has 2 different driving wheels,
- 2 DOF steering wheel type which is similar to tri-cycle type vehicle, and
- 3 DOF omni-directional cart.

The following table shows the classification of the existing mobile robots.

Table 3-1. *Table of Different Wheel Configurations. (Redrawn from Winters, 1992.)*

TWO DOF Differential	**TWO DOF Steered**	**THREE DOF Omni-directional**
Shakey	Neptune	Uranus
Newt	Hero-I	Unimation robot
Jason	Avatar	Easy Rollers
Hilare	Stanford Cart	Rover
Yamabiko	Blanche	Hermies III
ROBART II		

The crack sealing operation requires very accurate path tracking capability and big traction force to carry out powerful tasks, such as routing and sealing. The omni-directional cart has 3 degree of freedom motion and flexible path tracking capability but its traction force is not big enough to carry such a big unit due to the complexity of its wheel structure. The differential drive wheeled cart produces fairly good traction force compare to the others. Another big advantage compare to the steered type is very sharp turning capability, which makes it possible to follow very complex roadway crack path. The differential drive wheeled robot can turn on a very small circle like a dime. *Consequently, the 2 DOF differential drive wheeled type has been selected as the basic wheel/cart configuration of the Tethered mobile robot.*

3-1-2. Multiple Cart System - 2 Cart

Most of highway maintenance operations consist of multiple sequential tasks. For example, the crack sealing operation consists of 4 major sequential sub-tasks, routing, cleaning, heating, and finally sealing the crack. In order to adapt these characteristics of the highway maintenance operations, a new idea is proposed, which is separating the whole system into multiple robots like a train. So, one robot performs one or two sub-tasks. In terms of multiple robot idea, Kumar and Waldron (1989) proposed an actively coordinated vehicle system. But this system was designed to have actively actuated articulations as opposed to having passive two bar linkages as in the TMR design.

3-1-3. Robot Position Tracking System

There are several types of tracking devices for automatic guided vehicles. The majority of automatic guided vehicles use dead reckoning as their tracking method, while other systems include sonar, light beams, radar, and vision systems. Various position tracking sensors are compared in the table 3-2. After examining the advantages and disadvantages of the possible tracking methods, the linkage system which has encoders on each joints has been decided as a position tracking system for the TMR. This is same as a SCARA type robot manipulator but totally passive arm which has no driving capability. By measuring the joint angles of the linkage, the position and the angular position can be decided. There are several advantages of this position tracking system. First of all, this system is very reliable, which is the most concern in the harsh environment like outdoor highway surface. And this is easy to build and relatively cheap compare to other methods such as vision, radar, or sonar system, etc. One more reason to decide the linkage system as the position tracking system for the TMR is that material and power should be supplied to the TMR from the supporting vehicle. The TMR works in the vicinity of the supporting vehicle while the necessary material and power are being supplied from the vehicle. Some

hoses and power cables are therefore necessary. These can be carried to the TMR over the mechanical linkage.

Table 3-2. *Comparisons of different position tracking sensors.*

Tracking Method	Advantages	Disadvanteges
Dead Reckoning	• Low cost, compact size • Low computation time	• Error accumulation • Wheel slip, uncertainty in wheel radius
Vision Systems	• Accurate positioning • Absolute positioning	• Computation intensive • Outdoor lighting, vibration • Expensive, bulky
Infrared Systems	• Absolute positioning • Accurate positioning • Medium cost • Compact size	• Sunlight, vibration • Obstacles
Sonar Systems	• Absolute positioning • Accurate positioning • Medium cost	•Reflections, router noise
Linkage System	• Absolute positioning • Accurate positioning • Simple, low cost, reliable	• Singularity points • Link deflections, vibration • Linkage jamming

3-1-4. Actuator Selection

Electric motor has been decided as the actuator to drive the TMR wheels. Electric motor has good controllability and control flexibility compared to other actuators (e.g., hydraulic motors, gasoline engine, etc.). There are generally three kinds of electric motors, DC motors, brushless DC (BLDC) motors, and AC induction motors. Table 3-3 shows a qualitative performance comparison. In this table, it is evident that the BLDC motor is most adequate for our purposes even though it is costly and somewhat difficult to control.

The DC motor has a maintenance problem even though its torque characteristics are excellent.

Table 3-3. *Performance comparison of electric motors.*

	Low Speed	High Speed	Starting Torque	Speed Regulation	Maintenance
BLDC motor	Excellent	Excellent	Excellent	Excellent	Excellent
DC motor	Good	Poor-due to brush wear	Excellent	Good	Good, Brush Replacement
AC motor	Poor	Excellent	Poor, trouble with high inertia	Good, limited by slip of motor	Excellent

The Figure 3-2 and 3-3 show the assembly drawing of the TMR platform and its overall picture, respectively. The real TMR system will contain multiple mobile robot platforms linked together. For the crack sealing application, the TMR consists of 2 platforms and the Robot I carries the routing unit and the Robot II carries the sealing unit. But one robot platform is enough to perform the purpose of this research, since the focus of this research is the control system development for the TMR. The coordination of each robots in the multiple robot system is beyond the scope of this research. With the platform and the linkage system shown in the Figures, the developed control laws are implemented and their performances are assessed.

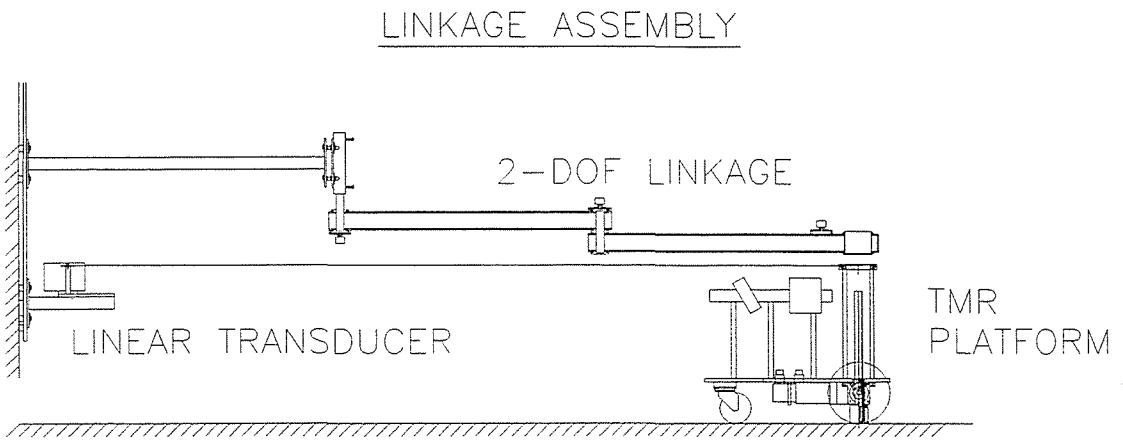

Figure 3-2. *Assembly drawing of the TMR platform and the linkage.*

3-2. TMR Configuration - Control System Aspects.

The TMR control system consists of three different modes running under different situations. The first is *Manual Control with Joystick* performed by human operator with a joystick. This control mode can be used for the cases when the operator needs to manually place the TMR at a specific position or to make the TMR trace a path manually.

The second is *Automatic Trajectory Tracking Control.* Using this mode, the TMR can automatically track a specific path without any manual operations. The reference path for this mode can be a pre-defined curve in a disk file form. The roadway sign stenciling, for example, needs a sequence of pre-defined reference path commands to follow a pre-defined roadway sign. And it can be generated with a real-time sensor, which forms a sensor based real time navigation problem. The current posture of the TMR from the position tracking system (linkage) and the reference posture from the laser range sensor are utilized for this mode to trace a path (the term "posture" was defined as a vector that contains *X, Y*

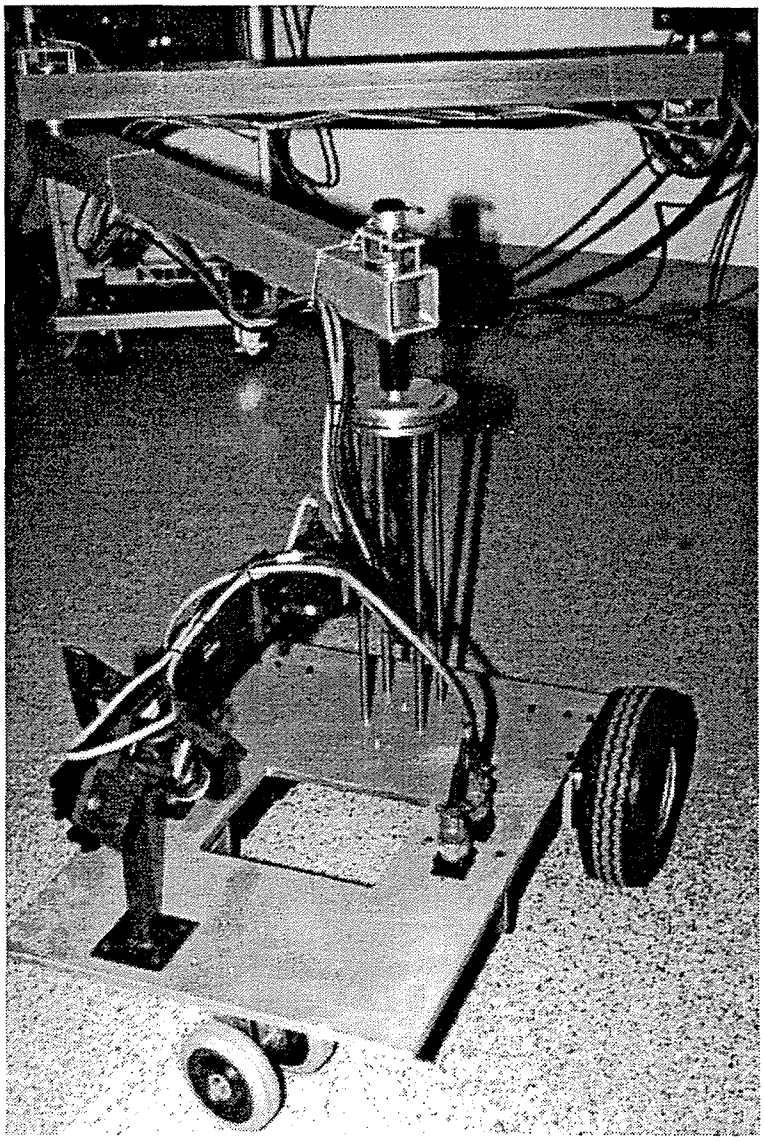

Figure 3-3. *The overall picture of the TMR platform and the linkage.*

translation and ψ rotation by Kanayama, 1988 as shown in the Figure 3-4). The TMR can track a crack path under this mode without any intervention by operators.

The third one is *Robust TMR Velocity Control.* Many of highway maintenance operations require very robust control system to external force disturbances that are hard to estimate. The routing process for the crack sealing operation is a good example. The routing force is difficult to predict and also severely fluctuating during the process. This mode is provided to surmount these difficulties.

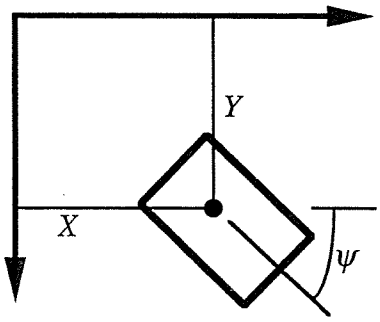

Figure 3-4. *Rigid body motion on X-Y plane, (X,Y,y) forms a posture vector..*

The Figure 3-5 shows the simplified control block diagrams of each control modes. The details of each modes are developed in the subsequent chapters. The Automatic Trajectory Tracking Control is derived based on kinematic model of the TMR. The Robust Velocity Control is developed with dynamic model on the other hand.

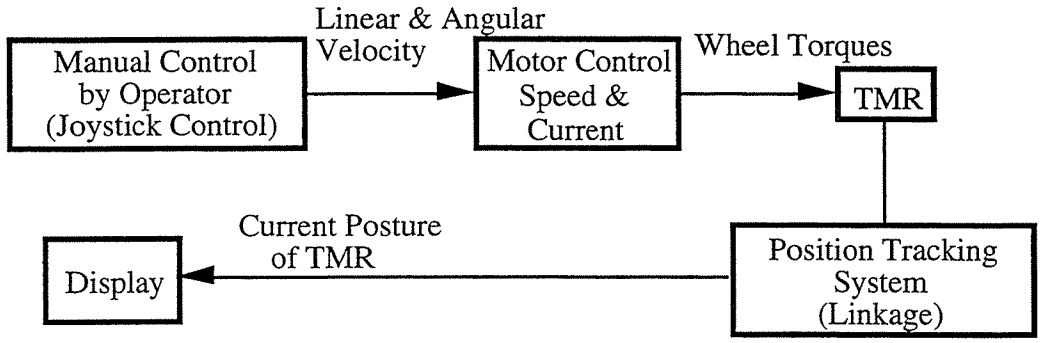

(a) Manual Control with Joystick.

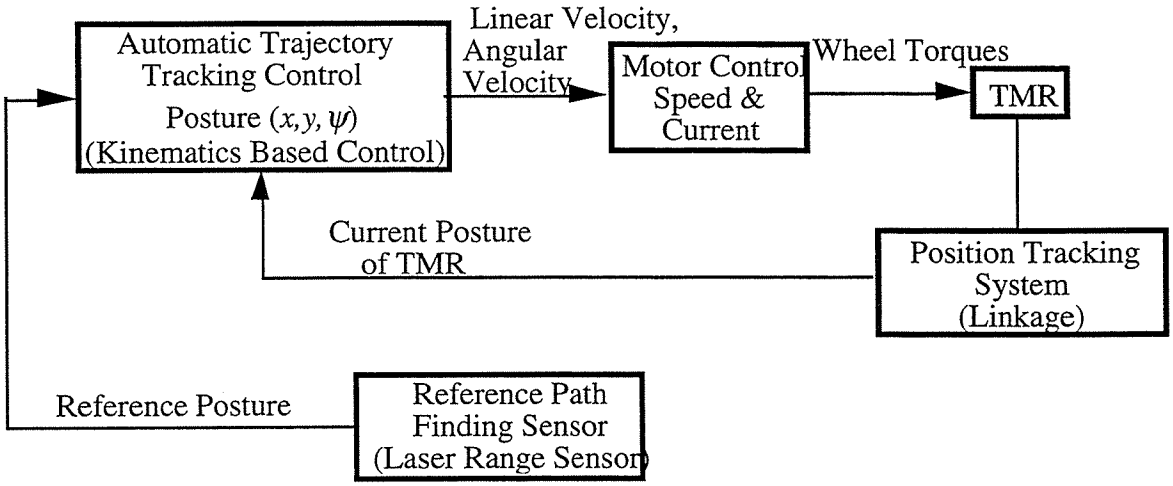

(b) Automatic Trajectory Tracking Control.

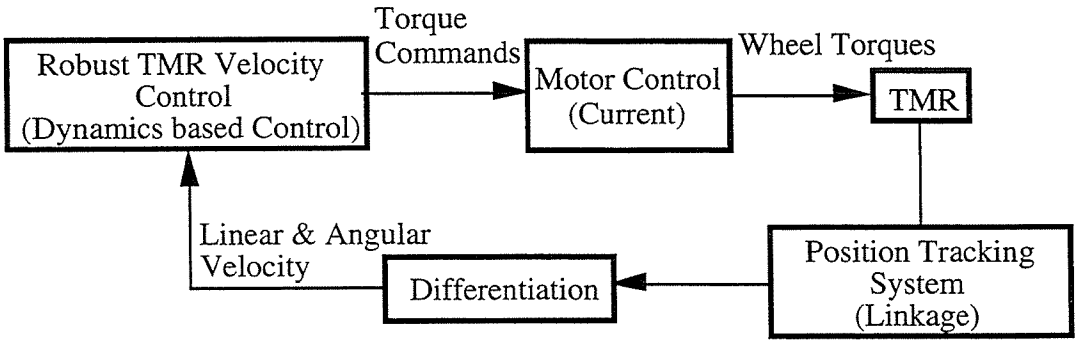

(c) Robust TMR Velocity Control.

Figure 3-5. *Overall control system configuration of the TMR.*

Chapter 4. Manual Control with Joystick

The manual control is manually performed by a human operator with a joystick. The joystick has 2 potentiometers in it and thus produces 2 axis coordinates which are orthogonal to each other. The following relationships between the joystick coordinates and the velocity commands to the TMR are appropriate in terms of human feeling,

Joystick Movements		Velocity Commands
Forward Movement	-->	Linear Velocity, u
Lateral Movement	-->	Angular Velocity, r

The velocity commands that are calculated from the joystick data are needed to be filtered due to their undesired high frequency contents. The filtered velocity commands are given to the wheel velocity controllers. The command filter makes the motion of the robot smoother than the unfiltered one.

The second order Butterworth filter is used as a filter design model. 20 Hz cut-off frequency is chosen since joystick operation is fulfilled by human who is not sensitive to high frequency motion. The following equation is the designed filter.

$$Y(z) = \frac{b(1) + b(2)z^{-1} + b(3)z^{-2}}{a(1) + a(2)z^{-1} + a(3)z^{-2}} X(z) \tag{4-1}$$

where $a = [1 \; -1.561 \; 0.6414]^T$, $b = [0.0201 \; 0.0402 \;]^T$. $X(z)$ is input and $Y(z)$ is filtered output.

This equation can be rewritten in recursive form which is useful when implementing the designed filter in real control code as

$$\begin{aligned} y[n] = {} & b(1)x[n] + b(2)x[n-1] + b(3)x[n-2] \\ & - a(2)y[n-1] - a(3)y[n-2] \end{aligned} \tag{4-2}$$

The Figure 4-1 (a) shows frequency response of the designed filter and (b) does phase delay versus frequency. The phase delay around the cut off frequency is 80 degrees which is reasonable. The Figure 4-2 through 4-5 show some experimental examples. The plots in the Figures contain the unfiltered velocity command that is transformed with the joystick output, its filtered velocity command, and the real command following for the left wheel. The control gains for the wheel motor control are varied. The control algorithm for the wheel motor control is Proportional and Integral (PI) control law. The performance of the joystick control was good when the proportional control gain is 20000 and the integral control gain is 1500. The details of motor control algorithm is included in Section 8-4.

This joystick control is successfully implemented with 80486 computer. The joystick is connected to the game port. The game port can be read using DOS BIOS interrupt routines. The joystick values are converted to the linear velocity and the angular velocity with the relation explained earlier. Then, these velocity commands are filtered with the developed second order Butterworth filter. These filtered velocity commands are sent to the motor controller boards through ISA bus interface (this interface will be explained in Chapter 8). The position and orientation of the TMR are displayed on screen. The control sampling time was about 0.029 second including the display.

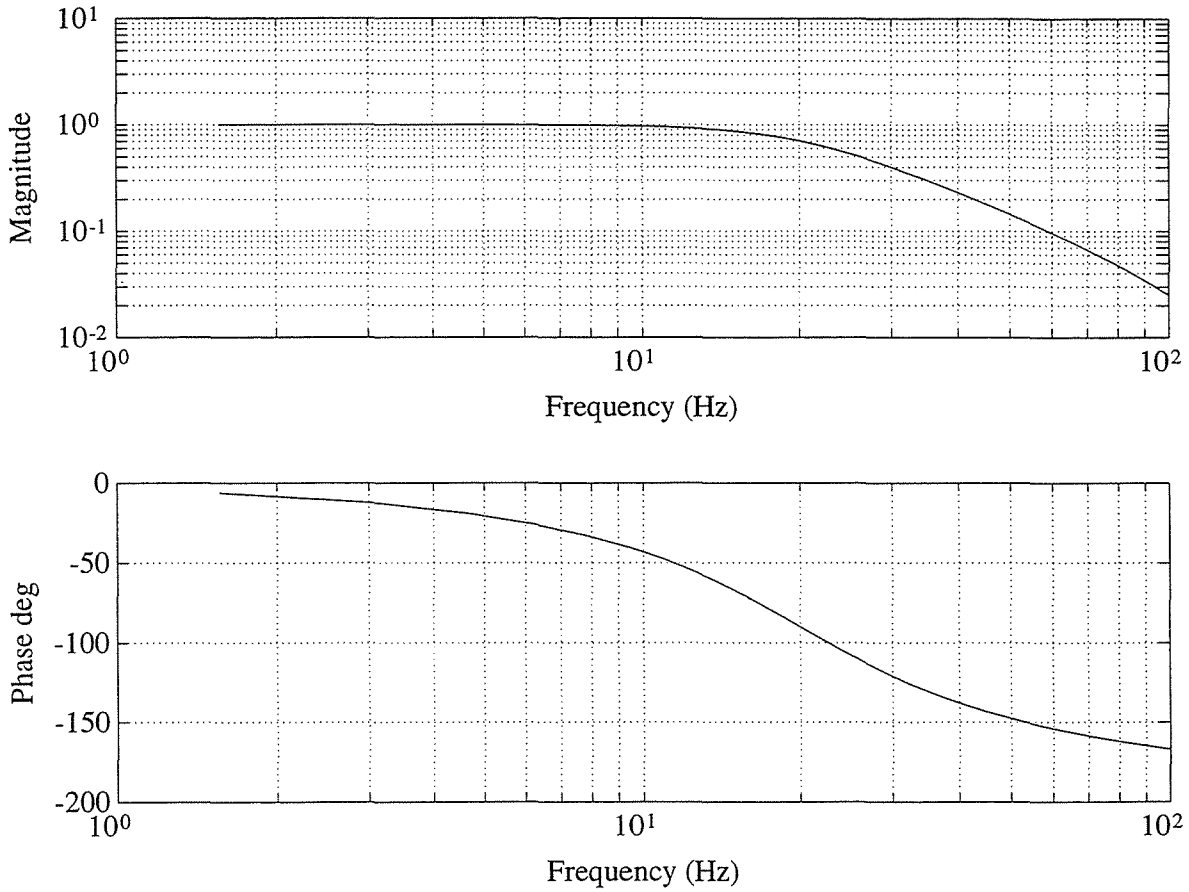

Figure 4-1. *Frequency response of designed filter, magnitude and phase plot .*

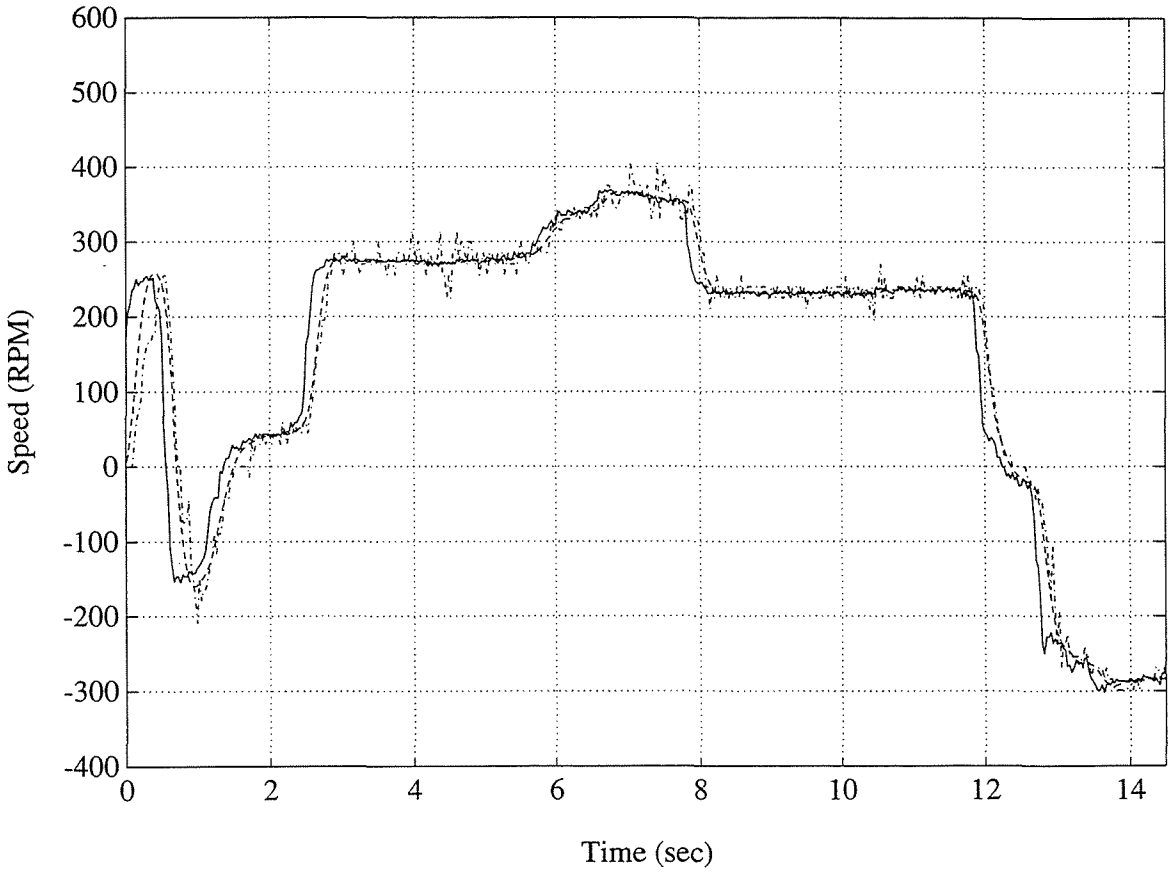

Figure 4-2. *An example of the joystick control, joystick command following of the left wheel when* K_P*=20000,* K_I*=1500, solid: unfiltered reference command from joystick, dashed: filtered reference command, dashdot: actual response of the left wheel motor.*

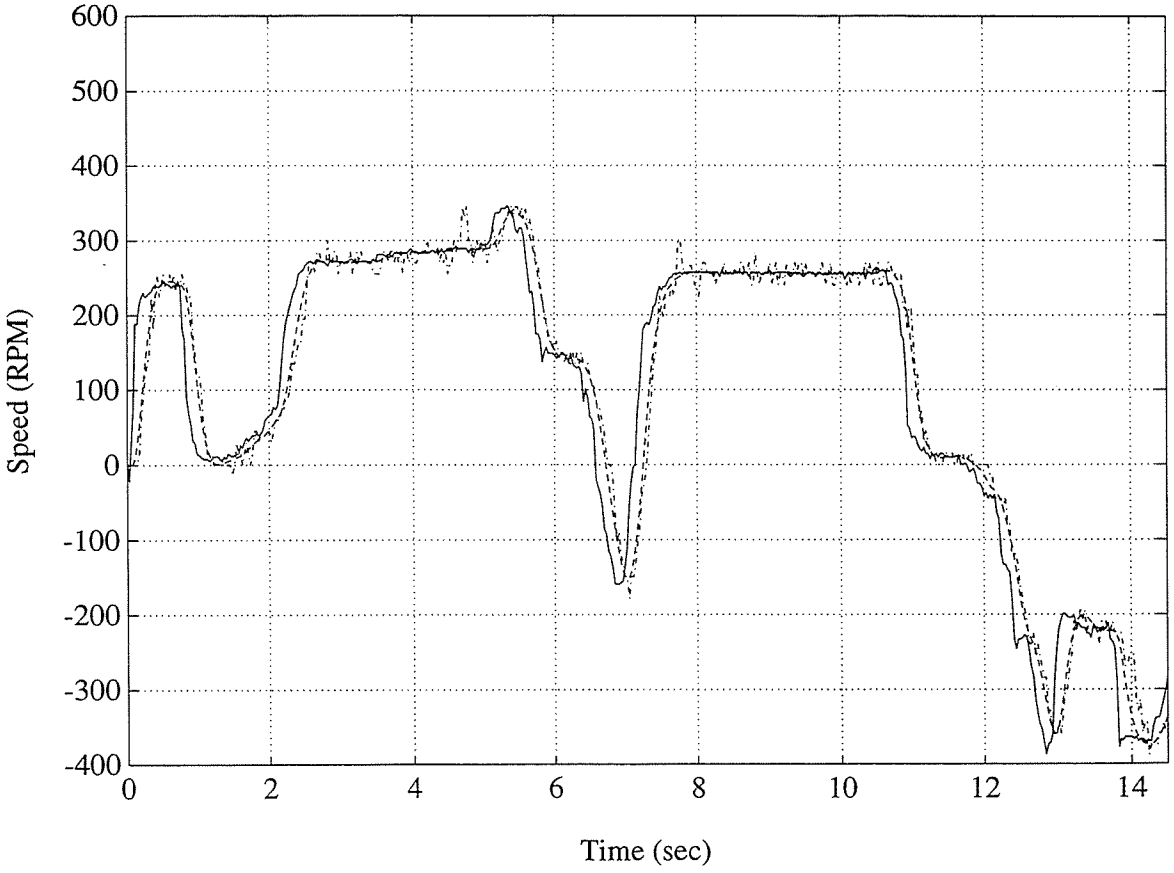

Figure 4-3. *An example of the joystick control, joystick command following of the left wheel when* K_P*=20000,* K_I*=1500, solid: unfiltered reference command from joystick, dashed: filtered reference command, dashdot: actual response of the left wheel motor.*

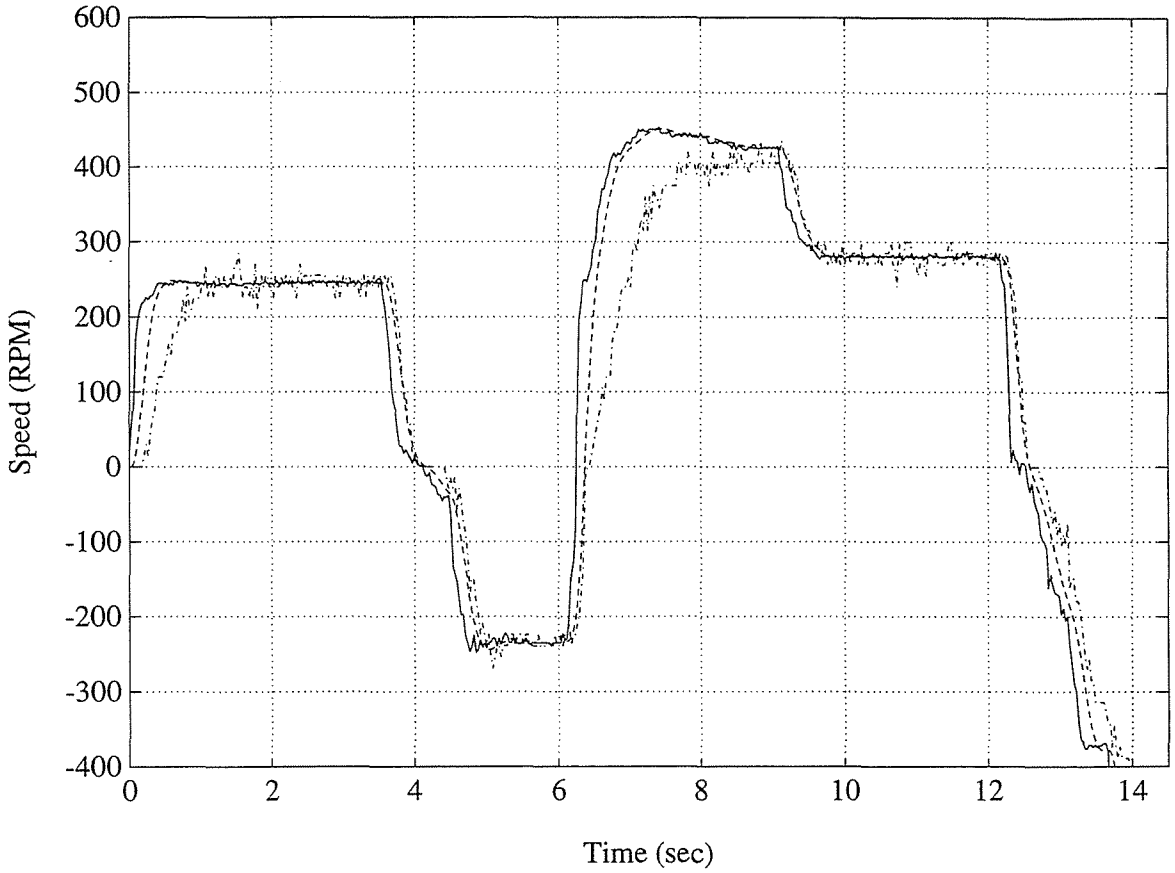

Figure 4-4. *An example of the joystick control, joystick command following of the left wheel when* K_P*=10000,* K_I*=1000, solid: unfiltered reference command from joystick, dashed: filtered reference command, dashdot: actual response of the left wheel motor.*

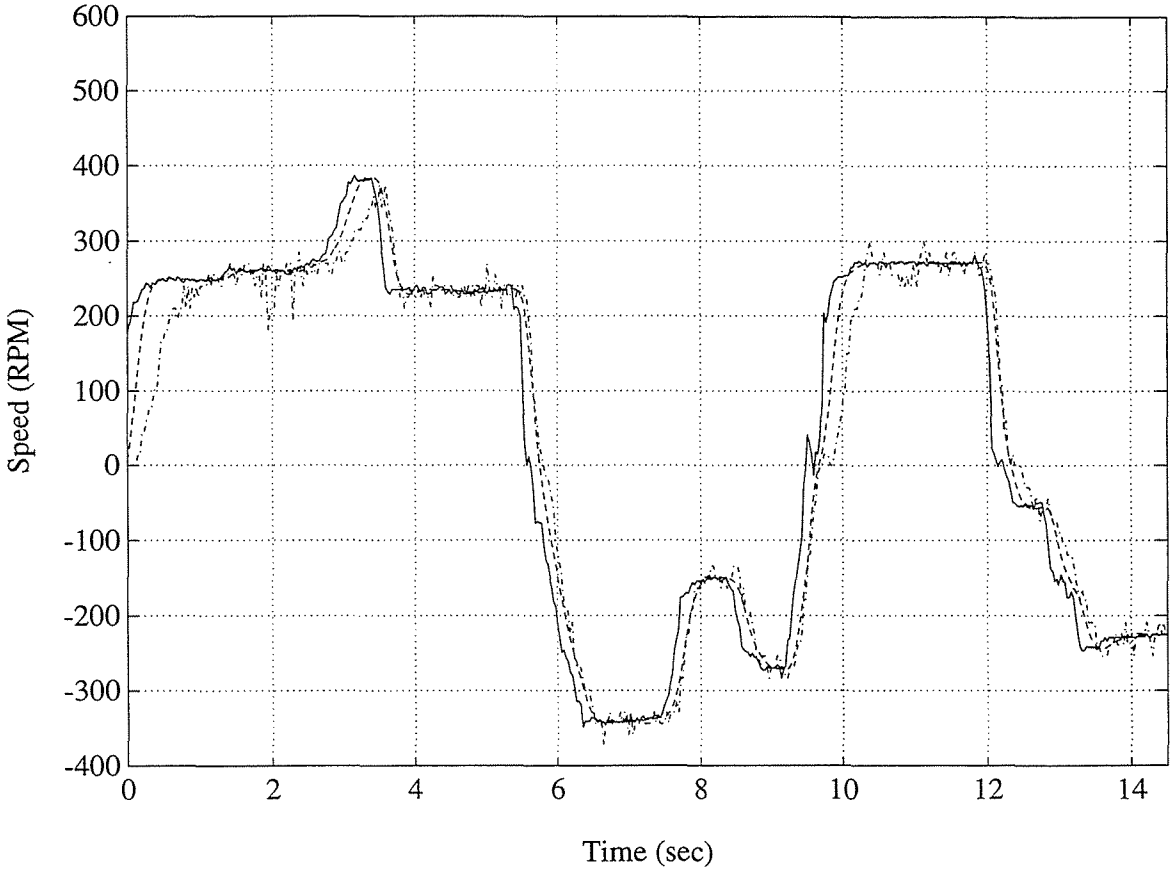

Figure 4-5. *An example of the joystick control, joystick command following of the left wheel when* K_P*=10000,* K_I*=1000, solid: unfiltered reference command from joystick, dashed: filtered reference command, dashdot: actual response of the left wheel motor.*

Chapter 5. Automatic Trajectory Tracking Control

This section deals with kinematic modeling of the TMR and its automatic trajectory tracking control algorithm. The modeling is based on the assumptions that there is no wheel slip and no pitch, roll, and bounce motions of the platform. The assumptions are valid due to the fact that the TMR runs on relatively flat paved road at slow speed. The mathematical model to develop a control algorithm is rather restricted to just essential kinematics of the target system since more detailed model including higher order terms requires more computational burden for control calculation but not much benefit is obtained. The effects of the ignored realities can be absorbed into feedback control action.

5.1 Kinematic Model of the TMR.

In order to describe the motion of the TMR, two reference coordinate systems are introduced as shown in Figure 5-1. The coordinate system *(X,Y)* is attached on the supporting vehicle. The equations of motion are described based on the assumption that this coordinate is stationary, so that it becomes *global coordinate system* fixed on the ground. The effect of the supporting vehicle's motion can be easily compensated later since it is mainly translational motion. The other is the *body coordinate system* attached on the TMR whose one component x represents forward direction of the robot and y is perpendicular to it. The origin of the body coordinate system coincides with the control point C whose position is controlled to track a prescribed path. On the control point, an applicator unit, sealant nozzle in crack sealing operation, for example, is located. The control point C is assumed to be on the center line, that is, on the x axis and e distant from the center of the wheel base Q.

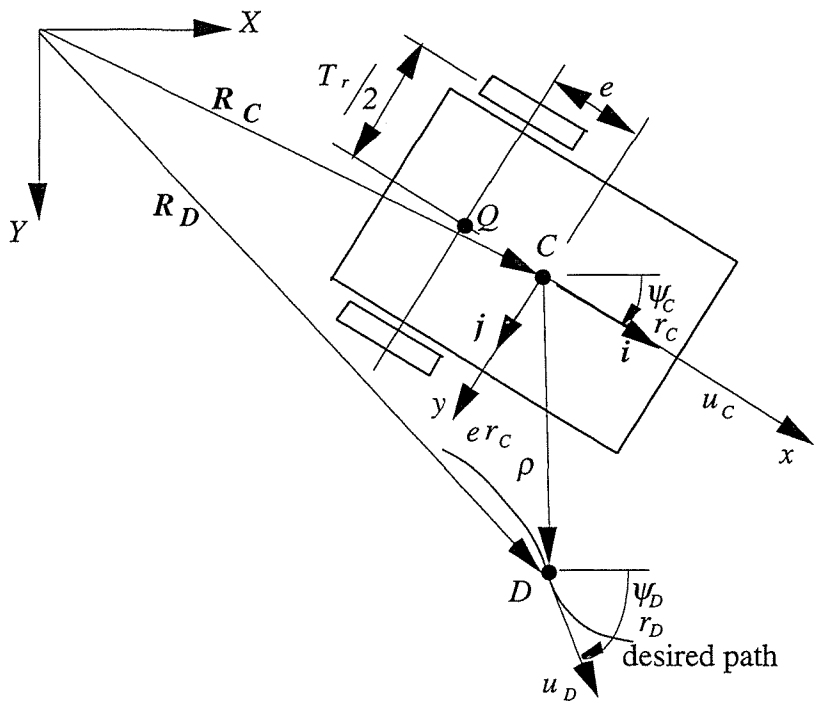

Figure 5-1. *TMR model and coordinate systems.*

For developing the kinematic model and the control algorithm, a term called *posture* which was used by Kanayama et al. (1988) is adopted. The posture vector consists of the x, y translation and the angular position ψ as its elements. And let us define some more terminologies for convenience.

- The current posture: the current posture of the TMR platform.
- The reference posture: the desired posture on which the TMR should be.
- The crack posture: the detected crack path and its tangent with a sensor.

The first derivative of the posture vector of the TMR at the point C in the global coordinate is

$$\begin{bmatrix} \dot{X}_C \\ \dot{Y}_C \\ \dot{\psi}_C \end{bmatrix} = \begin{bmatrix} \cos\psi_C & -\sin\psi_C & 0 \\ \sin\psi_C & \cos\psi_C & 0 \\ 0 & 0 & 1 \end{bmatrix} \begin{bmatrix} u_C \\ v_C \\ r_C \end{bmatrix} \tag{5-1}$$

where the first and the second rows represent linear velocities in x-y plane and the third row represents yaw rate of the robot. From the no slip condition, the lateral velocity v_C becomes er_C. Then, the above equation (5-1) is rewritten as

$$\begin{bmatrix} \dot{X}_C \\ \dot{Y}_C \\ \dot{\psi}_C \end{bmatrix} = \begin{bmatrix} \cos\psi_C & -e\sin\psi_C \\ \sin\psi_C & e\cos\psi_C \\ 0 & 1 \end{bmatrix} \begin{bmatrix} u_C \\ r_C \end{bmatrix}. \tag{5-2}$$

The posture $(X_C, Y_C, \psi_C)^T$ of the robot at C in the global coordinate is obtained after integrating the equation (5-2) given the linear and the angular velocities of the robot.

The position vector of the desired position D on the desired path at which the control point should reach is

$$\boldsymbol{R}_D = \boldsymbol{R}_C + \rho$$

where $\boldsymbol{R}_C$ is the position vector of the control point C which is identical to the origin of the body coordinate system and ρ is the relative position vector of the desired position D to the body coordinate system. Taking the first time derivative of the above equation, we can get

$$\dot{\boldsymbol{R}}_D = \dot{\boldsymbol{R}}_C + \dot{\rho} = \dot{\boldsymbol{R}}_C + \dot{\rho}_r + \omega \times \rho \tag{5-3}$$

where ω is the angular velocity vector of the body coordinate which is same to the one of the robot and $\dot{\rho}_r$ is the relative velocity vector to the body coordinate.

5.2 Control Algorithm Development.

A control problem generally falls into one of two categories, tracking control problem (or servo problem), and stabilization problem (or regulator problem). From a theoretical point of view, tracking control problem can be viewed as stabilization problem by changing state variables to errors. For instance, if we are to design a tracker law for the plant

$$\ddot{y} + f(\dot{y}, y, u) = 0$$

so that $e(t) = y(t) - y_d(t)$ goes to zero, the problem is equivalent to the asymptotic stabilization of the system

$$\ddot{e} + f(\dot{e}, e, u, y_d, \dot{y}_d, \ddot{y}_d) = 0$$

whose state components are e and $\dot{e}$ (Slotine and Li, 1991). Our control problem is to design a tracker following a pre-defined path. However, it becomes designing a stabilizer if we handle it with tracking errors as state components. Furthermore, Canudas and Roskam (1991) stated that there existed no smooth stabilization feedback in fixed global coordinates. Based on these facts, we will formulate the equation of motion with error terms and in the body coordinate system.

In the equation (5-3), the vectors ρ, $\dot{\rho}_r$ are respectively position vector of the desired point D and its time derivative relative to the body coordinate, which are equivalent to position error and its time derivative of the robot.

$$\rho = x\boldsymbol{i} + y\boldsymbol{j}, \quad \dot{\rho}_r = \dot{x}\boldsymbol{i} + \dot{y}\boldsymbol{j}.$$

The angular velocity of the moving coordinate has one component in $\boldsymbol{k}$ and its value is r_C, therefore,

$$\omega = r_C \boldsymbol{k}$$

since we ignored pitch, roll, and bounce motion. The desired velocity vector, $\dot{\boldsymbol{R}}_D$, which is expected to be tangent to the desired path, so that it does not have normal component to the path, is

$$\dot{\boldsymbol{R}}_D = u_D \cos\psi \boldsymbol{i} + u_D \sin\psi \boldsymbol{j}$$

and the velocity vector of the robot at C under no slip condition is

$$\dot{\boldsymbol{R}}_C = u_C \boldsymbol{i} + e r_C \boldsymbol{j}$$

in the body coordinate system. Plugging these equations into (5-3) and arranging in terms of errors, we can get

$$\dot{x} = yr_C - u_C + u_D \cos\psi$$
$$\dot{y} = -(e+x)r_C + u_D \sin\psi$$

And the first time derivative of angular position error that is the last component of the error posture is

$$\dot{\psi} = r_D - r_C.$$

In matrix form, these equations can be rewritten as

$$\begin{bmatrix} \dot{x} \\ \dot{y} \\ \dot{\psi} \end{bmatrix} = \begin{bmatrix} u_D \cos\psi \\ u_D \sin\psi \\ r_D \end{bmatrix} + \begin{bmatrix} -1 & y \\ 0 & -(e+x) \\ 0 & -1 \end{bmatrix} \begin{bmatrix} u_C \\ r_C \end{bmatrix}. \tag{5-4}$$

We already converted the tracking control problem to a stabilization problem by formulating the equation of motion in terms of the error posture $(x, y, \psi)^T$. Thus, our control problem can be defined as

finding a control law $(u_C, r_C)^T$ *such that, starting from anywhere in a region* Ω, *the state* $(x, y, \psi)^T$ *tend to 0 as* $t \to \infty$, *given a nonlinear system described by (5-4).*

The system has three outputs and two control inputs, so that it is not a square. Therefore, the coefficient matrix of the control input $(u_C, r_C)^T$ is not a square and thus is not invertable, which makes the problem very difficult.

Here, let us introduce a new variable,

$$z = y + c\psi, \quad c > 0, \; c \text{ is a positive constant.} \tag{5-5}$$

The new variable z can be used for a new state variable if the following lemma can be proved,

y and ψ both go to zero, when z goes to zero. (5-6)

First, (5-6) is apparent, when $y\psi$ is positive, that is when the signs of both variables are same. Second, (5-6) is also valid from physical intuition, when $y\psi$ is negative, that is when the signs of both variables are different. In Figure 5-2, we can see that the robot tends to the desired path when $y\psi$ is negative. So, y goes to zero and therefore ψ also goes to zero since z does. Consequently, we can use the new state component z instead of y and ψ, which makes the equation of motion (5-4) square as

$$\begin{bmatrix}\dot{x}\\ \dot{z}\end{bmatrix}=\begin{bmatrix}u_D\cos\psi\\ u_D\sin\psi+cr_D\end{bmatrix}+\begin{bmatrix}-1 & y\\ 0 & -(e+x+c)\end{bmatrix}\begin{bmatrix}u_C\\ r_C\end{bmatrix} \tag{5-7}$$

plugging the equations (5-4) into (5-5).

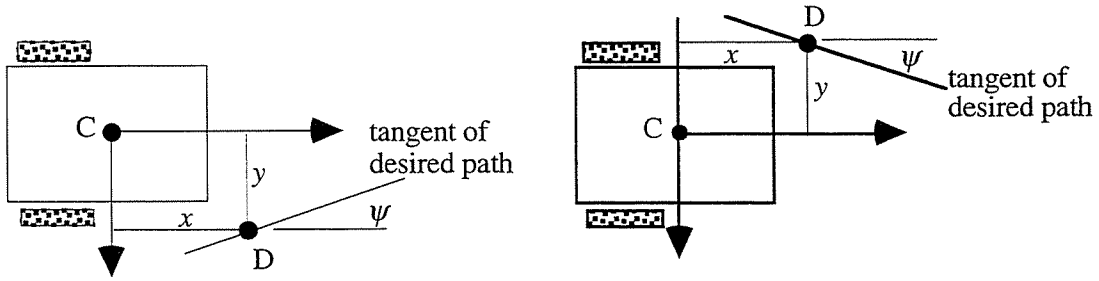

(a) $y>0$, $\psi<0$ *(b) $y>0$, $\psi<0$*

Figure 5-2. *The cases that the robot goes toward to the desire path and z thus goes to zero.*

Let us use a simple notation form for the equation (5-7), then

$$\dot{\boldsymbol{x}} = \boldsymbol{f}(\boldsymbol{x};t)+\boldsymbol{E}(\boldsymbol{x};t)\boldsymbol{u} \tag{5-8}$$

where

$$\boldsymbol{x}=\begin{bmatrix} x \\ z \end{bmatrix},\ \boldsymbol{f}(\boldsymbol{x};t)=\begin{bmatrix} u_D\cos\psi \\ u_D\sin\psi + cr_D \end{bmatrix},\ \boldsymbol{E}(\boldsymbol{x};t)=\begin{bmatrix} -1 & y \\ 0 & -(e+x+c) \end{bmatrix},\ \boldsymbol{u}=\begin{bmatrix} u_C \\ r_C \end{bmatrix}.$$

The matrix $\boldsymbol{E}(\boldsymbol{x};t)$ is invertable if and only if $x \neq -(e+c)$.

Finding a control law is fairly straight forward using 'feedback linearization' method ('computed torque' in robotics literature). Choose a control law

$$\boldsymbol{u}=\boldsymbol{E}^{-1}(-\boldsymbol{f}-\boldsymbol{K}\boldsymbol{x}) \tag{5-9}$$

and this control law transforms the equation (5-8) to

$$\dot{\boldsymbol{x}}+\boldsymbol{K}\boldsymbol{x}=\boldsymbol{0} \tag{5-10}$$

and this is exponentially stable choosing the gain matrix $\boldsymbol{K}$, such that the eigenvalues of the equations lie in the left-half plane.

5.3 Feasibility Study by Simulation

In order to verify the developed tracking control law, some computer simulations are performed. The stability and the robustness of the control law are expected to be proved through the simulations.

The control procedure is summarized in Figure 5-3. The desired posture and the current posture are given in the global coordinates and then they are transformed into the body coordinate to employ the control law (5-9).

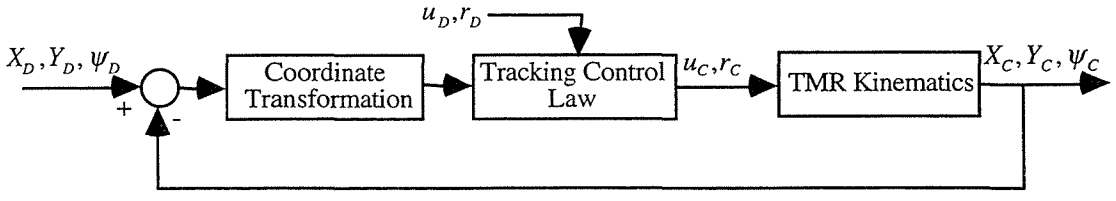

Figure 5-3. *Control block diagram of the Tracking Control.*

To verify the tracking control law (5-9), some simulation results are presented in Figure 5-4,5. A diagonal matrix is chosen for the gain matrix $\boldsymbol{K}$. The Figure 5-4 shows successfully tracking the desired path that has some discontinuities, y jump at the initial position and abrupt angle changes at $(50,25)^T$, $(50,0)^T$, and $(100,0)^T$.

The sinusoidal reference path (a) in the Figure 5-5 that has fairly steep curvature is used to simulate pavement crack path. The figure (b) shows error posture $(x,y,\psi)^T$ following the path (a). The control law (5-9) is exponentially stable as we can see in the equation (5-10). But the robustness of the control law especially for a non-linear system can not be concluded from its stability. In order to prove the robustness of our control law, some simulations are conducted. The most concerned uncertainty in controlling mobile robot is wheel slippage. Since we do not include any dynamics of the robot platform, there is no explicit term in the system equation that reflects the effect of the wheel slippage. From physical intuition, we can see that the wheel slippage effect could be absorbed into the parameter e even though we can not find out explicit relationship. The parameter e in the kinematic equation (5-4) is modified as $e = e_o(1+0.2\sin(\pi t))$, which is fluctuating ± 20% around the nominal value e_o. The figure (c) represents the tracking error when following the path (a) and including the uncertainty.

From the simulations shown above, it is concluded that the developed control law is stable and robust. The tracking error bounds in the sinusoidal path simulation are very small, so that we can expect good tracking control performance for real crack path tracking control of the TMR. All necessary requirements of the control algorithm are proved through the simulations. We are now ready to develop an optimal control system hardware to implement the control law.

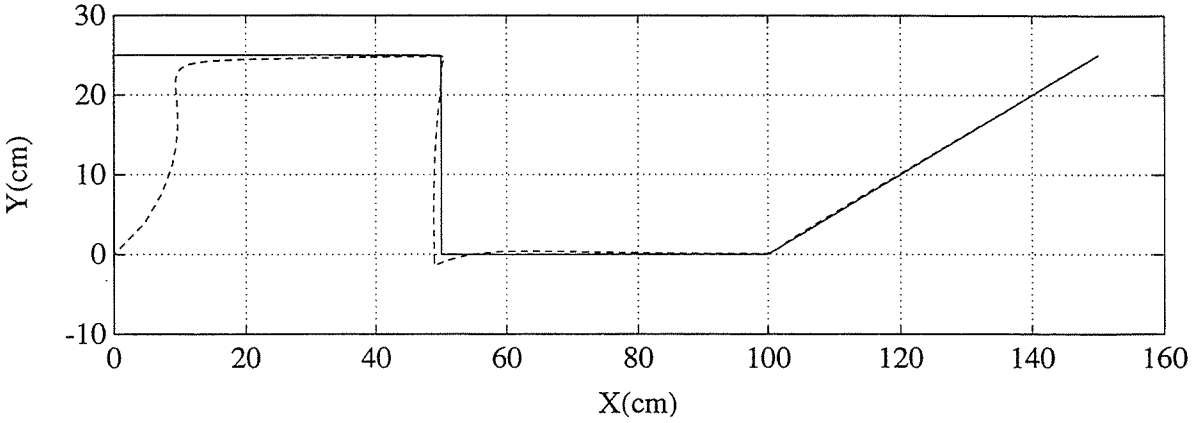

*(a) Test for discontinuous path ,e=20, **K**=[10 0;0 3] , solid: reference path, dashed: real trajectory.*

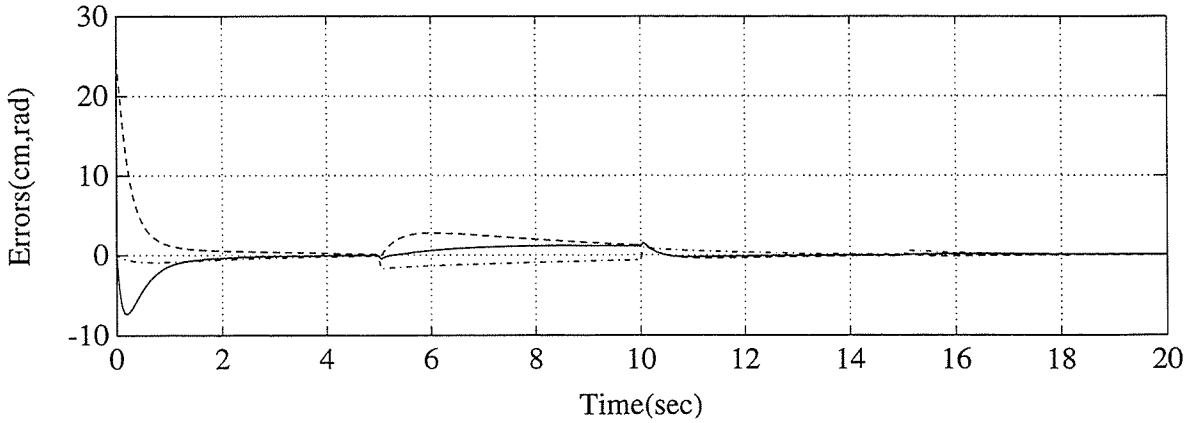

(b) Error posture when tracking the discontinuous path shown in (a).

Figure 5-4. *Simulation results for the discontinuous reference path.*

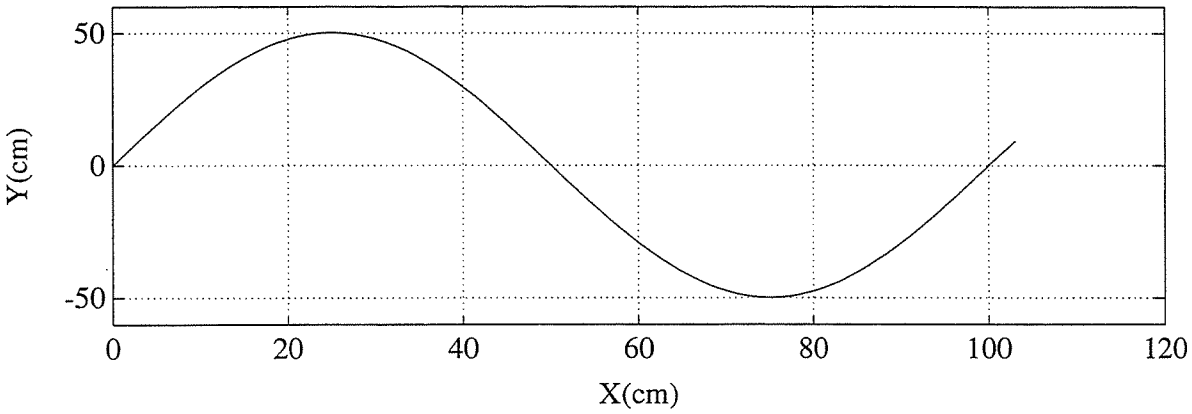

(a) Sinusoidal reference path used for simulation.

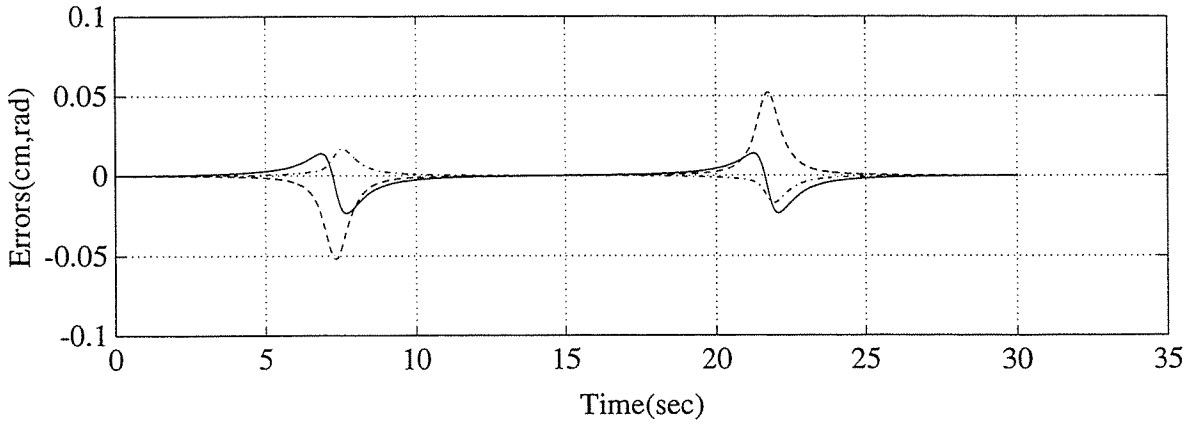

*(b) Error posture when tracking the path shown in (a), e=20, **K**=[10 0;0 3], solid: x, dashed: y, dashdot: θ.*

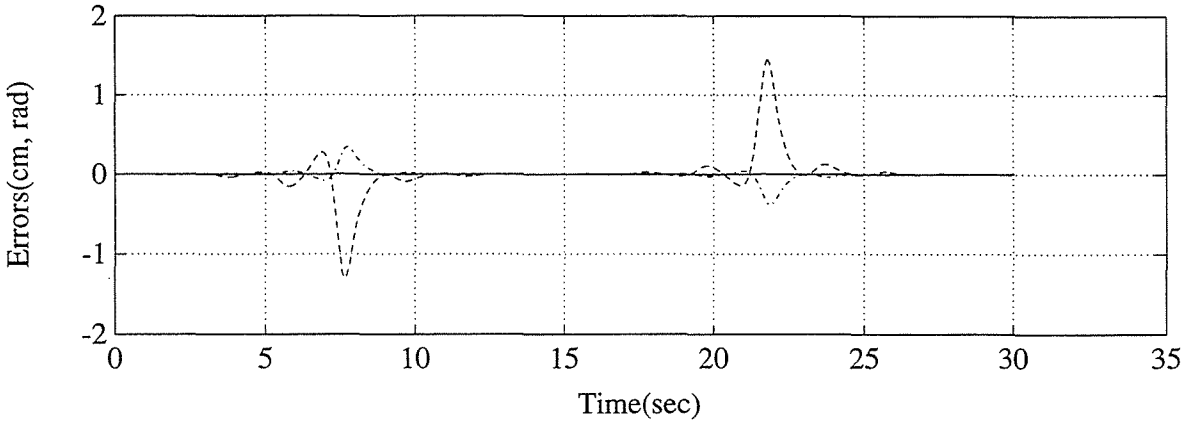

(c) Error posture when tracking the path shown in (a) and including the uncertainty in e, $e = e_o(1 + 0.2\sin(\pi t))$, *e=20, K=[10 0;0 3], solid: x, dashed: y, dashdot: θ.*

Figure 5-5. *Simulation results for the continuous sinusoidal reference path.*

5-4. Crack Path Finding with Laser Range Sensor

A variety of sensor technologies have been researched in order to select a sensing system which best meets the requirements in the crack sealing application (Krulewich and Velinsky, 1992). Then, the laser range sensor has been decided as a crack detecting device, which has been proved to be the best on both Asphalt Concrete (AC) and Portland Cement Concrete (PCC). The laser range sensor is attached at the front of the robot platform. The laser range sensor scans the profile of the road surface under the sensor based on the principle of triangulation. The profile data is used to determine the *offset* error which is the distance between the sensor center and the real crack reservoir. The detail crack finding algorithm is shown in Velinsky, 1993. In this thesis, it is assumed that the time history of the offset value is given.

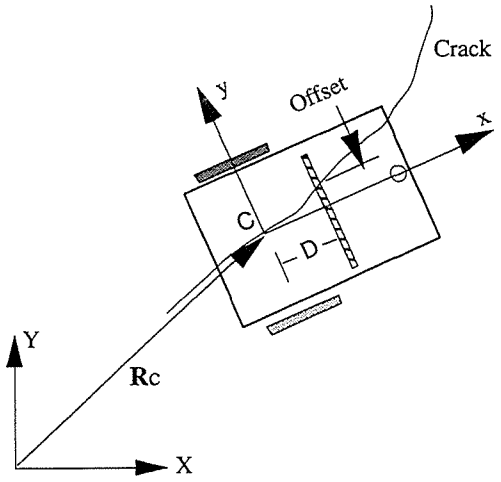

Figure 5-6. *Robot platform with laser range sensor.*

The Figure 5-6 shows the laser range sensor location and related parameters. The distance D of the laser range sensor from the origin of the body coordinates in x direction is fixed. The sensor is arranged perpendicular to the x axis. The y component of the detected crack position in the body coordinate is the *offset* value (the crack position relative to the center of the sensor). Then the global coordinates of the detected crack position is obtained by coordinate transformation. The following equation represents these relationships:

$$\begin{bmatrix} X_i \\ Y_i \end{bmatrix} = \begin{bmatrix} X_{c_i} \\ Y_{c_i} \end{bmatrix} + \begin{bmatrix} \cos\theta_{c_i} & -\sin\theta_{c_i} \\ \sin\theta_{c_i} & \cos\theta_{c_i} \end{bmatrix} \begin{bmatrix} D \\ offset \end{bmatrix}, \tag{5-11}$$

where the subscript i denotes a sampling instance. With the time function of the X and Y in discrete form, the tangent angle of the crack path is obtained as

$$\theta_i = atan\left(\frac{Y_i - Y_{i-1}}{X_i - X_{i-1}} \right) \tag{5-12}$$

where i represents the current sampling time and $i\text{-}1$ denotes the previous. Consequently, the equation (5-11) and (5-12) form the crack posture. This series of the crack posture is stored in the memory and utilized to determine the reference posture.

5-5. Reference Command Generation

The developed tracking control algorithm requires knowing the error posture *(x, y, θ)* and the desired linear velocity u_D and the angular velocity r_D of the robot platform. The reference posture obtained from the laser range sensor and the current posture measured by the TMR position tracking system (the mechanical linkage that has the optical encoders on each joints) are utilized to generate the reference commands.

The desired linear velocity is first determined based on the required task characteristics. The velocity is set to be very slow for a deep and wide routing task for example. If the controlled linear velocity of the robot is very close to the desired linear velocity u_D, the desired next position at the next control sampling step is

$$x_d = u_D dt \tag{5-13}$$

along x in the current body coordinates, where dt is sampling interval.

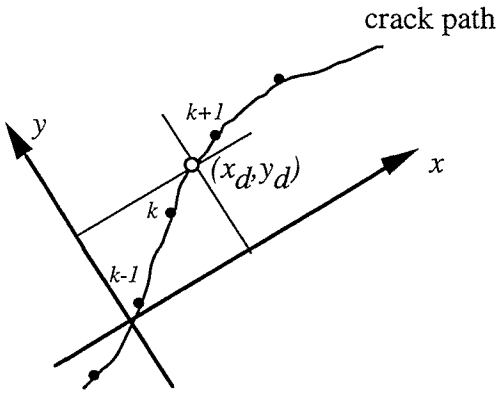

Figure 5-7. *Determination of the reference position.*

The desired lateral deviation from the reference path is the y component of the intersection of the reference path and the vertical line which passes through $(x_d, 0)$ and parallel to y axis as shown in the Figure 5-7. The crack posture is stored in a buffer memory in discrete form. As such, it is necessary to employ an interpolation method. Since one component, x_d, of the desired coordinates is known, it can be used as an

interpolation parameter. Before interpolating, the coordinates of the crack path must be first transformed to the body coordinates since the crack posture is stored in the global coordinate form:

$$\begin{bmatrix} x \\ y \end{bmatrix} = \begin{bmatrix} \cos\theta_c & \sin\theta_c \\ -\sin\theta_c & \cos\theta_c \end{bmatrix} \left\{ \begin{bmatrix} X \\ Y \end{bmatrix} - \begin{bmatrix} X_c \\ Y_c \end{bmatrix} \right\}. \tag{5-14}$$

Through interpolation, the desired y in the body coordinate system is expressed as

$$y_d = \frac{(y_{k+1} - y_k)(x_d - x_k)}{x_{k+1} - x_k} + y_k \tag{5-15}$$

for k such that $x_k < x_d \le x_{k+1}$. Similarly, the desired θ can be found as

$$\theta_d = \frac{(\theta_{k+1} - \theta_k)(x_d - x_k)}{x_{k+1} - x_k} + \theta_k \tag{5-16}$$

for k such that $x_k < x_d \le x_{k+1}$ since these scalar quantities are stored in same location as x_d in the data structure buffer.

5-6. Experimental Results

The developed tracking control law is implemented with the TMR platform shown in the Chapter 3. The details of the TMR controller hardware used for implementing the control law are explained in Chapter 8.

First, the table reference method for a reference posture is applied for tracking control performance test. The reference posture is generated in off-line program and stored in a disk file. Then, this reference posture is read every control sampling time within the tracking control program. There are two purposes that this table reference method is tested. First of all, this method can be utilized for the applications that require tracking a pre-programmed path, such as highway stenciling operation. We can draw a roadway sign by making the TMR follow pre-defined path representing a roadway sign. And another

purpose is that it is a pre-test before implementing the tracking control with a real time sensor, the laser range sensor for the crack sealing operation.

The reference path shown in the Figure 5-8 (a) is used for the tests. The reference path consists of two sinusoidal curves. The first part of the reference curve is one cycle of sine curve and the other is negative sine back to the initial position. Various control gain matrices are tested as shown in the Figures 4-8, 9, 10, 11, 12. Each figure shows trajectory tracking on *X-Y* plane, angular position tracking, tracking errors, and control inputs during the TMR is following the reference posture. We can see that the control performance becomes better as control gain is bigger, which we expect from control theory. But high control gain causes high frequency chattering. For the test shown in the Figure 5-12, big control gains compare to other tests are used. We can see that the control inputs in the Figures 5-12 (d) are more shakier than the control inputs for the other tests even though the tracking errors become smaller. It was also noticed that robot motion was not smooth in that test. From the tests, it is concluded that the gain matrix [20 0;0 20] would be good for the given reference path. But the appropriate gain also depends on how complex the reference curve is. That is, lower control gain is more appropriate when the reference path is very complex in order to get smooth motion of robot platform. Trade off for the smooth motion is bigger tracking errors.

After successfully implementing the tracking control law with the reference path table method, offset table is used to generate the reference posture instead of giving all the posture information in a file. Detail theory to get the posture from the offset data is given in Sections 4 and 5. This test is a pre-test before the tracking control with the real time laser range sensor is implemented. This test is basically same to the tracking control with the laser sensor except that the offset data comes from the given table instead of coming from the laser sensor system. Since the laser sensor system itself is not a topic of this research, I just assumed that the offset data can be given from anywhere. So, the success of the

tracking control with the offset table promises the success of the tracking control with the laser sensor.

Figure 5-13 (b), (c), and (d) show examples of trajectory tracking on X-Y plane when the offset table shown in the Figure 5-13 (a) is being used. The reference posture that the TMR should track is calculated from the current posture of the TMR and the offset data. The offset data is already given but the current posture of the TMR at future sampling time can not be predicted because there always exist tracking errors. So, we can not see the final shape of the reference path even though the whole offset data is given as shown in the Figure 5-13 (a). This is why the shape of the reference path calculated from the offset table does not have smooth shape. But we can roughly suppose the shape of the reference path with the offset. The offset given in the Figure 5-13 (a) is always greater than or equal to zero and is sinusoidal. From these facts, we can expect a positively turning big circle and sinusoidally oscillating small curve on it like the reference paths shown in the Figure 5-13 (b), (c), and (d). The control gain is set to be relatively low, [10 0; 0 10], since we do not want to follow small high frequency curve on the reference curve. Tracking all detail high frequency curves shipped on low frequency curve makes our task even worse. Because non-holonomic cart like differentially steered vehicle requires very fast yaw motion in order to accurately track small curves during moving with constant linear speed. Three different speeds were tested and tracking performance was good at low speed as we expected.

The Figure 5-14 shows artificial cracks routed on plywood in order to test the tracking control with the laser range sensor in lab environment. Three different shape cracks, A, B, and C are used for the test. Crack A is one quarter inch wide. Crack B and C are half inch wide. The crack detection algorithm is well described in Krulwich and Velinsky, 1992. The Figure 5-15, 16 and 17 show tracking control results along the crack A, B, and C, respectively. The linear speed was 5 inch/sec. The lateral deviation of the actual TMR trajectory from the reference crack is very small along the crack except big curvature region. The lateral error around big curvature region is big relative to smooth

region. This is unavoidable to some extent for non-holonomic cart moving forward with a constant speed. This error is mainly caused by inertia of the robot platform. The control law developed here is based on the kinematics of the robot. Robust control law which includes dynamic effect will be developed in next chapter.

The solutions of the equation (5-10) are

$$x_1(t) = x_1(0)e^{-K_{11}t}$$
$$x_2(t) = x_2(0)e^{-K_{22}t} \tag{5-17}$$

when the diagonal matrix $\boldsymbol{K} = [K_{11}\ 0; 0\ K_{22}]$ is being used. These equations are interpreted as faster responses are obtained at higher control gains. But higher control gains may excite high frequency unmodeled modes since the tracking control law (5-9) is derived from the kinematic model. The responses could, therefore, go to unstable modes. So, the gains should be carefully selected after considering the system bandwidths. In this thesis, the control gains were selected through experiments. There is always trade off between the system performance and stability. Good control performance was obtained at high control gains but the TMR motion was not smooth. After carefully watching the TMR motion and control performance while changing the control gains, the gain matrix *[20 0;0 20]* was chosen for the smooth reference curve shown in the Figure 5-8 (a). But the control gain matrix *[10 0;0 10]* was more appropriate to tracking control of real crack path due to the complexity of the crack path. Higher control gains could be used for smooth reference path for better control performance but the control gains should be lowered for complex reference curve in order to avoid shaky motion of the platform.

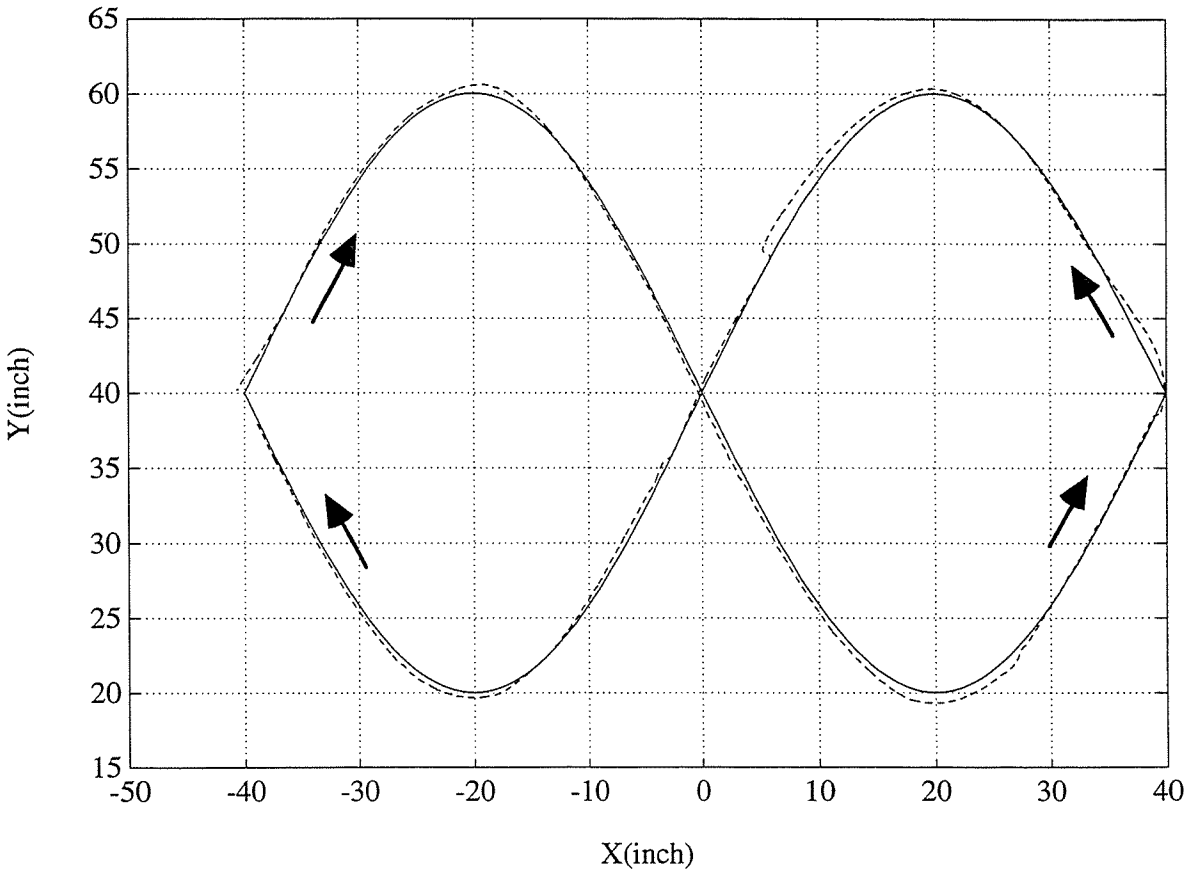

Figure 5-8 (a). Trajectory(x, y position) tracking of the TMR: solid line - reference path, dashed line - real TMR path tracking, K=[20 0; 0 20].

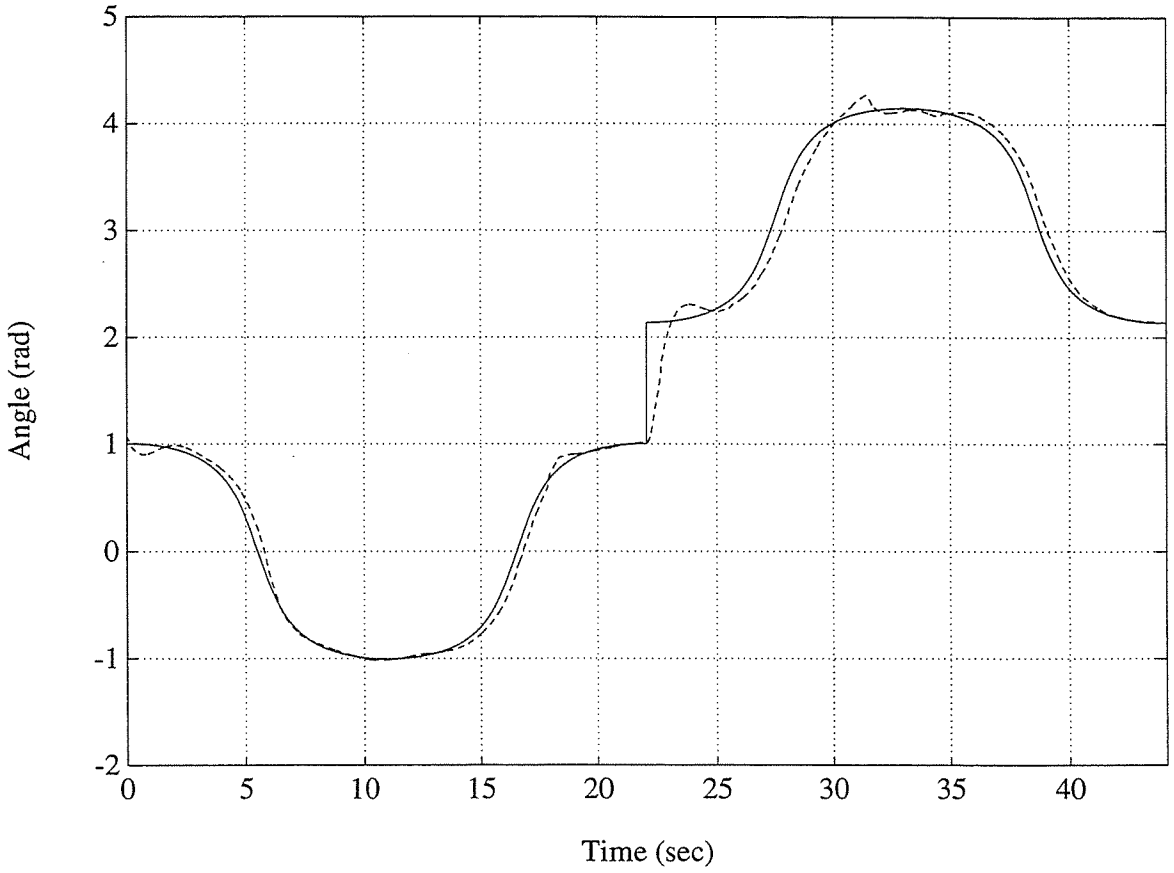

Figure 5-8 (b). Trajectory(θ rotation) tracking of the TMR: solid line - reference angular position, dashed line - real TMR tracking, K=[20 0; 0 20].

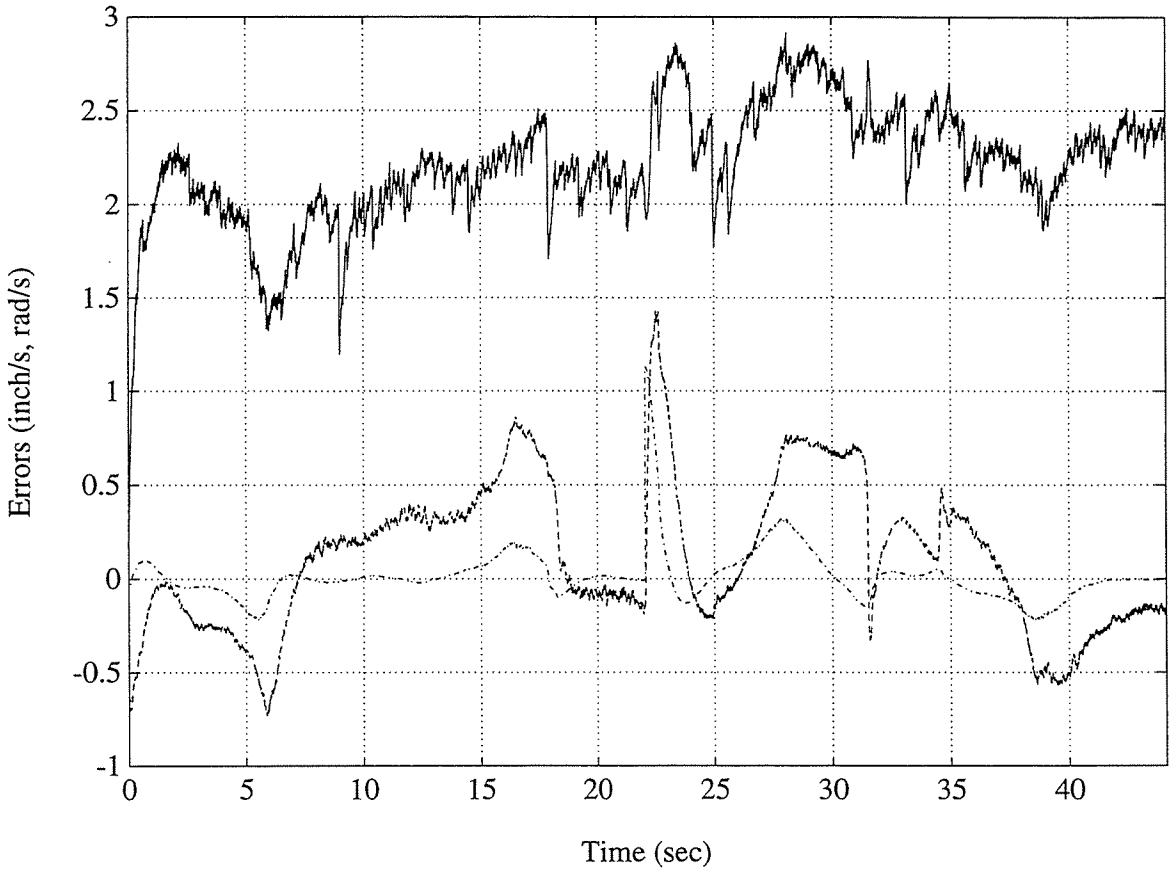

Figure 5-8 (c). Error posture when tracking the path shown in the Figure (a): solid line - x, dashed line - y, dashdot line - θ, K=[20 0; 0 20].

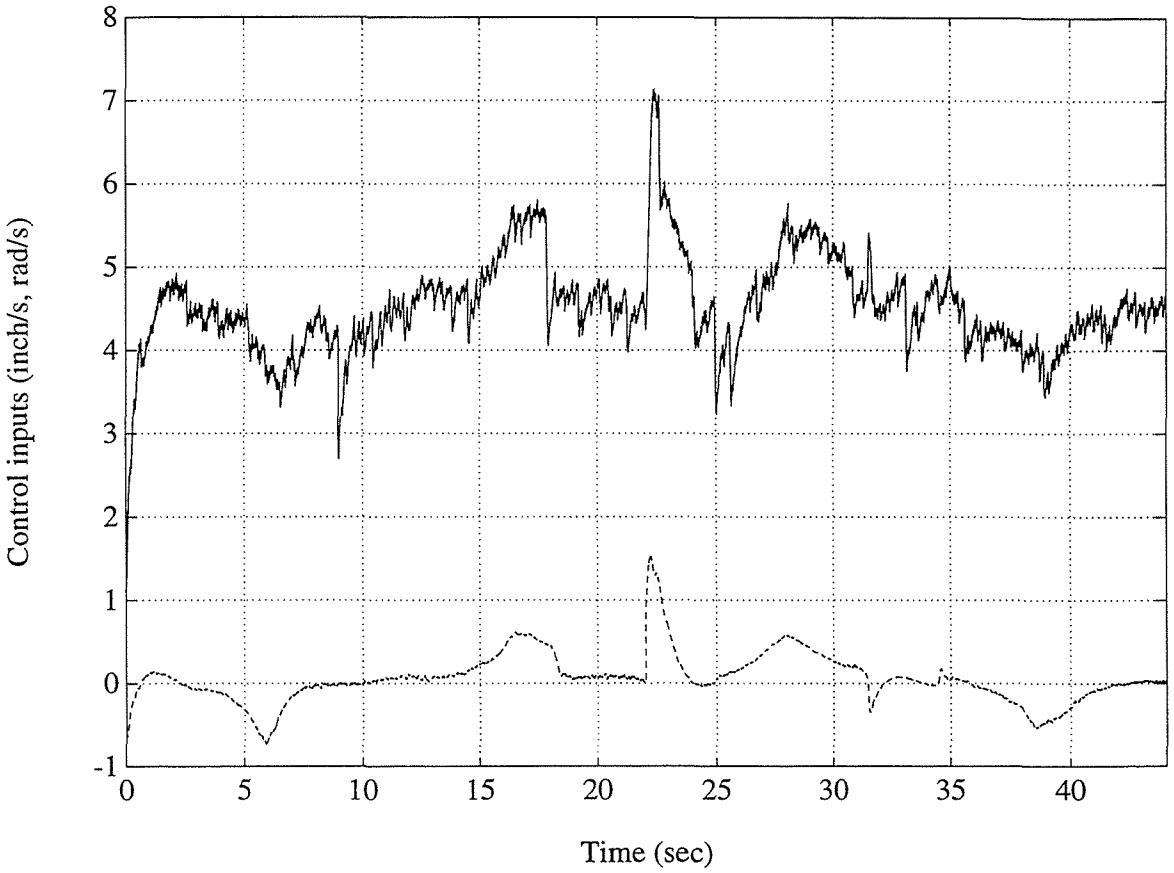

Figure 5-8 (d). Control commands when tracking the path shown in the Figure (a): solid line - linear speed, dashed line - angular speed, K=[20 0; 0 20].

***Figure 5-8**. An experimental result: K=[20 0; 0 20].*

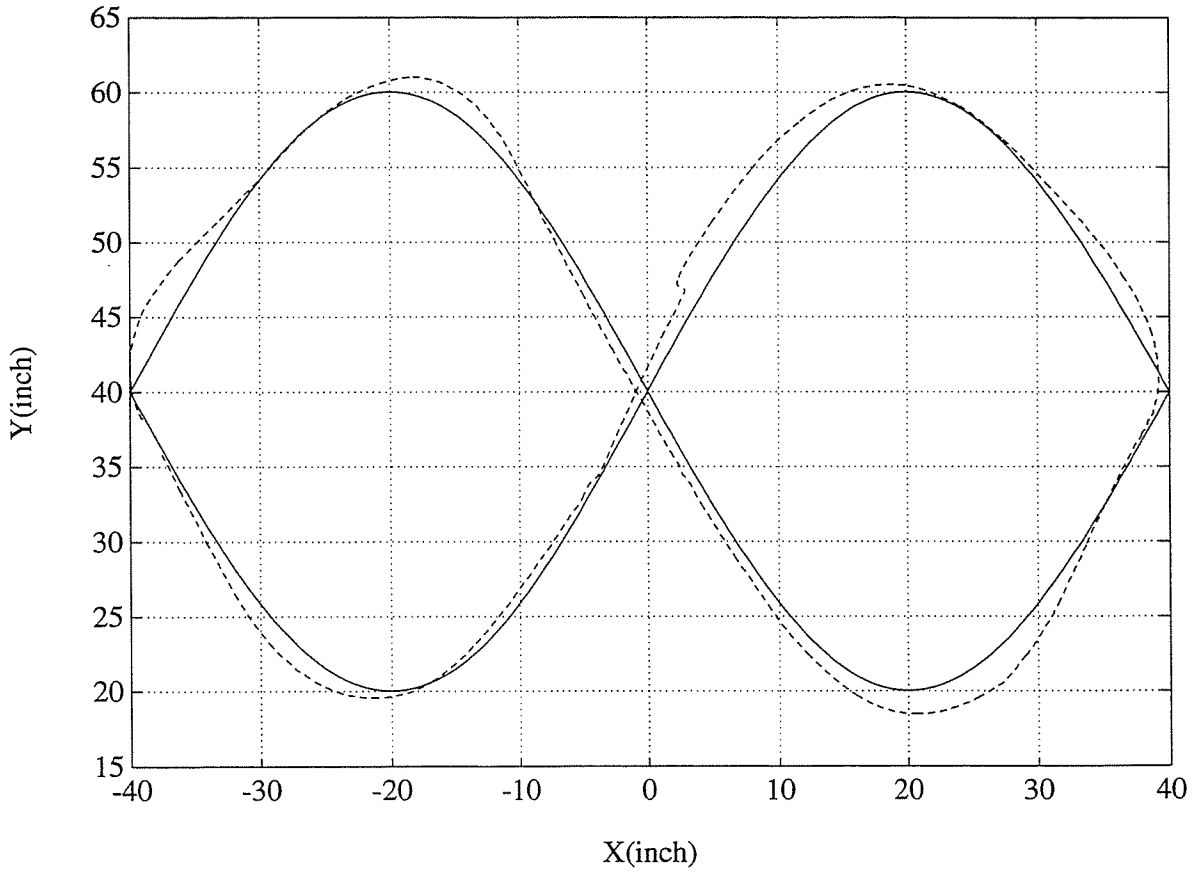

Figure 5-9 (a). Trajectory(x, y position) tracking of the TMR: solid line - reference path, dashed line - real TMR path tracking, K=[10 0; 0 10].

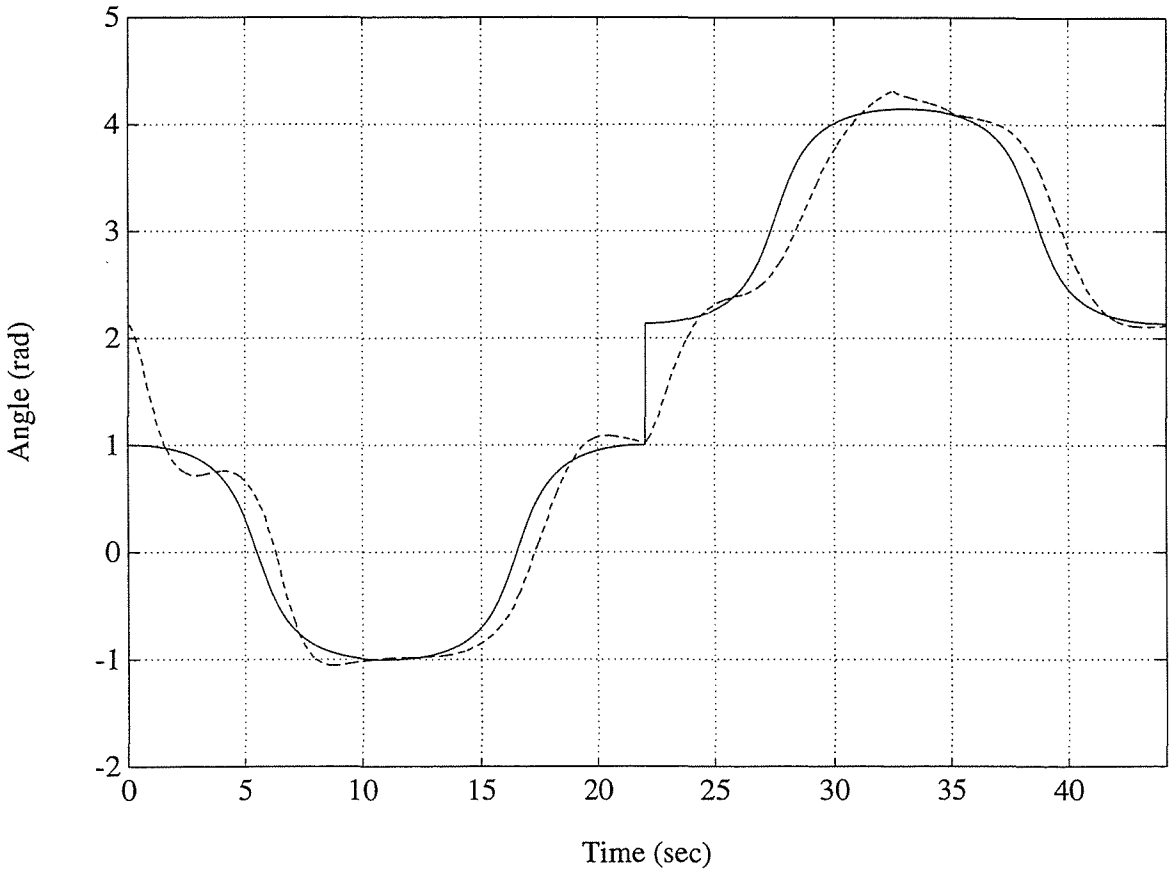

Figure 5-9 (b). Trajectory(θ rotation) tracking of the TMR: solid line - reference angular position, dashed line - real TMR tracking, K=[10 0; 0 10].

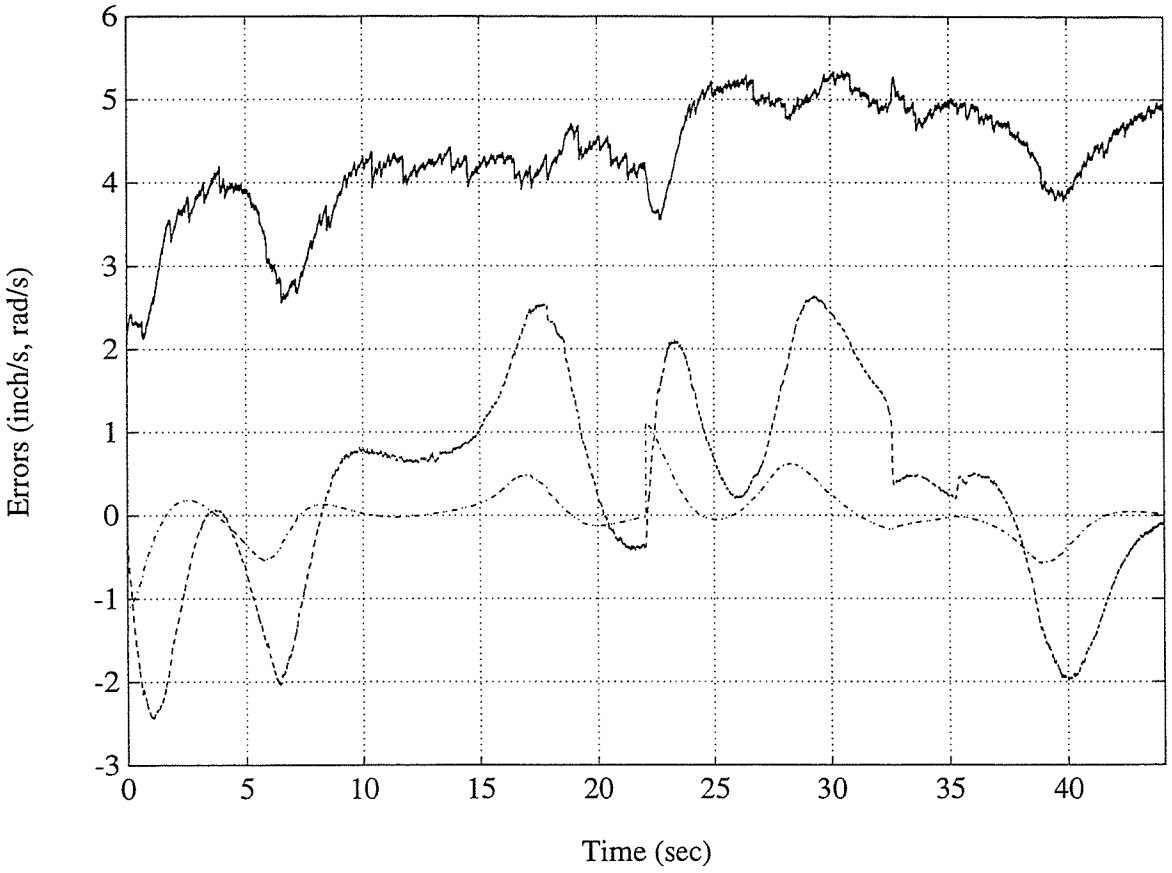

Figure 5-9 (c). Error posture when tracking the path shown in the Figure (a): solid line - x, dashed line - y, dashdot line - θ, K=[10 0; 0 10].

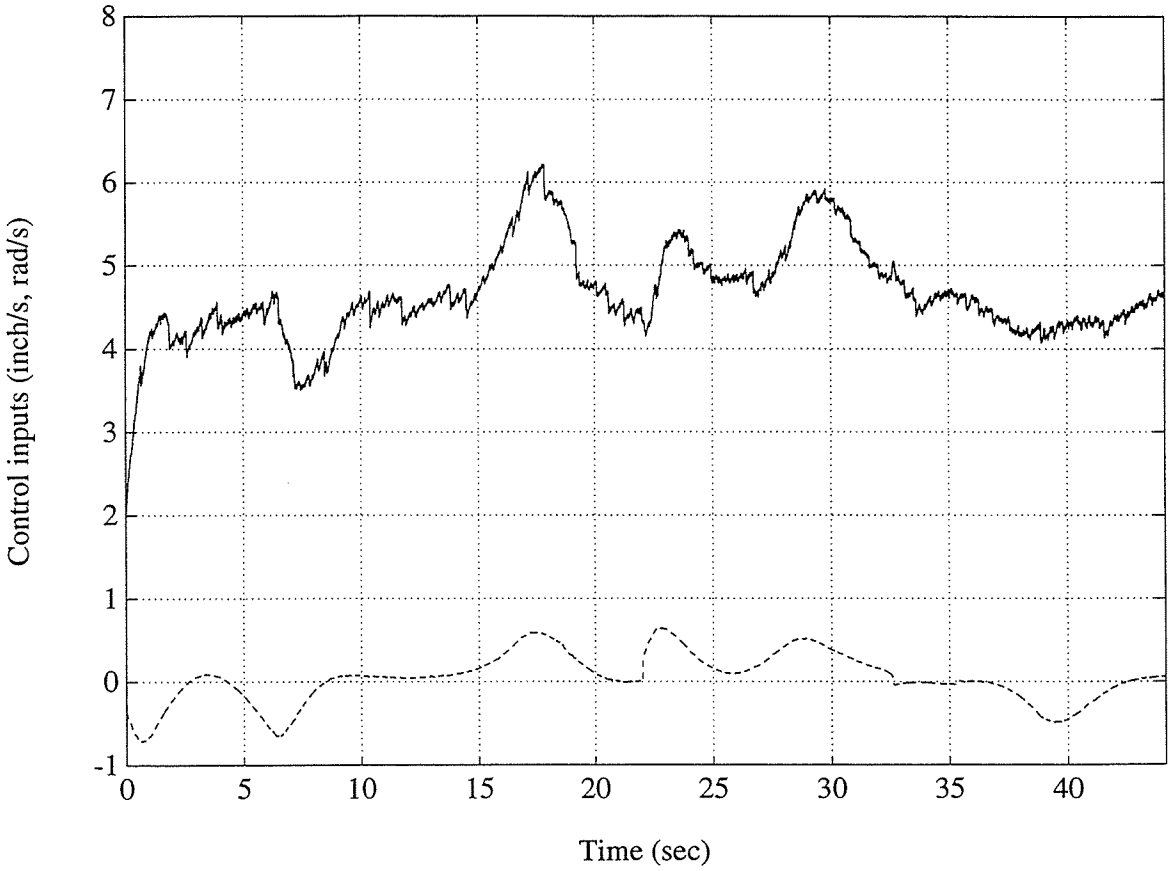

Figure 5-9 (d). Control commands when tracking the path shown in the Figure (a): solid line - linear speed, dashed line - angular speed, K=[10 0; 0 10].

***Figure 5-9**. An experimental result: K=[10 0; 0 10].*

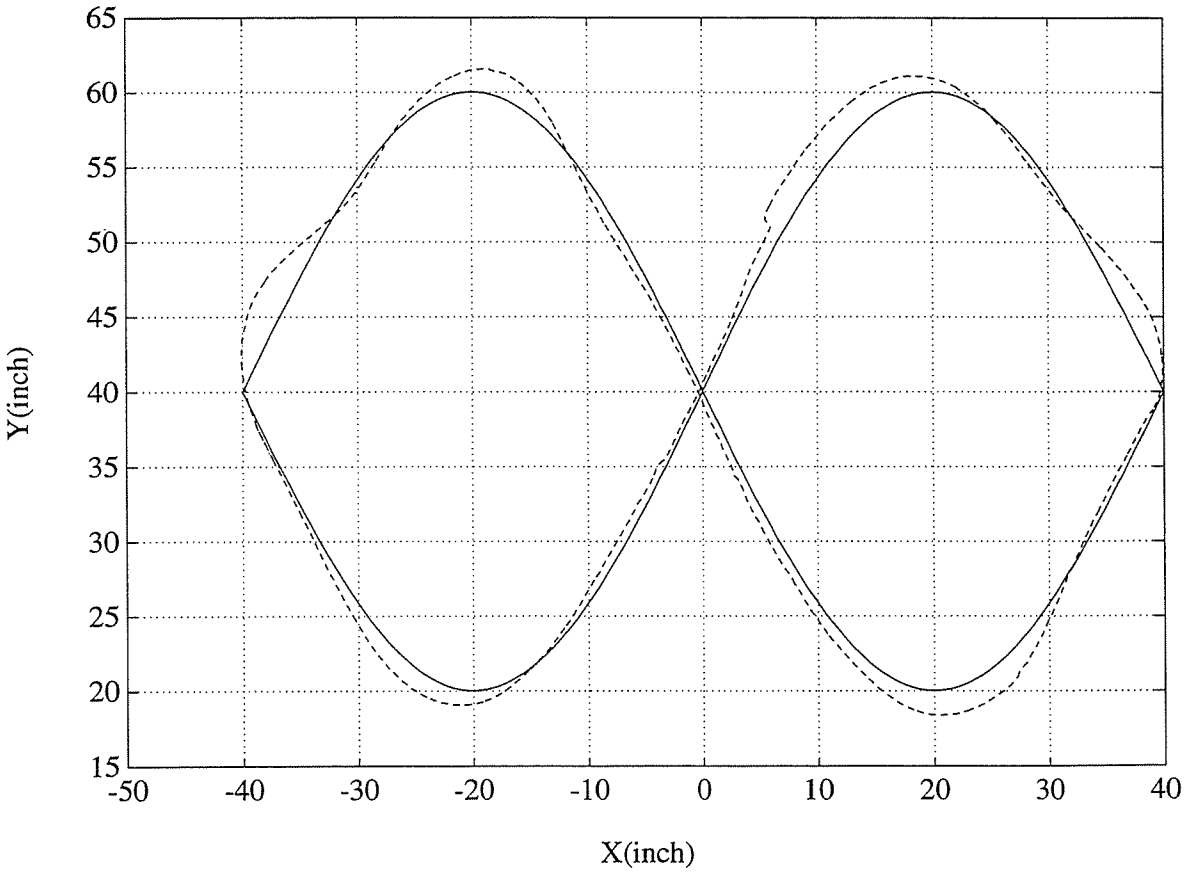

Figure 5-10 (a). Trajectory(x, y position) tracking of the TMR: solid line - reference path, dashed line - real TMR path tracking, [20 0; 0 10].

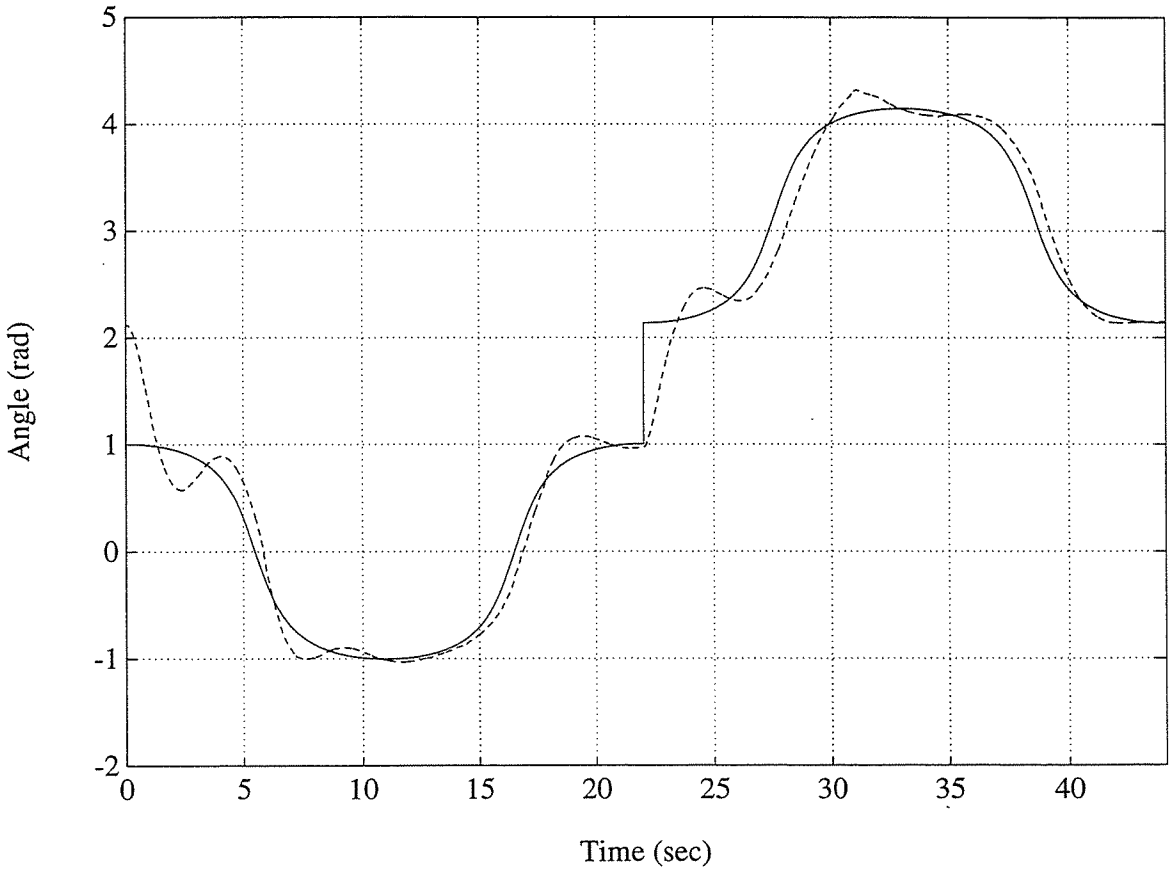

Figure 5-10 (b). Trajectory(θ rotation) tracking of the TMR: solid line - reference angular position, dashed line - real TMR tracking, [20 0; 0 10].

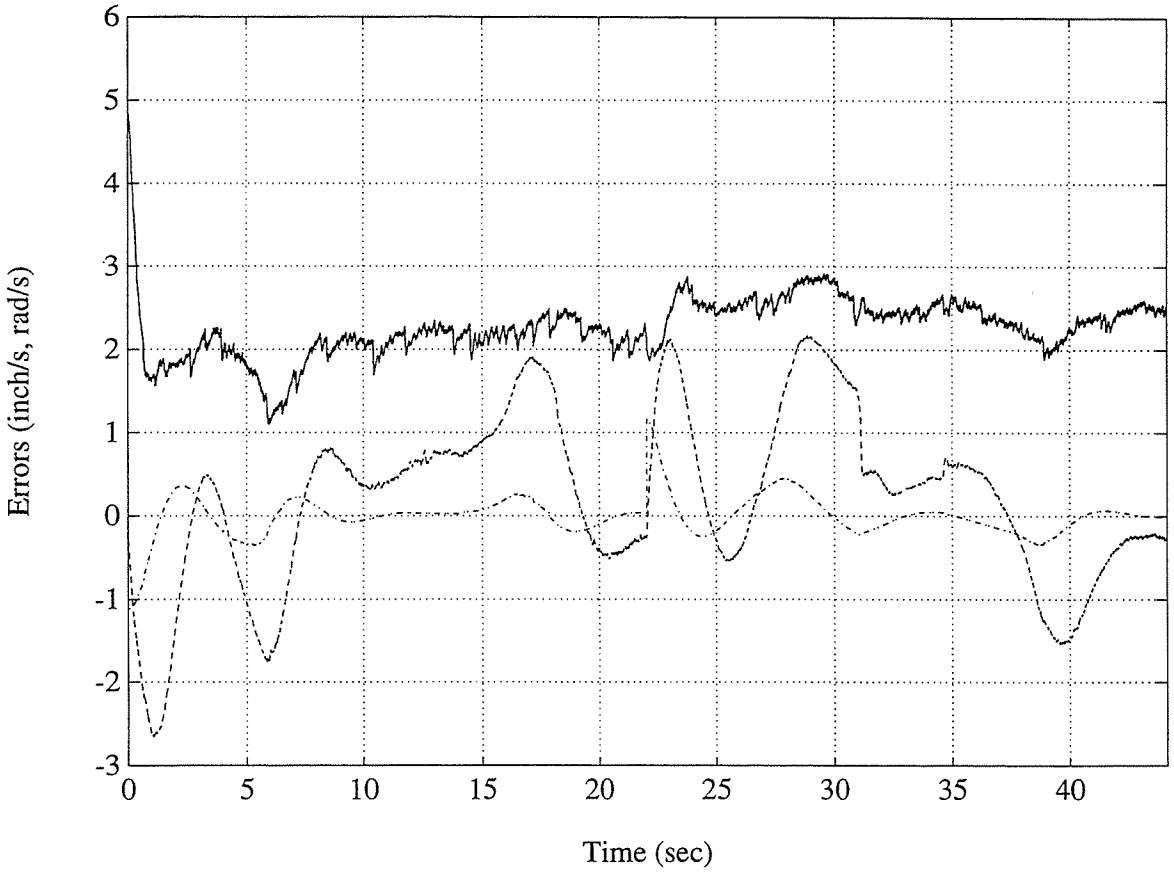

Figure 5-10 (c). Error posture when tracking the path shown in the Figure (a): solid line - x, dashed line - y, dashdot line - θ, [20 0; 0 10].

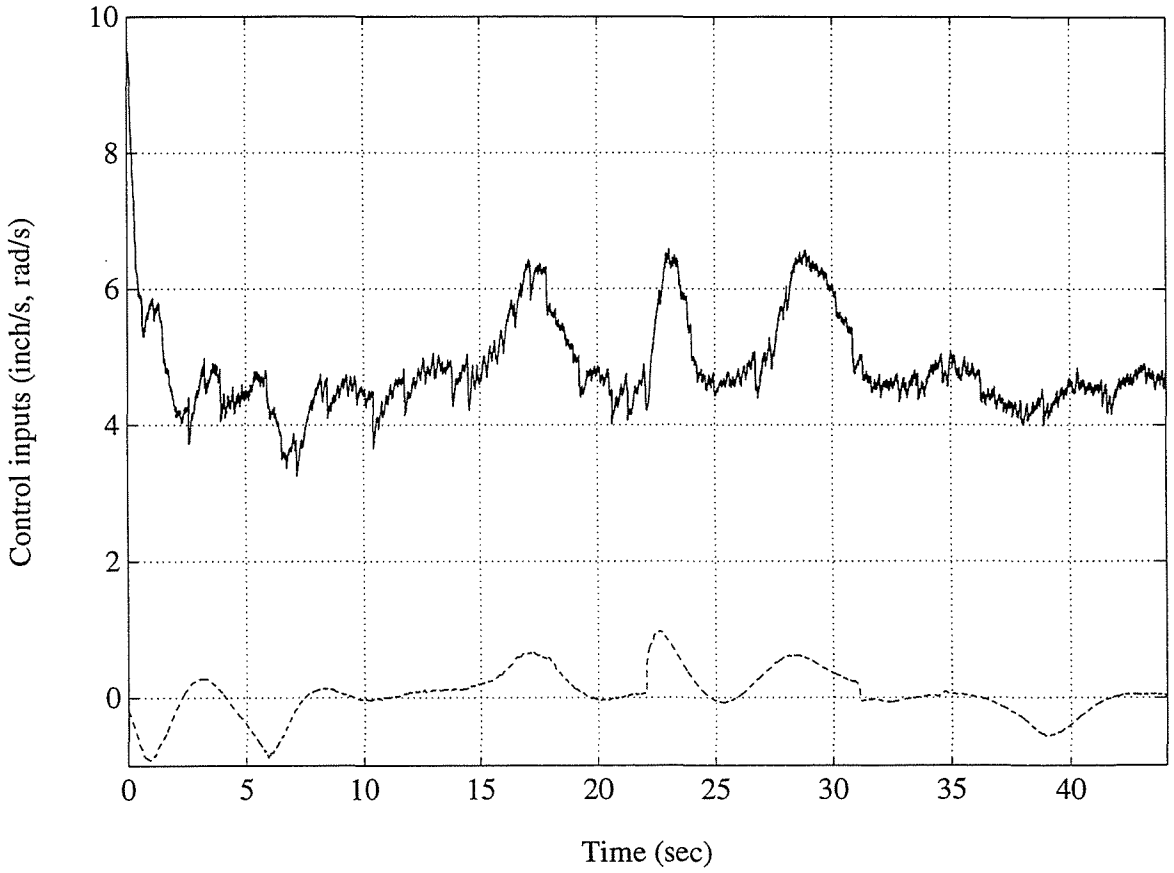

Figure 5-10 (d). Control commands when tracking the path shown in the Figure (a): solid line - linear speed, dashed line - angular speed, [20 0; 0 10].

Figure 5-10. *An experimental result: K=[20 0; 0 10].*

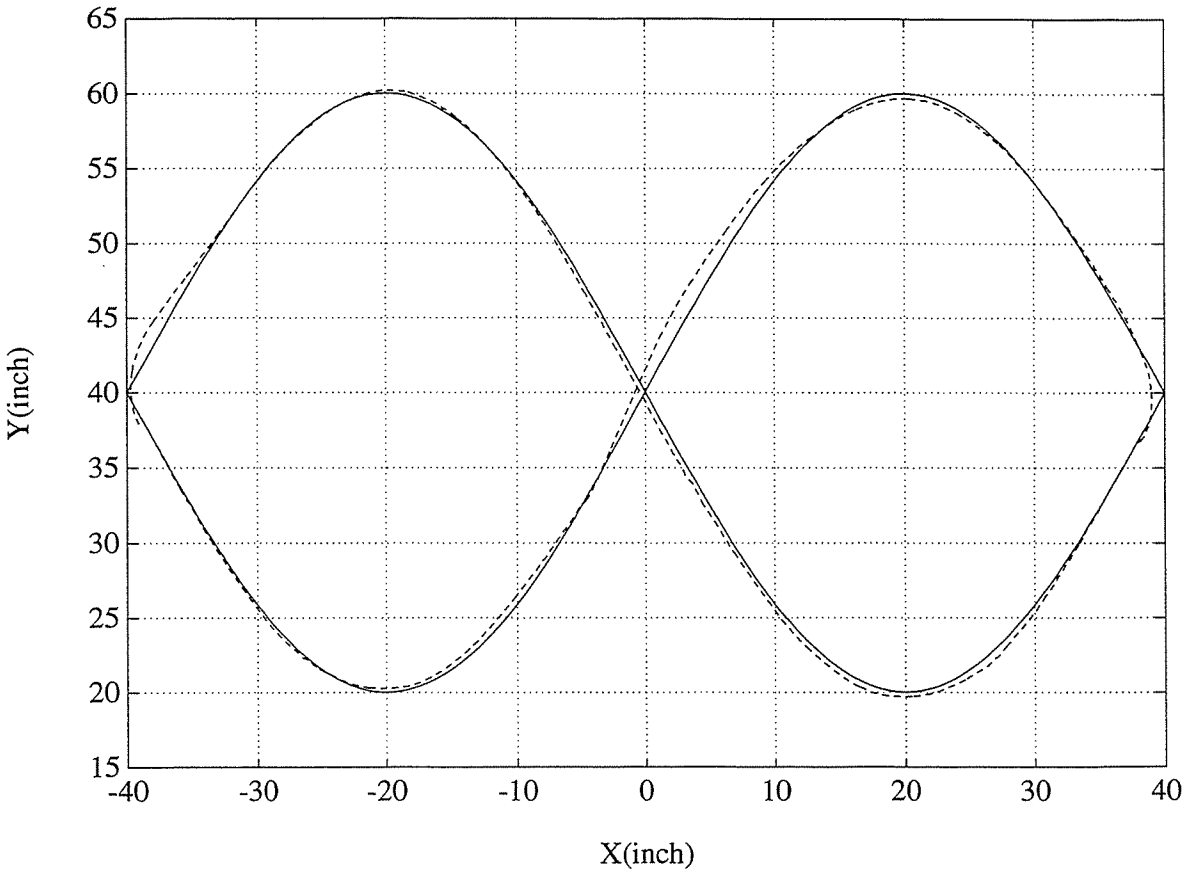

Figure 5-11 (a). Trajectory(x, y position) tracking of the TMR: solid line - reference path, dashed line - real TMR path tracking, K=[10 0; 0 20].

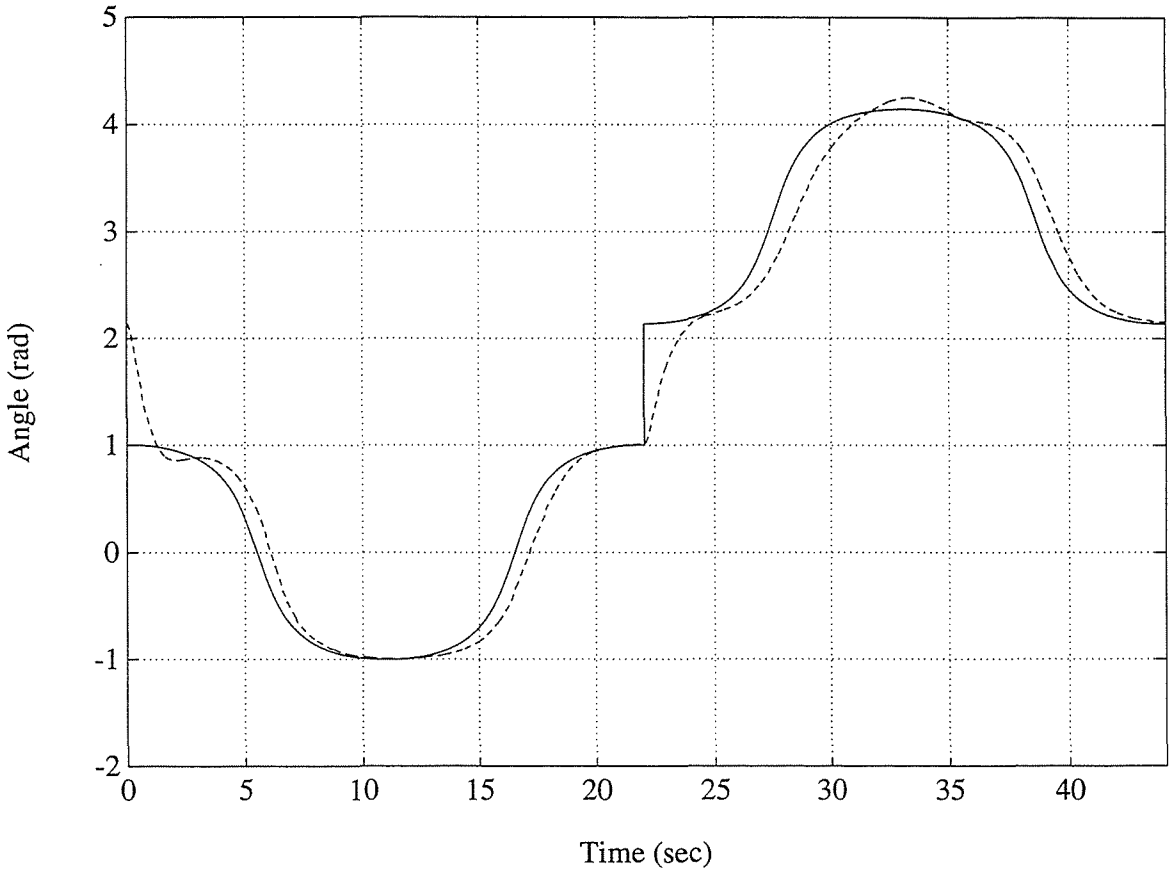

Figure 5-11 (b). Trajectory(θ rotation) tracking of the TMR: solid line - reference angular position, dashed line - real TMR tracking, K=[10 0; 0 20].

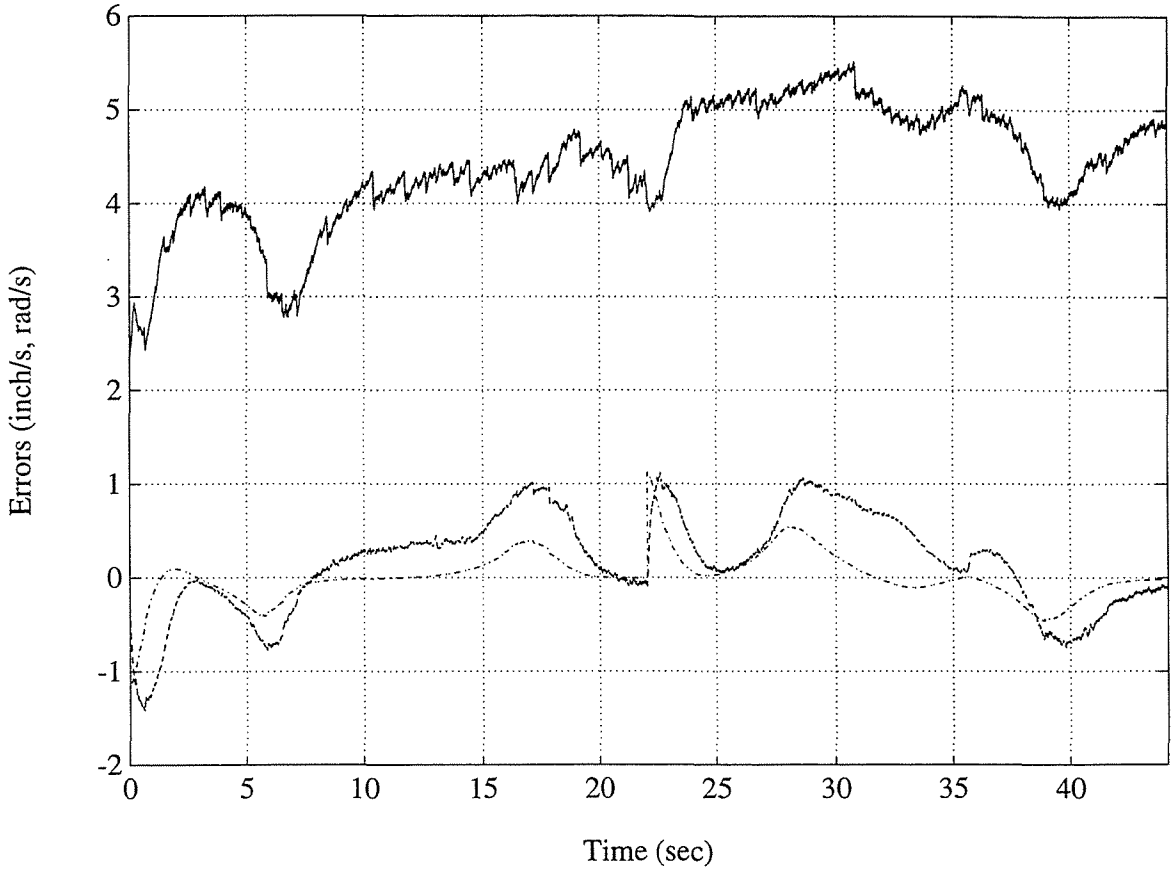

Figure 5-11 (c). Error posture when tracking the path shown in the Figure (a): solid line - x, dashed line - y, dashdot line - θ, K=[10 0; 0 20].

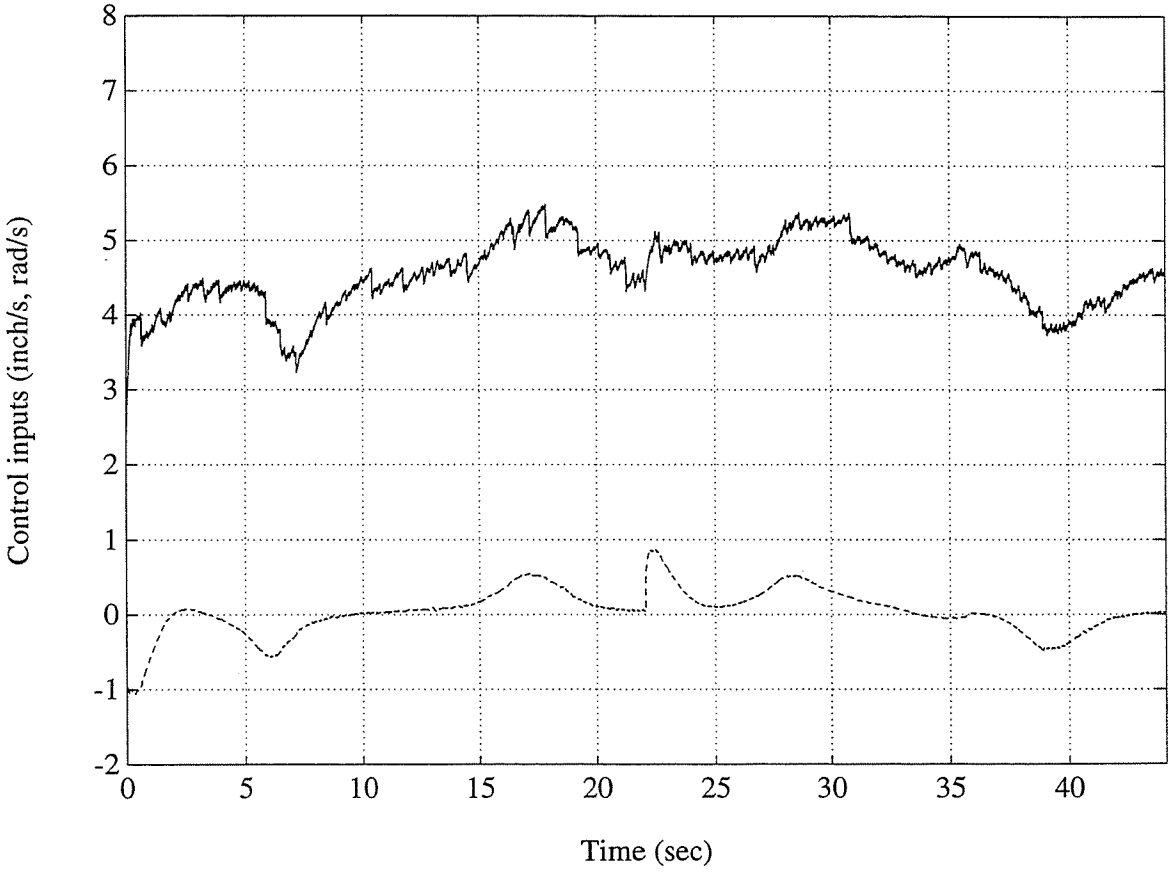

Figure 5-11 (d). Control commands when tracking the path shown in the Figure (a): solid line - linear speed, dashed line - angular speed, K=[10 0; 0 20].

***Figure 5-11**. An experimental result: K=[10 0; 0 20].*

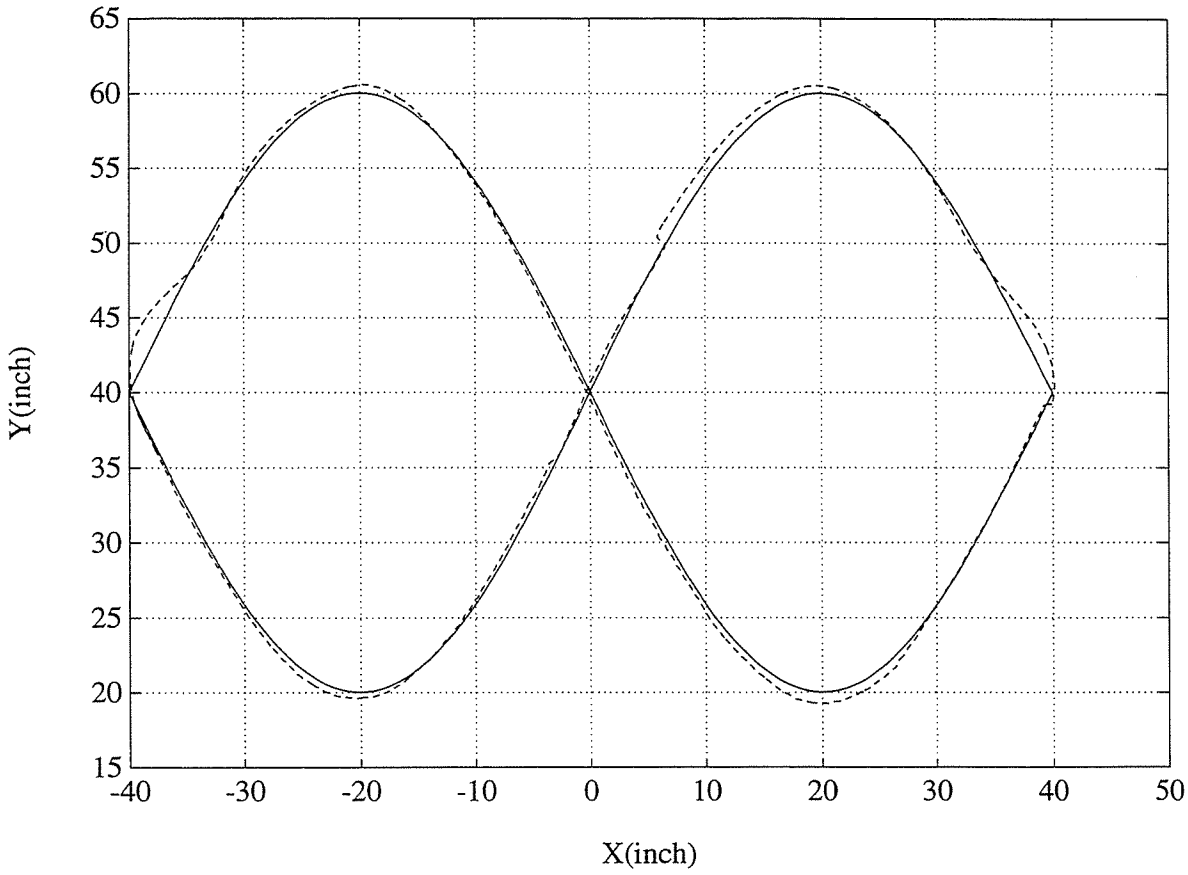

Figure 5-12 (a). Trajectory(x, y position) tracking of the TMR: solid line - reference path, dashed line - real TMR path tracking, K=[30 0; 0 20].

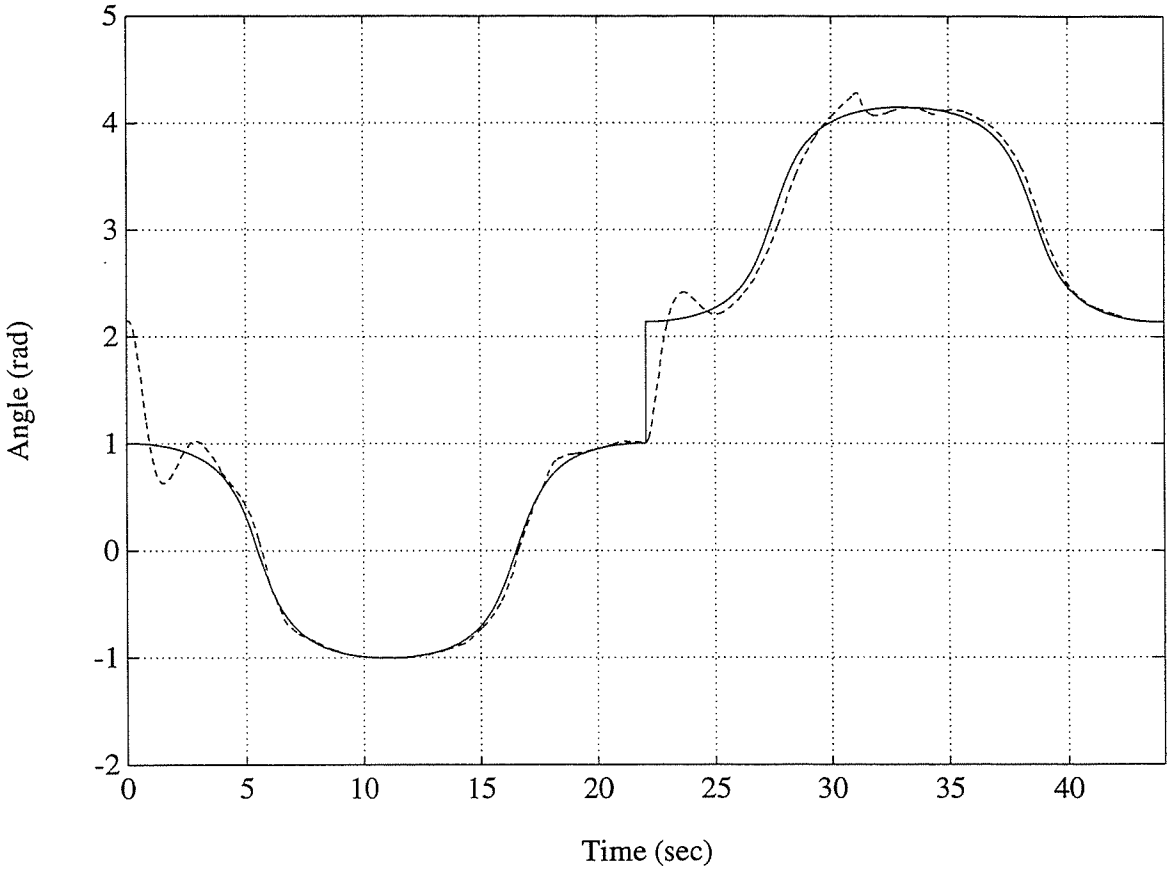

Figure 5-12 (b). Trajectory(θ rotation) tracking of the TMR: solid line - reference angular position, dashed line - real TMR tracking, K=[30 0; 0 20].

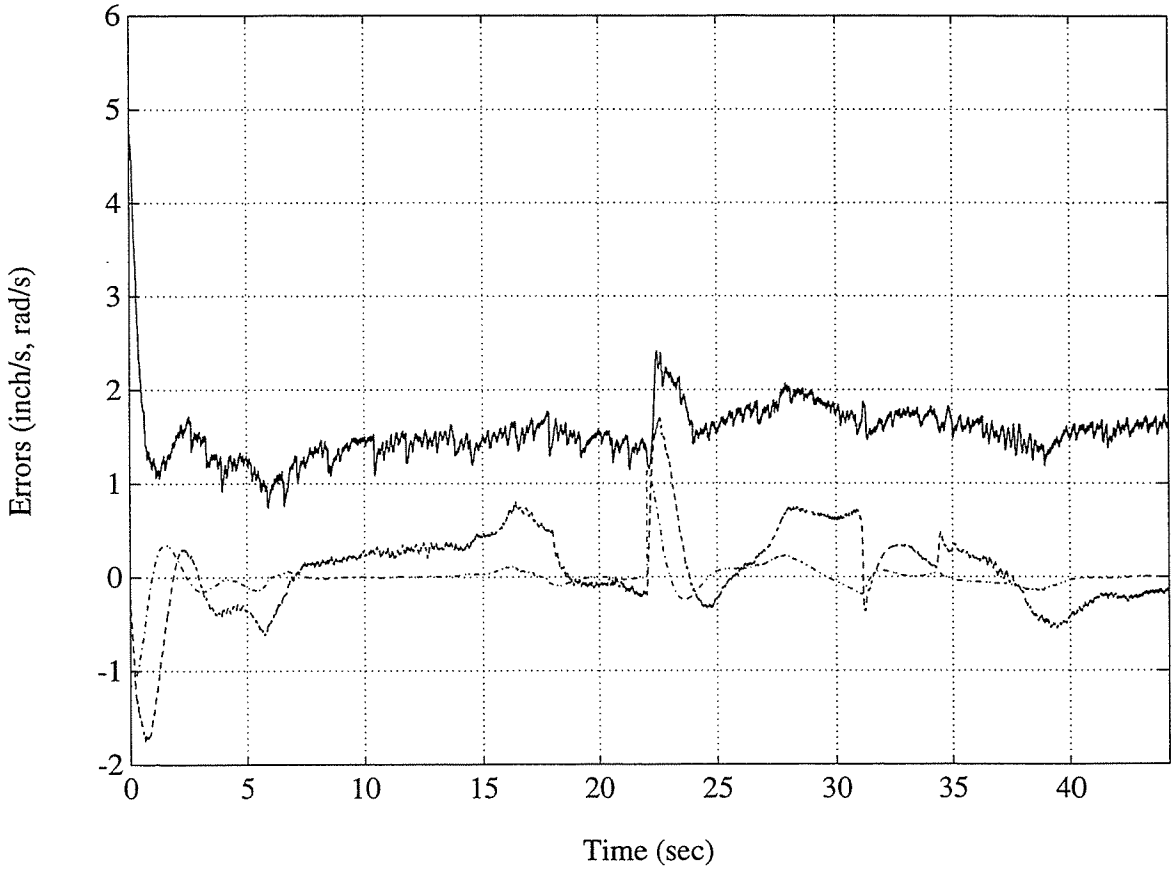

Figure 5-12 (c). Error posture when tracking the path shown in the Figure (a): solid line - x, dashed line - y, dashdot line - θ, K=[30 0; 0 20].

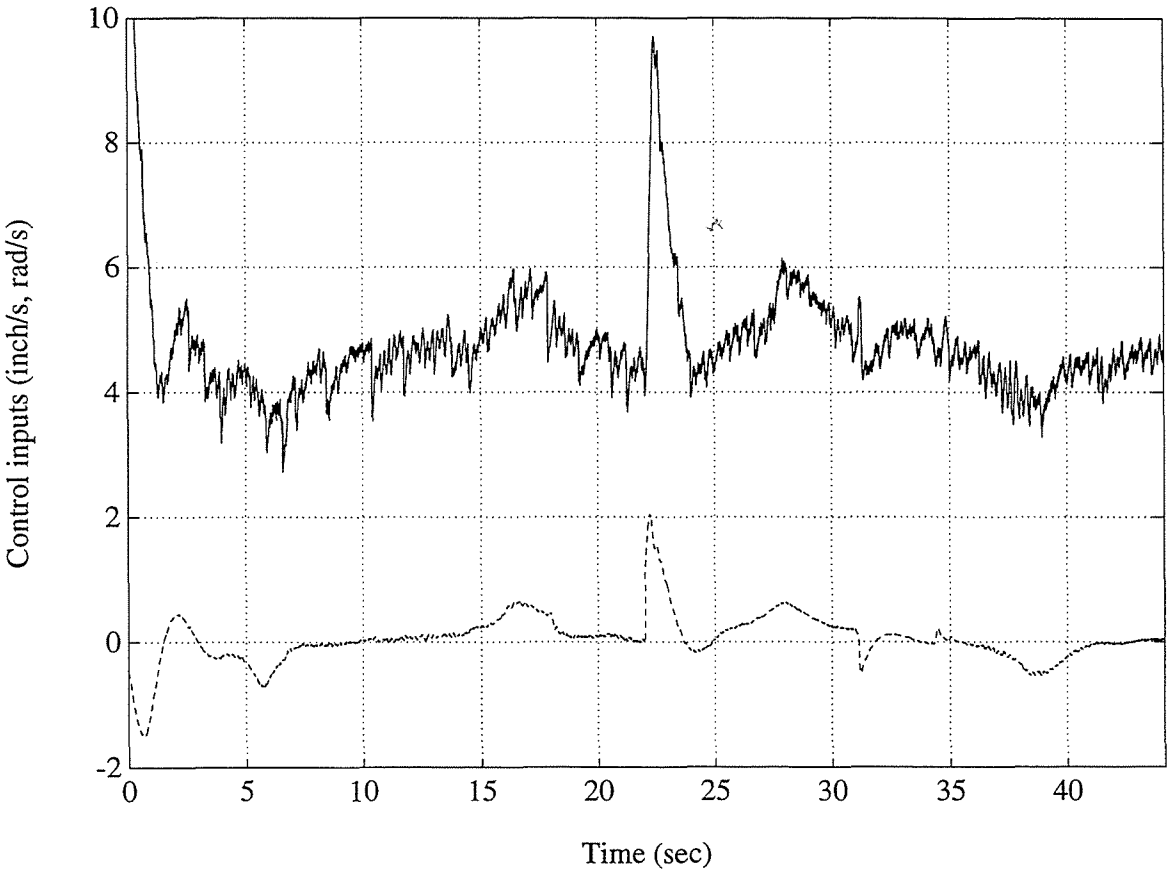

Figure 5-12 (d). Control commands when tracking the path shown in the Figure (a): solid line - linear speed, dashed line - angular speed, K=[30 0; 0 20].

Figure 5-12. *An experimental result with reference path table: K=[30 0; 0 20].*

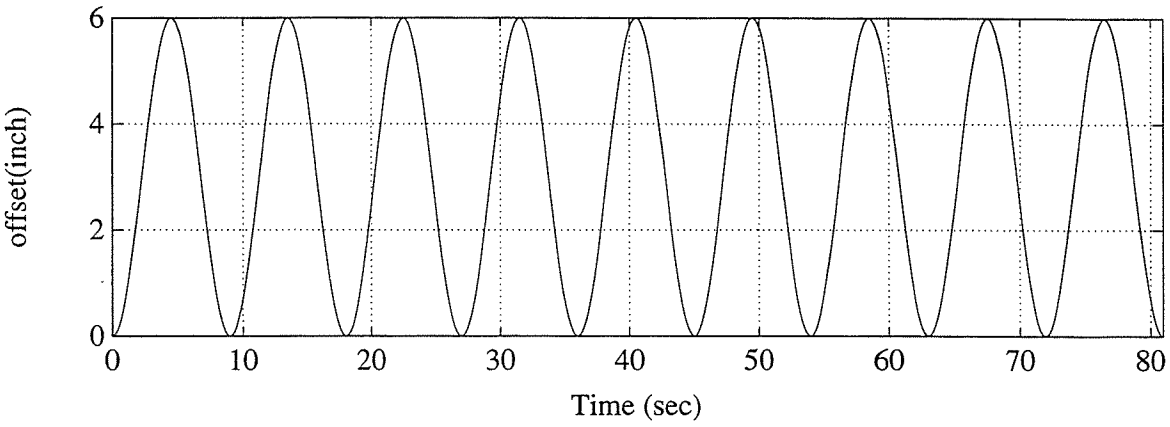

Figure 5-13 (a). Trajectory(x, y position) tracking of the TMR with offset table. Offset table used for the tests.

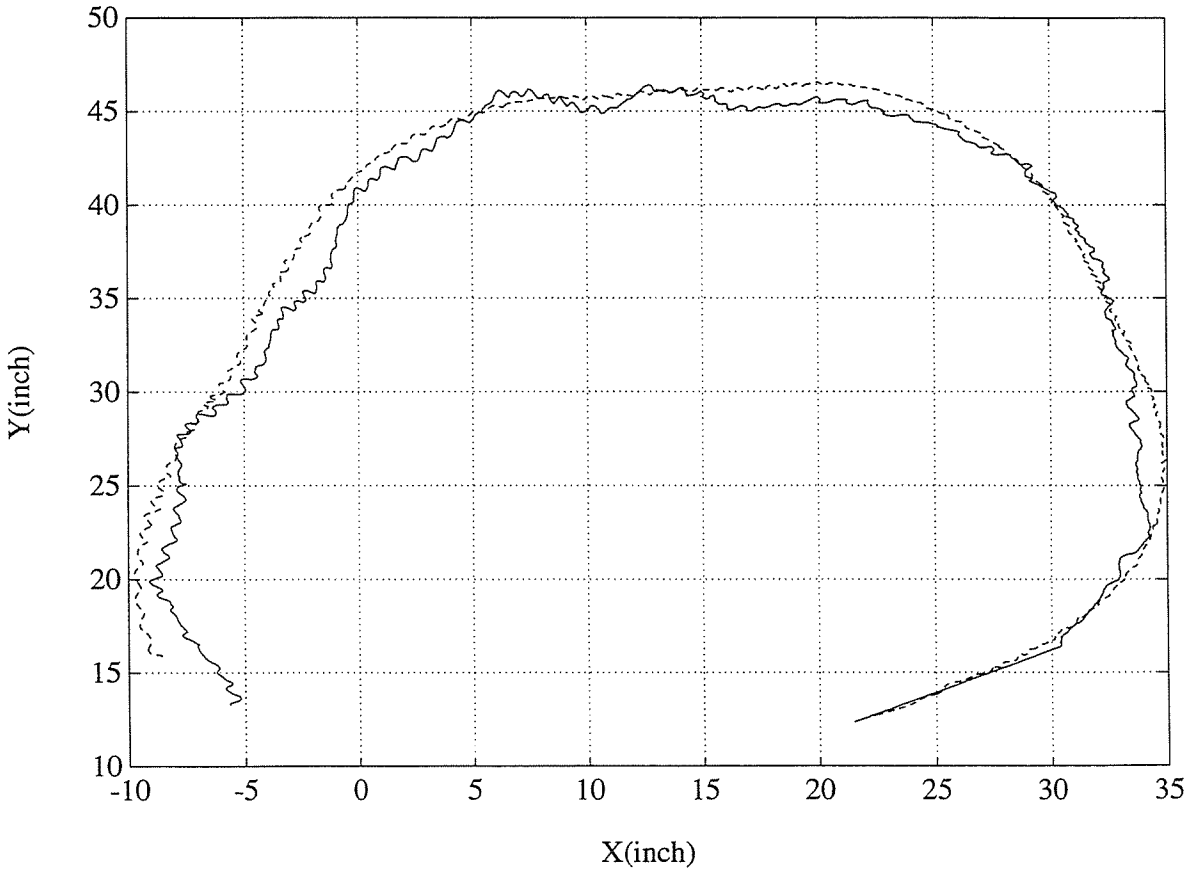

Figure 5-13 (b). Trajectory(x, y position) tracking of the TMR with offset table: solid line - reference path, dashed line - real TMR path tracking, u_D=4.0 in/sec, K=[10 0; 0 10].

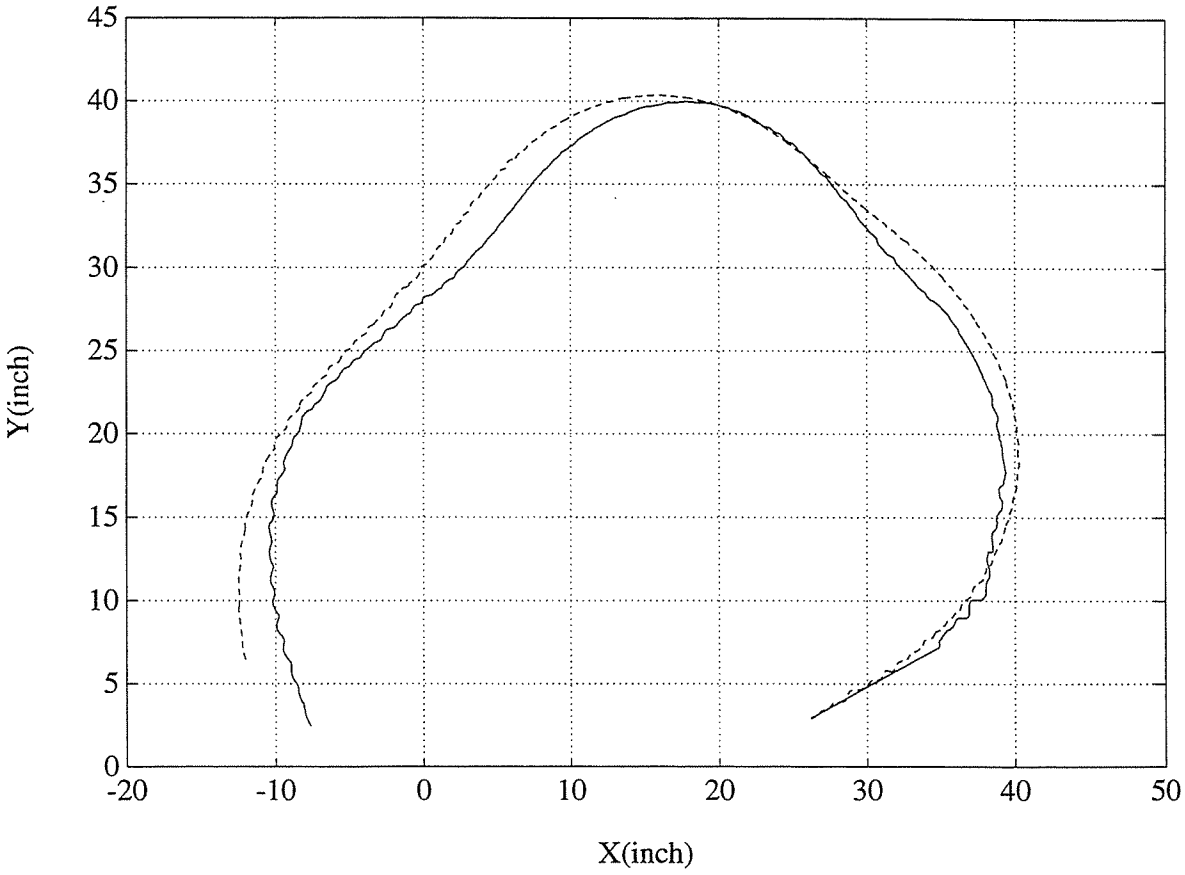

Figure 5-13 (c). Trajectory(x, y position) tracking of the TMR with offset table: solid line - reference path, dashed line - real TMR path tracking, u_D=8.0 in/sec, K=[10 0; 0 10].

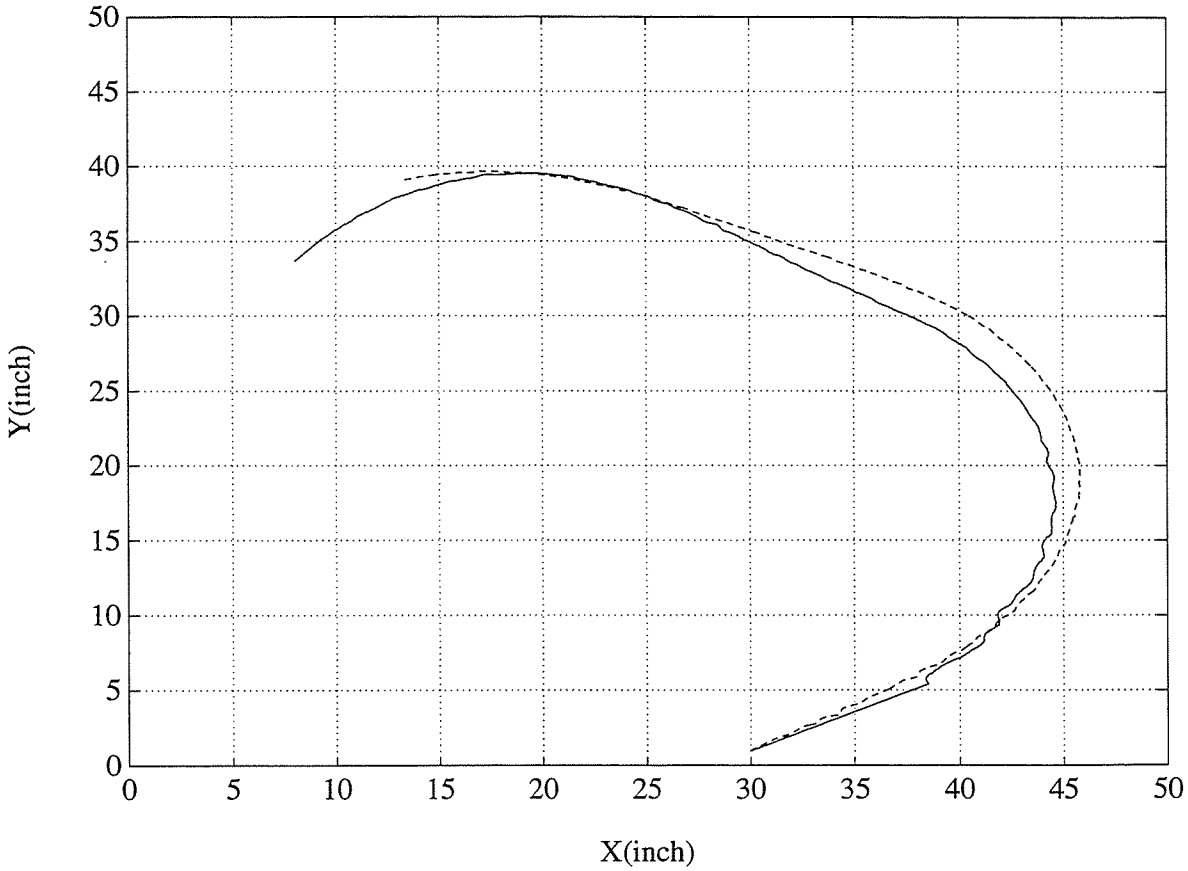

Figure 5-13 (d). Trajectory(x, y position) tracking of the TMR with offset table: solid line - reference path, dashed line - real TMR path tracking, u_D=12.0 in/sec, K=[10 0; 0 10].

***Figure 5-13**. Trajectory(x, y position) tracking of the TMR with offset table: solid line - reference path, dashed line - real TMR path tracking.*

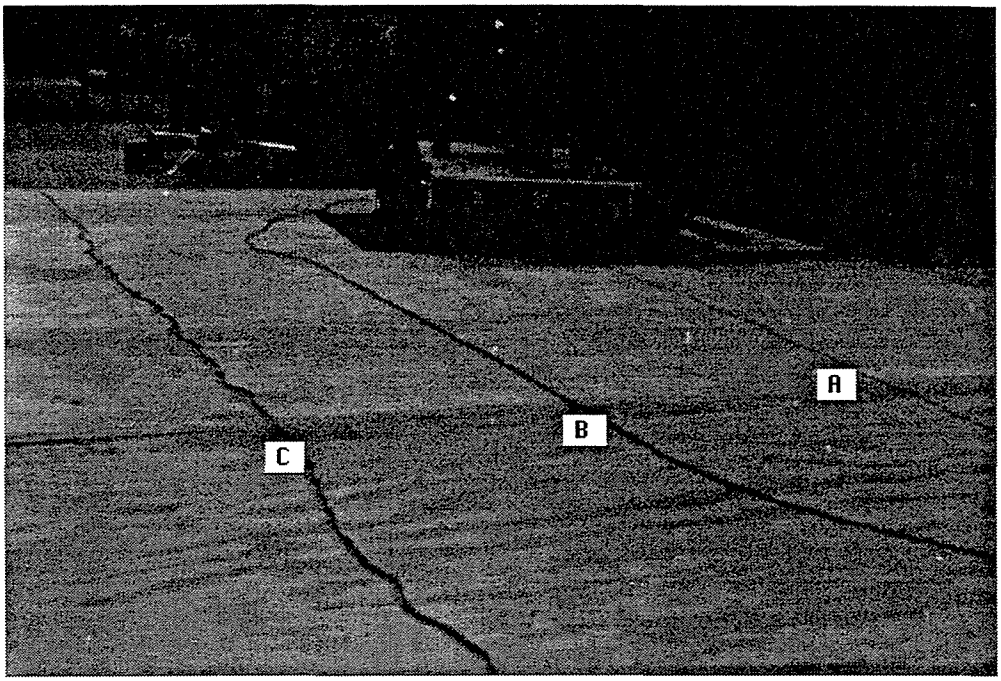

Figure 5-14. *Cracks on plywood used for laser tracking control experiment.*

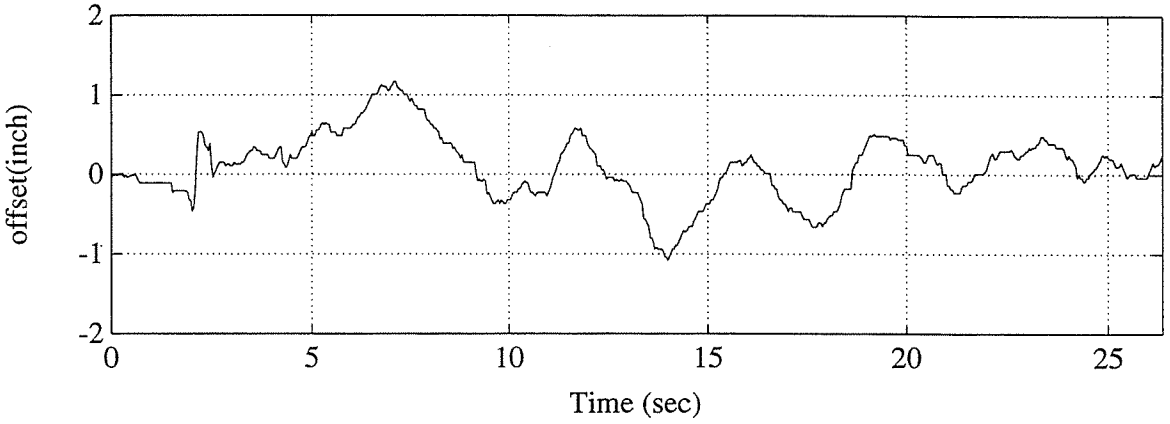

(a). Offset from the laser sensor along the crack A in the Figure 5-14.

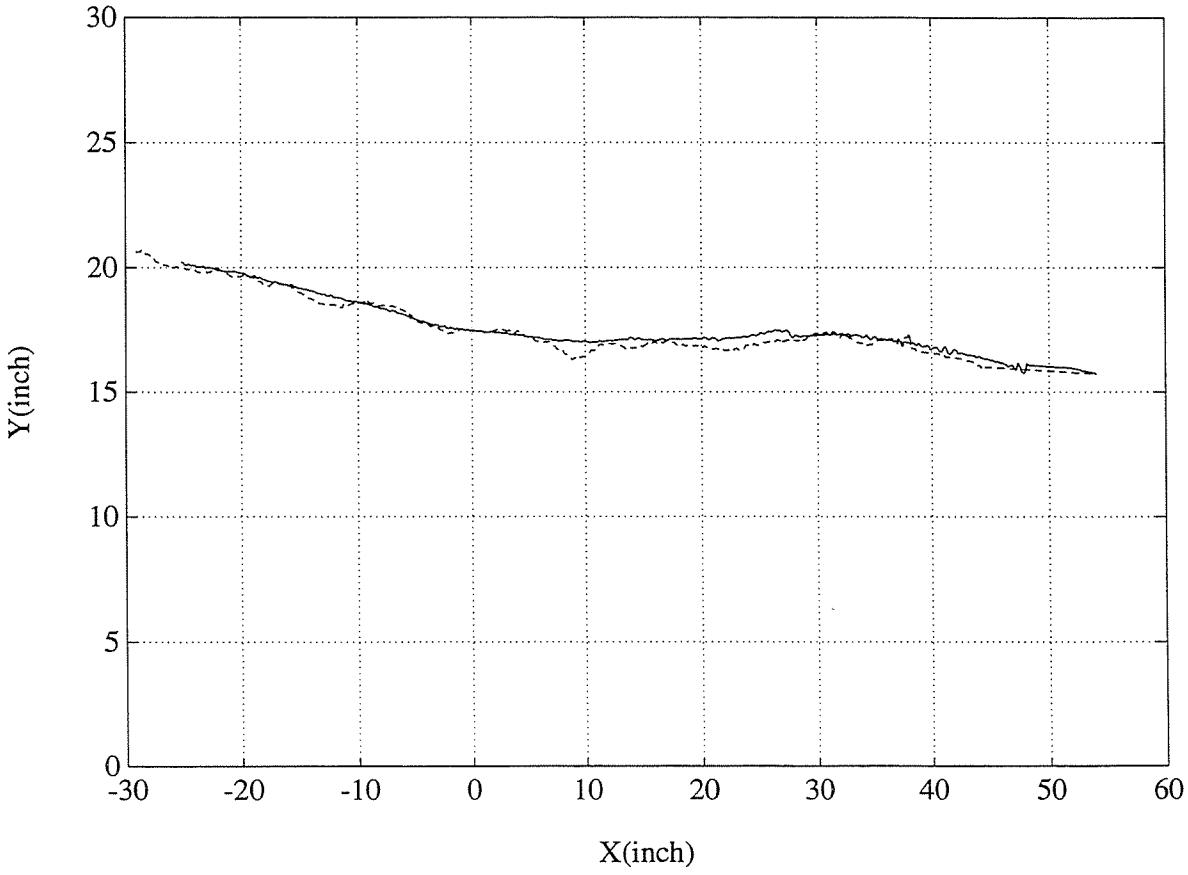

(b). Trajectory, solid - actual TMR trajectory, dashed - crack path detected by laser sensor.

***Figure 5-15**. A trajectory tracking test example with laser range sensor, crack A in the Figure 5-14.*

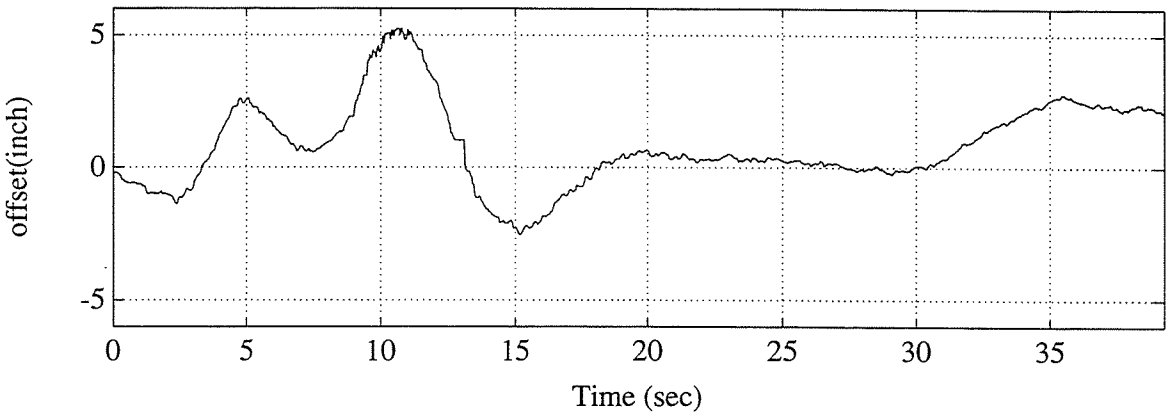

(a). Offset from the laser sensor along the crack B in the Figure 5-14.

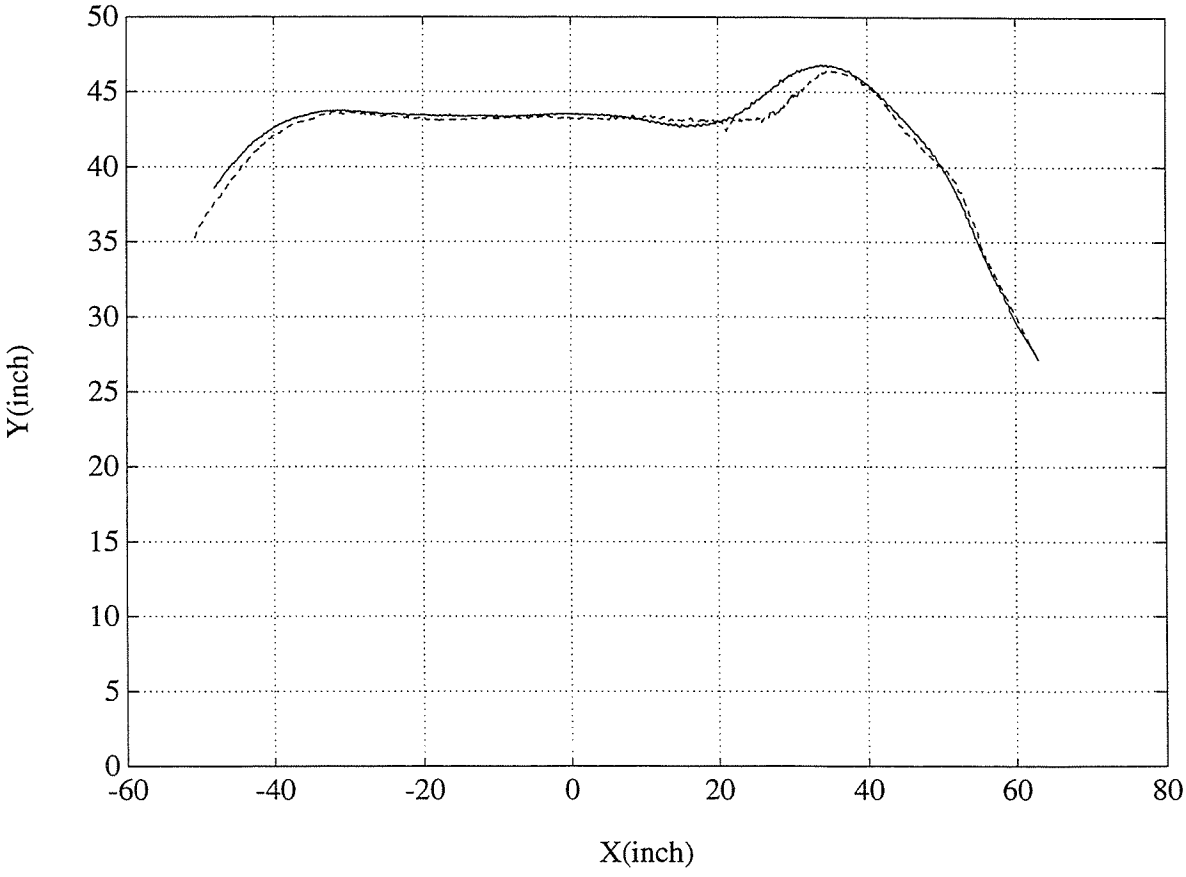

(b). Trajectory, solid - actual TMR trajectory, dashed - crack path detected by laser sensor.

***Figure 5-16**. A trajectory tracking test example with laser range sensor, crack B in the Figure 5-14.*

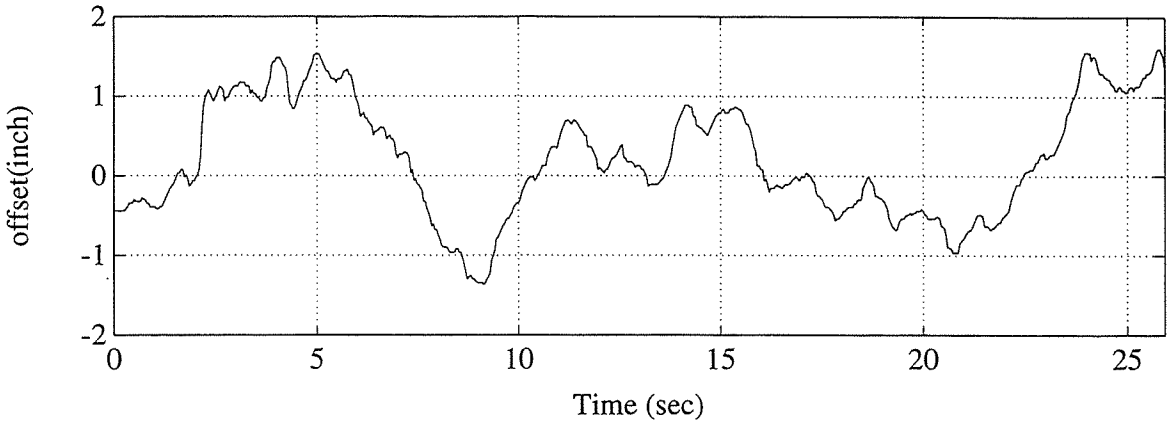

(a). Offset from the laser sensor along the crack C in the Figure 5-14.

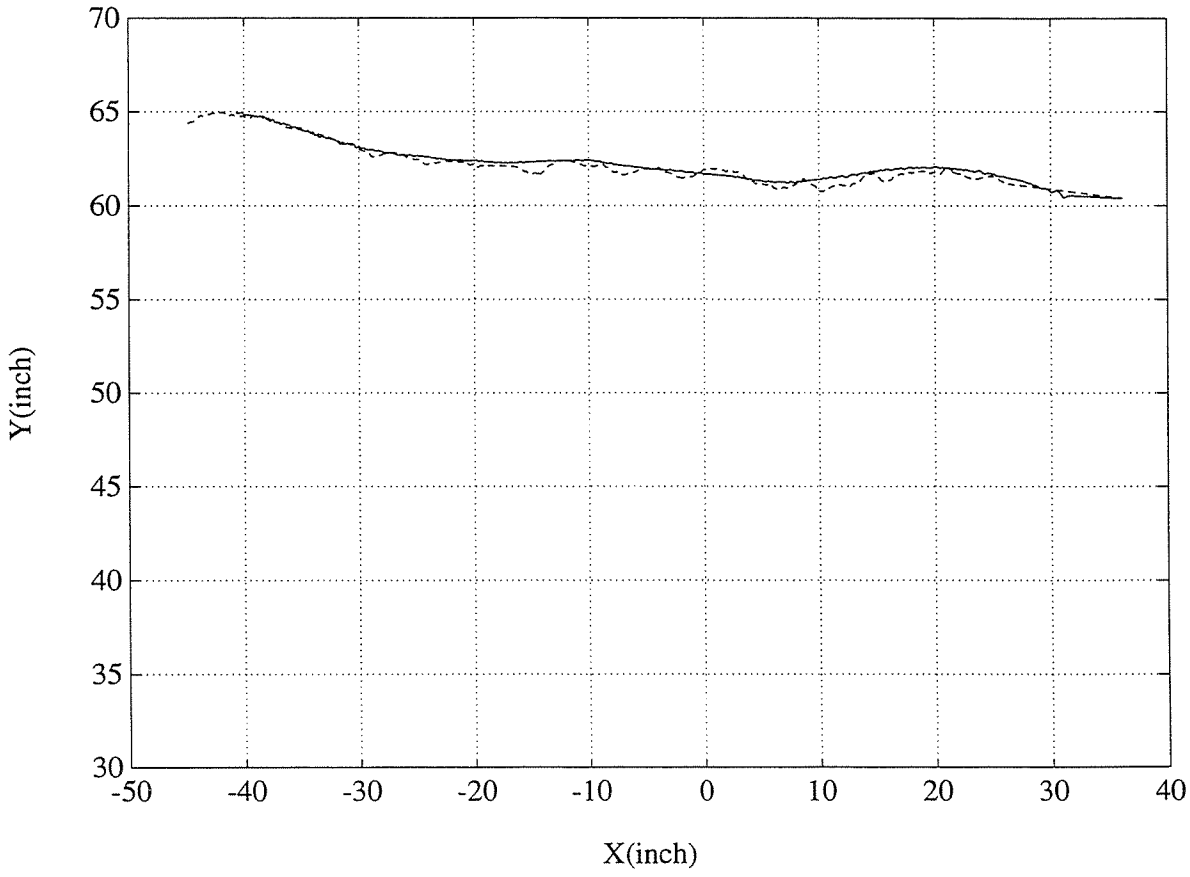

(b). Trajectory, solid - actual TMR trajectory, dashed - crack path detected by laser sensor.

Figure 5-17. *A trajectory tracking test example with laser range sensor, crack C in the Figure 5-14.*

Chapter 6. Robust TMR Velocity Control

The biggest concerns when controlling the TMR are its inertia effect as shown in the Automatic Trajectory Tracking Control in the Chapter 5 and the routing force (or friction force due to the sealant applicator during sealing process). The inertia effect is centrifugal force when following a curve, which is a non-linear form. And the routing force would be function of the linear velocity and the angular velocity of the TMR and also depend on cutting width and depth. We can measure the routing force through appropriate off-line experiment. This can be used to estimate the real routing force when controlling the TMR. But it is very hard to get precise prediction model for the routing force. Also, the routing force fluctuates in big range during real process. Acknowledging these facts, we can realize that the robustness issue of the control algorithm would be the biggest concern.

Many researches have been conducted about wheeled mobile robot control as cited in the Chapter 1. But there have not been any papers concerning the sliding mode control issue for a wheeled mobile robot. In the TMR control, the biggest concerns are the non-linear terms due to centrifugal forces and the routing force that is very hard to estimate. But we can figure out the upper and lower bounds of the fluctuating routing force using an appropriate experimental method. Therefore, the robust control using the sliding mode technique is very appropriate to the TMR control problem. In this research, the sliding mode control for a wheeled mobile robot was formulated and this is a unique control strategy for the TMR and a general wheeled mobile robot.

The sliding mode control promises the robustness of the control system when we can estimate the bound of parametric uncertainty and unmodeled dynamics. This control methodology can be a great tool for the Wheeled Mobile Robot that should maintain big fluctuating external forces like the TMR for highway maintenance operation. In this chapter, the sliding mode control algorithm for the TMR is formulated. This control algorithm can be applied for a normal WMR.

The dynamic mode of the TMR is presented in Section 1. Basic theory of the robust sliding control algorithm will be presented in Section 2 and the sliding control is formulated for the TMR tracking control in the following section. The TMR platform shown in the Chapter 3 is used to derive a dynamic model for control algorithm development. The simulation is also performed with the parameters of the real TMR platform and shown in Section 4.

6-1. Dynamics of the TMR

The Figure 6-1 shows the TMR platform and external forces exerted on its x-y plane. There are some external forces that would be applied to the TMR, such as the forces and the moment due to the linkage, the forces due to the router or the applicator unit, and the friction forces due to the front wheel castors. But the friction forces due to the front wheel castors are very small compare to others, so that we can ignore them when we derive the dynamic equations. And we assume no slip condition again like the kinematic modeling. In the Figure 6-1, the forces P_x, P_y and the moment M_P on the point P represent the resultant forces and moment due to the router and the sealant applicator forces and the linkage forces, based on the assumption that all forces are exerted on the center line, that is x-axis, of the TMR. This assumption is valid since all units are aligned on the center line.

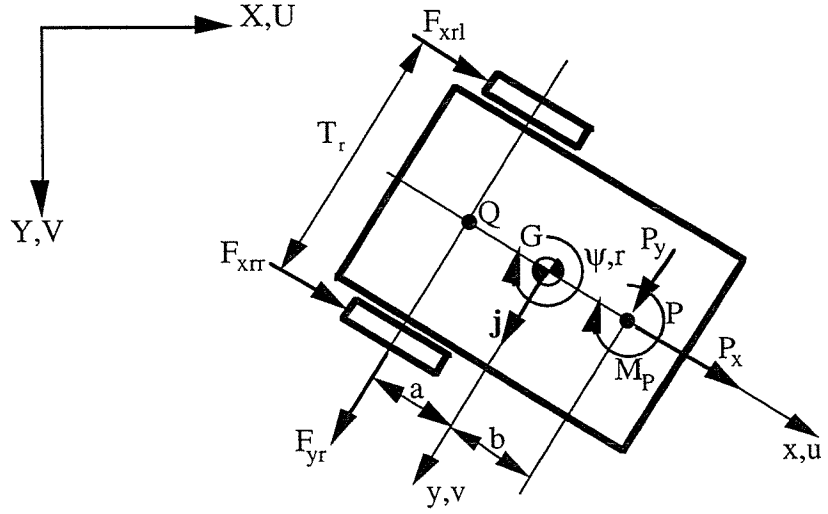

Figure 6-1. *The TMR platform and external forces exerted on its x-y plane.*

Taking force equilibrium and moment equilibrium at the center of gravity, G, we can get the following equations:

$$\begin{aligned} m(\dot{u} - rv) &= F_{xrl} + F_{xrr} + P_x \\ m(\dot{v} + ru) &= F_{yr} + P_y \\ I_{Gz}\dot{r} &= \frac{T_r}{2}(F_{xrl} - F_{xrr}) - F_{yr}a + bP_y + M_P. \end{aligned} \tag{6-1}$$

Recall that we assume no slip condition, such that $v = ar$, then the equation (6-1) becomes

$$\begin{aligned} m\dot{u} &= mar^2 + P_x + (F_{xrl} + F_{xrr}) \\ I_{ze}\dot{r} &= -maru + (a+b)P_y + M_P + \frac{T_r}{2}(F_{xrl} - F_{xrr}) \end{aligned} \tag{6-2}$$

where $I_{ze} = I_{Gz} + ma^2$, equivalent second moment of inertia.

The forces F_{xrl}, F_{xrr} exerted on the rear wheels can be replaced with the motor torques. A n to 1 speed reducer is inserted between the wheel and the driving motor in order to decrease the motor speed n to 1 and to increase the motor torque 1 to n (assuming no frictional loss in the reducer). The Figure 6-2 shows the wheel assembly including the speed reducer and the driving motor.

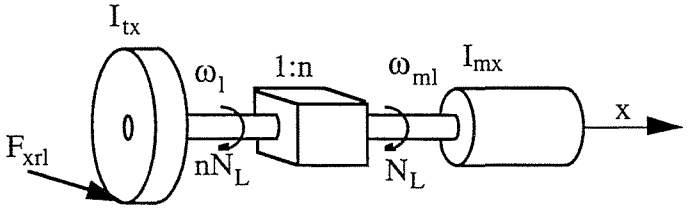

Figure 6-2. *The motor, speed reducer, and wheel assembly (left wheel).*

The motor speed is n times larger than the wheel speed,

$$\omega_{ml} = n\omega_l. \tag{6-3}$$

The motor torque is represented as

$$\tau_l = I_{mx}\dot{\omega}_{ml} + N_L \tag{6-4}$$

where N_L is a torque exerted on the motor axis. The torque becomes n times larger than N_L after the speed reducer.

$$nN_L = I_{tx}\dot{\omega}_l + F_{xrl}R_t. \tag{6-5}$$

Plugging (6-3) and (6-4) into (6-5), we can get

$$n\tau_l = (n^2 I_{mx} + I_{tx})\dot{\omega}_l + F_{xrl}R_t. \tag{6-6}$$

Similarly for the right wheel,

$$n\tau_r = (n^2 I_{mx} + I_{tx})\dot{\omega}_r + F_{xrr}R_t. \tag{6-7}$$

Rearranging the equations (6-6), (6-7) in terms of the forces exerted on the rear wheels,

$$F_{xrl} = \frac{n\tau_l}{R_t} - \frac{I_e}{R_t}\dot{\omega}_l, \quad F_{xrr} = \frac{n\tau_r}{R_t} - \frac{I_e}{R_t}\dot{\omega}_r \tag{6-8}$$

where $I_e = n^2 I_{mx} + I_{tx}$.

From the no slip condition, the wheel angular velocity can be expressed with the linear velocity and the angular velocity of the TMR platform like

$$\begin{aligned} u &= \frac{R_t}{2}(\omega_l + \omega_r) \\ r &= \frac{R_t}{T_r}(\omega_l - \omega_r) \end{aligned} \quad \text{or} \quad \begin{aligned} \omega_l &= \frac{1}{R_t}\left(u + \frac{T_r}{2}r\right) \\ \omega_r &= \frac{1}{R_t}\left(u - \frac{T_r}{2}r\right). \end{aligned} \tag{6-9}$$

Therefore, the equation (6-8) becomes the following (6-10) in terms of the linear velocity and the angular velocity of the TMR platform.

$$F_{xrl} = \frac{n\tau_l}{R_t} - \frac{I_e}{R_t^2}\left(\dot{u} + \frac{T_r}{2}\dot{r}\right) \tag{6-10-a}$$

$$F_{xrr} = \frac{n\tau_r}{R_t} - \frac{I_e}{R_t^2}\left(\dot{u} - \frac{T_r}{2}\dot{r}\right) \tag{6-10-b}$$

With the equation (6-10-a,b), the original equations of motion (6-2) become

$$\left(m + \frac{2I_e}{R_t^2}\right)\dot{u} = mar^2 + P_x + \frac{n}{R_t}\left(\tau_l + \tau_r\right), \tag{6-11-a}$$

$$\left(I_{Qz} + \frac{T_r^2 I_e}{2R_t^2}\right)\dot{r} = -maru + (a+b)P_y + M_P + \frac{nT_r}{2R_t}\left(\tau_l - \tau_r\right). \tag{6-11-b}$$

Rearranging these equations, we can get

$$\dot{u} = \frac{R_t^2}{mR_t^2 + 2I_e}\left(mar^2 + P_x\right) + \frac{nR_t}{mR_t^2 + 2I_e}\left(\tau_l + \tau_r\right), \tag{6-12-a}$$

$$\dot{r} = \frac{2R_t^2}{2R_t^2 I_{Qz} + T_r^2 I_e}\left\{-maru + (a+b)P_y + M_P\right\} + \frac{nT_r R_t}{2R_t^2 I_{Qz} + T_r^2 I_e}\left(\tau_l - \tau_r\right). \tag{6-12-b}$$

We can use matrix form for the above equation (6-12) for simplicity as

$$\dot{\boldsymbol{q}} = \boldsymbol{f}(\boldsymbol{q}) + \boldsymbol{B}\tau \tag{6-13}$$

where

$$\tau = \begin{bmatrix} \tau_l \\ \tau_r \end{bmatrix}, \tag{6-14-a}$$

$$\boldsymbol{q} = \begin{bmatrix} u \\ r \end{bmatrix}, \tag{6-14-b}$$

$$\dot{\boldsymbol{q}} = \begin{bmatrix} \dot{u} \\ \dot{r} \end{bmatrix}, \tag{6-14-c}$$

$$f(\boldsymbol{q}) = \begin{bmatrix} \dfrac{R_t^2}{mR_t^2 + 2I_e}\left(mar^2 + P_x\right) \\ \dfrac{2R_t^2}{2R_t^2 I_{Qz} + T_r^2 I_e}\left\{-maru + (a+b)P_y + M_P\right\} \end{bmatrix}, \qquad \text{(6-14-d)}$$

and

$$\boldsymbol{B} = \begin{bmatrix} \dfrac{nR_t}{mR_t^2 + 2I_e} & \dfrac{nR_t}{mR_t^2 + 2I_e} \\ \dfrac{nT_r R_t}{2R_t^2 I_{Qz} + T_r^2 I_e} & -\dfrac{nT_r R_t}{2R_t^2 I_{Qz} + T_r^2 I_e} \end{bmatrix}. \qquad \text{(6-14-e)}$$

6-2. Robust Control Using Sliding Mode Control

The sliding control for non-linear system was established by Slotine, 1983. This methodology has been applied to numerous research areas: Slotine (1985), Lin and Chin (1989), Cho, et al. (1993), Jo, et al. (1994). Recent trend of using the sliding control is combining it with other control methodologies such as adaptive control, fuzzy control, neural network, etc. (Su and Leung, 1993). The theory of sliding control was well described by Slotine and Li, 1991. In this section, basic sliding control theory is described based on Slotine and Li, 1991 and Yoerger and Slotine, 1983.

The sliding control guarantees a nonlinear feedback controller with good tracking precision for given nonlinear model, parametric uncertainty, and frequency range of unmodeled dynamics. Also, the sliding control guarantees robustness to the uncertainty of the model, so that simplified models are allowed to be used while keeping stability.

There are several ways to represent a single input nonlinear system (this will be expanded to multi input output nonlinear system). The following form will be used for the single input nonlinear system:

$$x^{(n)} = f(\boldsymbol{x}) + b(\boldsymbol{x})u \qquad \text{(6-15)}$$

where the scalar x is the output of interest, the scalar u is the control input, and the vector $\boldsymbol{x} = \left[x\ \dot{x} \ldots\ x^{(n-1)}\right]^T$ is the state vector. In this equation, the nonlinear function $f(\boldsymbol{x})$ and the control gain $b(\boldsymbol{x})$ are not exactly known in real control problems. That is those terms always contain certain amount of uncertainties. However the extents of the uncertainties on them are upper bounded by a known function of $\boldsymbol{x}$. For a second-order mechanical system, $b(\boldsymbol{x})$ is the reciprocal of the inertia and $f(\boldsymbol{x})$ is equivalent to force, and u is the applied force to control the system.

The nonlinear function $f(\boldsymbol{x})$ can contain the uncertainty $\Delta f(\boldsymbol{x})$, such that

$$f(\boldsymbol{x}) = \hat{f}(\boldsymbol{x}) + \Delta f(\boldsymbol{x}) \tag{6-16}$$

where $\hat{f}(\boldsymbol{x})$ is the estimate of the nonlinear term $f(\boldsymbol{x})$. The uncertainty $\Delta f(\boldsymbol{x})$ is bounded as

$$\left|\Delta f(\boldsymbol{x})\right| \le F(\boldsymbol{x}). \tag{6-17}$$

Similarly, $b(\boldsymbol{x})$ is known to be of constant sign and is bounded by a known function of time $\hat{b}(\boldsymbol{x})$ such that

$$\frac{1}{\beta} \le \frac{\hat{b}(\boldsymbol{x})}{b(\boldsymbol{x})} \le \beta. \tag{6-18}$$

The parameter β can be interpreted as *gain margin* of the control system.

The trajectory tracking problem is defined as making the state $\boldsymbol{x}$ track a desired state $\boldsymbol{x}_d$ in the presence of uncertainties. The tracking error vector is defined as

$$\tilde{\boldsymbol{x}} = \boldsymbol{x} - \boldsymbol{x}_d. \tag{6-19}$$

Let us define a time-varying surface $S(t)$ in the state space $\boldsymbol{R}^{(n)}$ by the scalar equation $s(\boldsymbol{x};t) = 0$, such that

$$s(\boldsymbol{x};t) = \left(\frac{d}{dt} + \lambda\right)^{n-1} \tilde{x} \tag{6-20}$$

where λ is a strictly positive constant. This equation has a low-pass characteristic and the desired closed-loop response is expected to behave in this way. The time-varying surface $S(t)$ is called *sliding surface*. Perfect tracking can then be defined as remaining (or *sliding*) on the sliding surface $S(t)$. Remaining on the sliding surface implies that $\tilde{\boldsymbol{x}} \to \boldsymbol{0}$ if the system originally starts on the sliding surface, that is, $\boldsymbol{x}_d(0) = \boldsymbol{x}(0)$.

From the equation (6-20), it is evident that the convergence $\tilde{\boldsymbol{x}}$ to 0 follows directly from the convergence of s to 0. Therefore, the system is stable if s goes to zero. The problem thus falls into how to choose a control input u to make s go to zero. Slotine (1991) chose the following *sliding condition*:

$$\frac{1}{2}\frac{d}{dt}s^2(\boldsymbol{x};t) \le -\eta|s| \tag{6-21}$$

where η is a positive constant. This stability criterion is derived from Liapunov theory and Filipov's work on differential equations containing discontinuities (Slotine, 1983). This equation states that the squared distance to the sliding surface decreases along all system trajectories. Thus, trajectories tend towards the surface $S(t)$. The system trajectories remain on the surface once reaching on the surface. The surface, therefore, becomes *invariant set* after satisfying the sliding condition (6-21). Furthermore, the sliding condition implies that disturbances and dynamic uncertainties can be tolerated while keeping the surface an invariant set.

The typical system behavior satisfying the sliding condition (6-21) is shown in Figure 6-3 for n=2. The sliding surface is a line in the phase plane. The slope of the line is $-\lambda$ and contains the desired point $\boldsymbol{x}_d = \begin{bmatrix} x_d & \dot{x}_d \end{bmatrix}^T$. The state trajectory reaches the time-varying sliding surface in a finite time smaller than $|s(t=0)|/\eta$ starting from any initial condition, and then slides along the surface towards $\boldsymbol{x}_d$ exponentially, with a time-constant equal to $1/\lambda$.

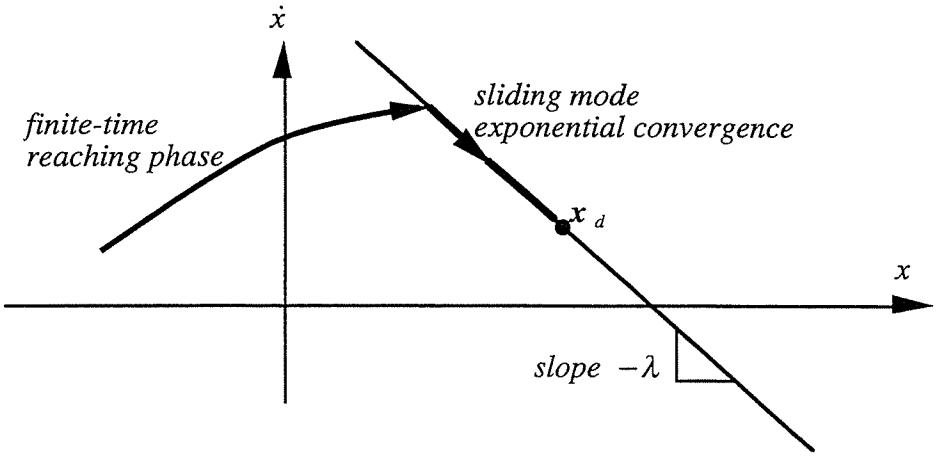

Figure 6-3. *Graphical interpretation of the sliding control for n=2. (Redrawn from Slotine and Li, 1991.)*

6-3. Application of Sliding Mode Control to the TMR

This section discusses formulation of the sliding control for the TMR trajectory tracking control using the basic theory described in the Section 6-2. Single input nonlinear system was the target of the previous development in the Section 6-2. The discussion will be extended to multi-input multi-output (MIMO) system, because the TMR control problem is a MIMO.

Let us rewrite the system equation (6-13),

$$\dot{\boldsymbol{q}} = \boldsymbol{f}(\boldsymbol{q}) + \boldsymbol{B}\tau. \tag{6-22}$$

This system equations have 2 control inputs, τ , and 2 outputs, $\boldsymbol{q}$. Our control problem is to set up the control law τ to make the state $\boldsymbol{q}$ track a desired time-varying state $\boldsymbol{q}_d$, in the presence of parametric uncertainties.

The system equation (6-22) is the first order. For the first order linear system, the proportional control always generates steady-state error, so that the integral control is

usually added in order to remove the steady state error. From this fact, we would rather use the integral of the state, $\int_0^t q_i dr$, as the variable of interest. Let us define a new vector,

$$\xi_i = \int q_i dr \tag{6-23}$$

since the q_i is the component of the velocity vector, the component ξ_i has dimension of distance. Let $\tilde{\xi} = \xi - \xi_d$ be the tracking error vector in the new vector form ξ. And let us define a scalar function $s(\xi;t)$ in the state space $\boldsymbol{R}^n$ as

$$s_i = \left(\frac{d}{dt} + \lambda_i\right)\tilde{\xi}_i = \dot{\tilde{\xi}}_i + \lambda_i \tilde{\xi}_i, \quad i = 1,2 \tag{6-24}$$

where λ_i are strictly positive constant. This is the extension of the scalar function (6-20) to MIMO case and integral control.

As in the single input case (6-16), (6-17), and (6-18), the uncertainties on $\boldsymbol{f}$ is written in additive form,

$$\left|\hat{f}_i - f_i\right| \le F_i \quad i = 1,2, \tag{6-25}$$

and the uncertainties on the input matrix $\boldsymbol{B}$ is written in multiplicative from,

$$\boldsymbol{B} = (\boldsymbol{I} + \Delta)\hat{\boldsymbol{B}}, \quad \left|\Delta_{ij}\right| \le D_{ij} \quad i = 1,2 \quad j = 1,2, \tag{6-26}$$

where the symbol ^ represents an estimated value of a variable and $\boldsymbol{I}$ is 2×2 identity matrix.

The sliding mode controller design can be considered as finding a control law τ that satisfies the individual sliding conditions,

$$\frac{1}{2}\frac{d}{dt}s_i^2 \le -\eta_i |s_i|, \qquad \eta_i > 0, \qquad i = 1,2. \tag{6-27}$$

The first derivative of the vector $\boldsymbol{s}$ that contains the scalar function s_i is

$$\dot{\boldsymbol{s}} = \ddot{\tilde{\xi}} + \Lambda \dot{\tilde{\xi}} = \dot{\boldsymbol{q}} - \dot{\boldsymbol{q}}_d + \Lambda \tilde{\boldsymbol{q}} \tag{6-28}$$

where the matrix Λ is the diagonal matrix whose components are λ_i, $i=1,2$. Plugging the equatio of motion (6-22) into (6-28), the above equation becomes

$$\dot{s} = f + B\tau - \dot{q}_d + \Lambda\tilde{q}. \tag{6-29}$$

The dynamics while in sliding mode can be written as

$$\dot{s} = 0 \tag{6-30}$$

in a single-input case. The equivalent control $\hat{\tau}$ satisfying the above dynamics (but MIMO case) is

$$\hat{\tau} = \hat{B}^{-1}\left(\dot{q}_d - \Lambda\tilde{q} - \hat{f}\right), \tag{6-31}$$

which can be interpreted as the continuous control law that maintains the condition (6-30) while the dynamics were exactly known. Choosing the control input vector as

$$\tau = \hat{\tau} - \hat{B}^{-1}ksgn(\dot{s}) \tag{6-32}$$

makes the vector $\dot{s}$

$$\dot{s} = f + B\hat{B}^{-1}\left(\dot{q}_d - \Lambda\tilde{q} - \hat{f} - ksgn(\dot{s})\right) - \dot{q}_d + \Lambda\tilde{q}, \tag{6-33}$$

where the gain matrix k is a diagonal matrix whose diagonal components are k_i and $sgn(\dot{s})$ is sign function. After substituting the uncertainties (6-26) with the input matrix B, the equation (6-33) becomes

$$\dot{s} = f + (I + \Delta)\left(\dot{q}_d - \Lambda\tilde{q} - \hat{f} - ksgn(\dot{s})\right) - \dot{q}_d + \Lambda\tilde{q}.$$

Rearranging this equation,

$$\dot{s} = f - \hat{f} + \Delta\left(\dot{q}_d - \Lambda\tilde{q} - \hat{f}\right) + (I + \Delta)ksgn(\dot{s}). \tag{6-34}$$

So, the sliding conditions can be verified with the equation (6-34) if

$$(1-D_{ii})k_i \geq F_i + \sum_{j=1}^{2} D_{ij}\left|\dot{q}_{dj} - \lambda_j \tilde{q}_j - \hat{f}_j\right| - \sum_{j\neq i}^{2} D_{ij}k_j + \eta_i, \qquad i = 1,2. \tag{6-35}$$

Let us choose the following equations from the condition (6-35),

$$(1-D_{ii})k_i = F_i + \sum_{j=1}^{2} D_{ij}\left|\dot{q}_{dj} - \lambda_j \tilde{q}_j - \hat{f}_j\right| - \sum_{j\neq i}^{2} D_{ij}k_j + \eta_i, \qquad i = 1,2 \tag{6-36}$$

then the gain matrix $\boldsymbol{k}$ can be determined. Consequently, the sliding control law (6-32) is finally determined with the gain matrix obtained from the equation (6-36).

6-4. Sliding Mode Control Simulation

The control law (6-32) with the gain (6-36) is tested through computer simulations. The following reference trajectories are used to see the tracking performance as shown in the Figure 6-5,

$$\begin{aligned} q_{1d} &= 0.2 + 0.1\sin(2\pi t/5) \\ q_{2d} &= 0.5\sin(2\pi t/5) \end{aligned} \tag{6-37}$$

whose units are meters per second and radians per second, respectively. The TMR platform shown in the Chapter 3 is used as a dynamic model. And the following linear relationships are assumed for the external forces,

$$\begin{aligned} P_x &= -100u \\ P_y &= -10r \\ M_P &= -10r \end{aligned} \tag{6-38}$$

This relationships state that the routine forces and moment are proportional to the linear velocity and the angular velocity in negative sense. The first linear equation about P_x has been proved through simple test.

The control gains (6-36) can be rewritten in individual component forms as

$$\begin{aligned}(1-D_{11})k_1 + D_{12}k_2 &= F_1 + D_{11}\left|\dot{q}_{d1} - \lambda_1\tilde{q}_1 - \hat{f}_1\right| + D_{12}\left|\dot{q}_{d2} - \lambda_2\tilde{q}_2 - \hat{f}_2\right| + \eta_1 \\ D_{21}k_1 + (1-D_{22})k_2 &= F_2 + D_{21}\left|\dot{q}_{d1} - \lambda_1\tilde{q}_1 - \hat{f}_1\right| + D_{22}\left|\dot{q}_{d2} - \lambda_2\tilde{q}_2 - \hat{f}_2\right| + \eta_2.\end{aligned} \tag{6-39}$$

The control gains are determined with the bounds on uncertainties and the desired and current states using this equation. The bandwidth λ of low pass filter to the dynamics of s must be small compared to the frequency of the first unmodeled mode in the system.

The Figure 6-5 (a) and (b) show the tracking control performances. The Figure 6-5 (c) also shows the control input torques of both wheels when tracking the reference trajectories (6-37). The control chattering is extremely severe as shown in this Figure. The cause of this chattering is obviously the switching control action due to the sign function in the tracking control law (6-32).

Chattering must be eliminated for the tracking controller to work properly. For single input case, this can be achieved by smoothing out the control discontinuity in a thin boundary layer neighboring the switching surface

$$B(t) = \{x, |s(x;t)| \le \Phi\} \qquad \Phi > 0 \tag{6-40}$$

where Φ is the boundary layer thickness for a single input case. In other words, outside of $B(t)$, the control law is chosen as before and then the control input is interpolated once trajectories get inside $B(t)$, by replacing the term sgn(s) to s/Φ as shown in Figure 6-4 (Slotine and Li, 1991).

The control chattering implied by the switching gains $\boldsymbol{k}$ can be eliminated by using smooth interpolations, that is,

$$k_i sat(s_i / \Phi_i), \quad i = 1,2 \tag{6-41}$$

instead of using the sign function, where *sat* is the saturation function:

$$\begin{aligned}&sat(y) = y \quad if\ |y| \le 1, \\ &sat(y) = sgn(y) \quad otherwise.\end{aligned} \tag{6-42}$$

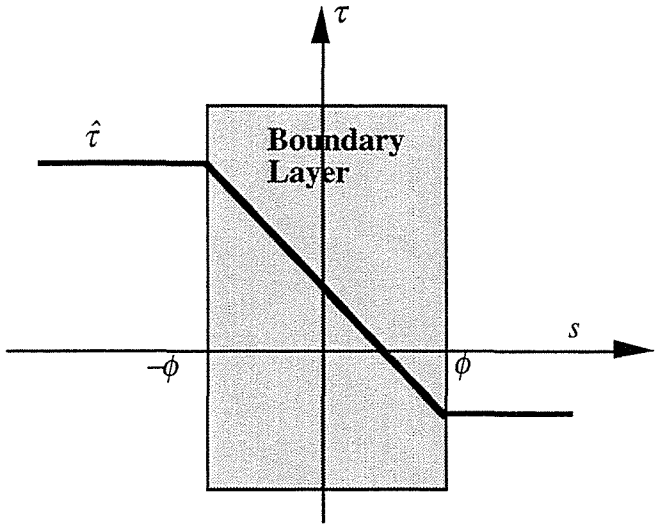

Figure 6-4. *Control interpolation in the boundary layer. (Redrawn from Slotine and Li, 1991.)*

The Figure 6-6 shows the tracking control performance when using the smooth control inputs with the saturation function. The Figure 6-6 (a) represents the tracking error when following the reference trajectory (6-38). The control inputs are smoothed out as shown in the Figure 6-6 (b) by using the saturation function.

In order to see the robustness of the control law to the uncertainties, some parameters are varied and then the control simulations are performed. The equation of motion (6-13) can be rewritten for easy programming as

$$\begin{aligned} \dot{u} &= a_1 r^2 + a_2 P_x + a_3(\tau_l + \tau_r) \\ \dot{r} &= b_1 ur + b_2 P_y + b_3 M_P + b_4(\tau_l - \tau_r) \end{aligned} \tag{6-43}$$

where the coefficients a_1, a_2, a_3, b_1, b_2, b_3, and b_4 are easily obtained from the equation of motion (6-13). The coefficients a_1, a_3, b_1, and b_4 are varied as

$$a_1 = \hat{a}_1(1 + 0.1\sin(\pi t)),$$
$$a_3 = \hat{a}_3(1 + 0.1\sin(0.5\pi t)),$$

$$b_1 = \hat{b}_1(1 + 0.1\sin(2\pi t)), \text{ and}$$
$$b_4 = \hat{b}_4(1 + 0.1\sin(1.5\pi t))$$

and the control simulation is performed in order to see the robustness to the parametric uncertainties. The Figure 6-7 (a) shows the tracking errors and (b) represents the control inputs. We can see that the tracking control performance and the robustness to the parametric uncertainties are very good from this Figure.

The Figure 6-8 shows the tracking control performance when the uncertainties on the external forces and moment are included as

$$P_x = \hat{P}_x(1 + 0.1\sin(\pi t)),$$
$$P_y = \hat{P}_y(1 + 0.1\sin(2\pi t)), \text{ and}$$
$$M_P = \hat{M}_P(1 + 0.1\sin(1.5\pi t)).$$

The plots of tracking errors shows that the control performance is very good even though the external forces are not exactly estimated. Also, the control chattering is disappeared as shown in the Figure 6-8 (b).

From the several simulations about the tracking control performance and the robustness, we can conclude that the developed sliding mode controller is very appropriate for our purposes.

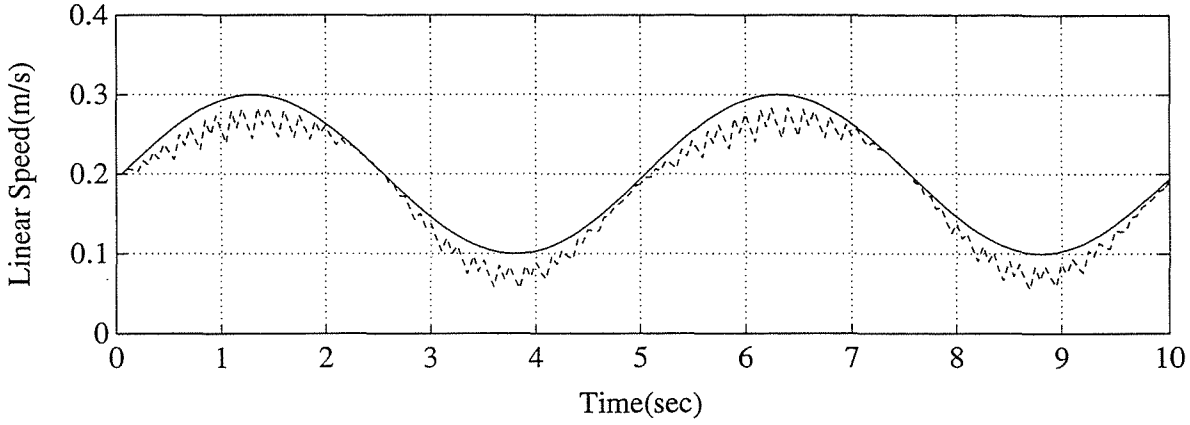

(a). Tracking performance of the linear speed, solid: reference input, dotted: real tracking.

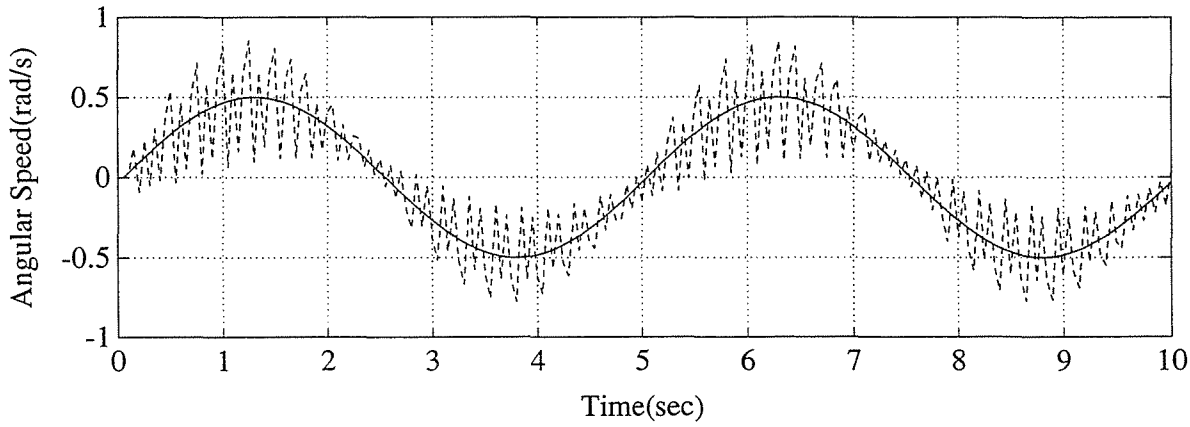

(b). Tracking performance of the angular speed, solid: reference input, dotted: real tracking.

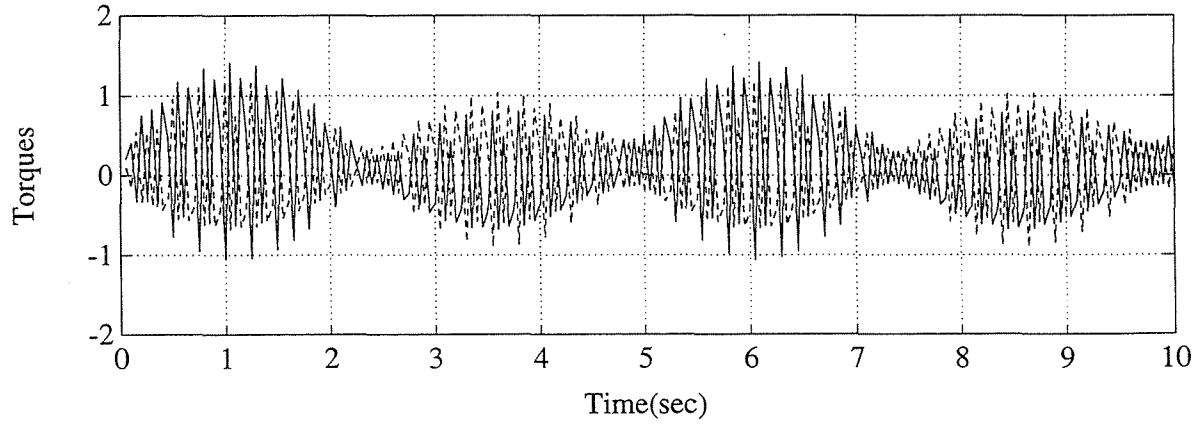

(c). Switching control inputs, solid: left wheel torque, dotted: right wheel torque.

Figure 6-5. *Switching control inputs and resulting tracking performances,* $\lambda = [20\ 0;\ 0\ 20]$, $\eta = [0.1;\ 0.1]$.

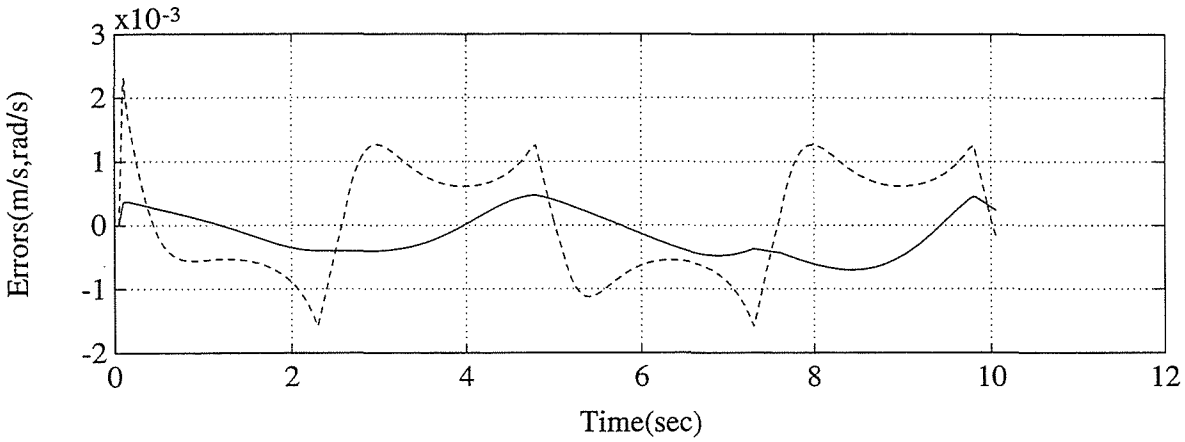

(a). Tracking errors, solid: linear speed, dotted: angular speed.

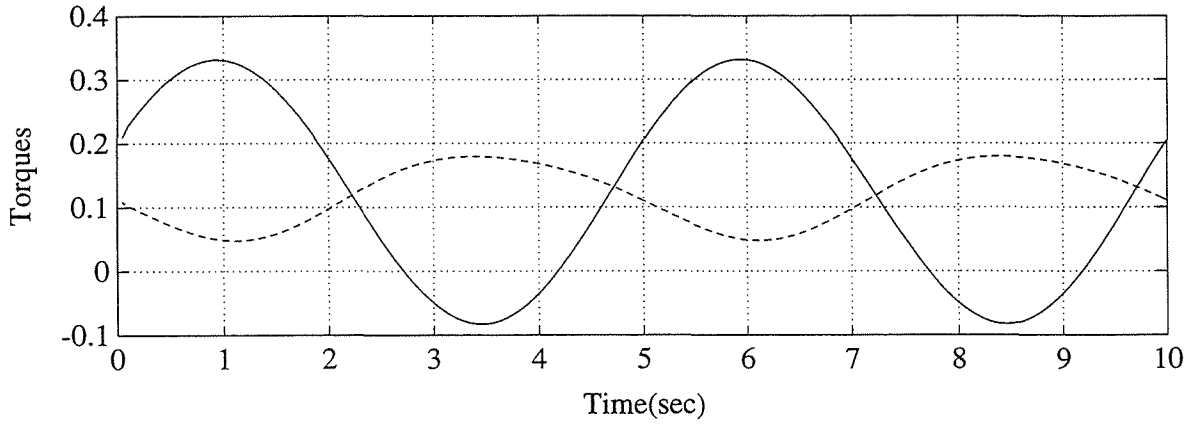

(b). Smooth control inputs, solid: left wheel torque, dotted: right wheel torque.

Figure 6-6. *Smooth control inputs and resulting control performances,* λ *=[20 0; 0 20],* η *=[0.1; 0.1],* Φ *=0.8.*

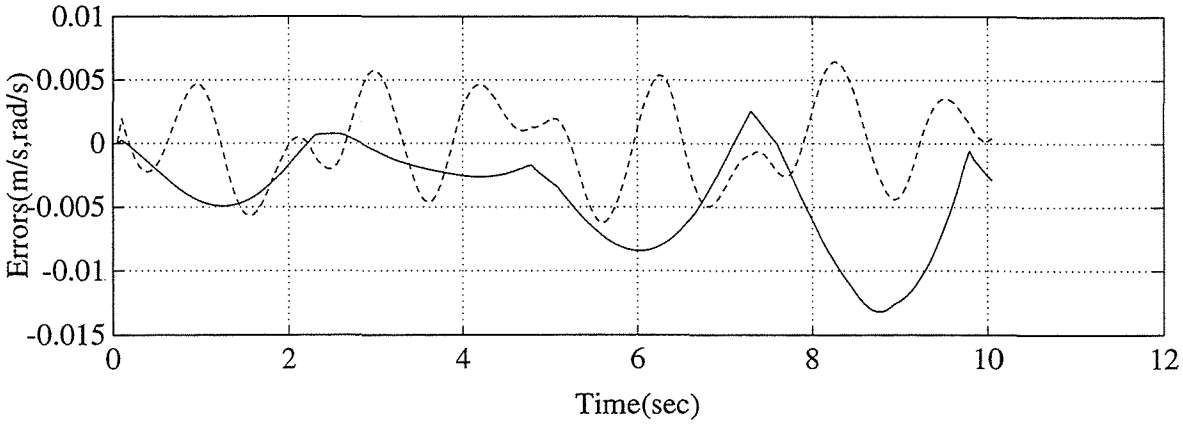

(a). Tracking errors, solid: linear speed, dotted: angular speed.

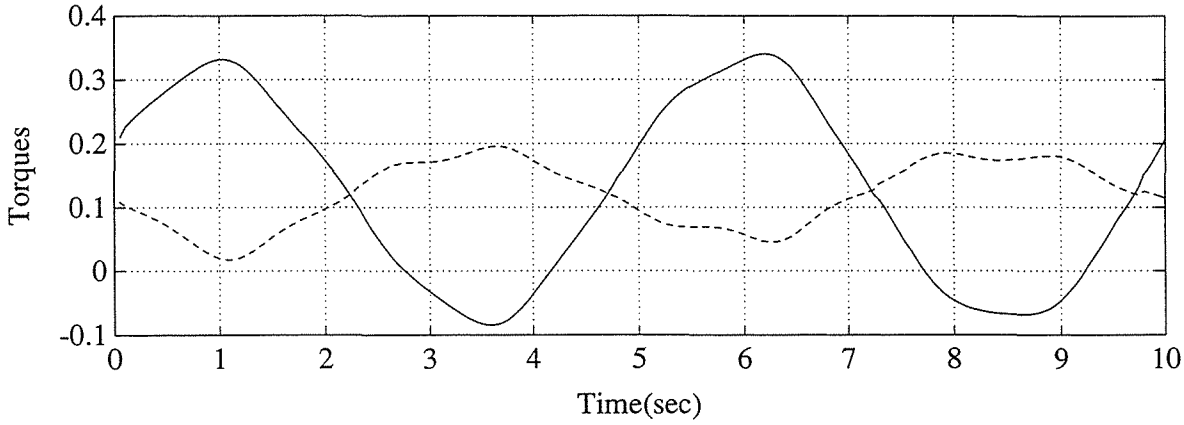

(b). Smooth control inputs, solid: left wheel torque, dotted: right wheel torque.

Figure 6-7. *Smooth control inputs and resulting control performances when including the uncertainties in the coefficients, such that* $a_1 = \hat{a}_1(1+0.1\sin(\pi t))$, $a_3 = \hat{a}_3(1+0.1\sin(0.5\pi t))$, $b_1 = \hat{b}_1(1+0.1\sin(2\pi t))$, *and* $b_4 = \hat{b}_4(1+0.1\sin(1.5\pi t))$; λ *=[20 0; 0 20],* η *=[0.1; 0.1],* Φ *=0.8.*

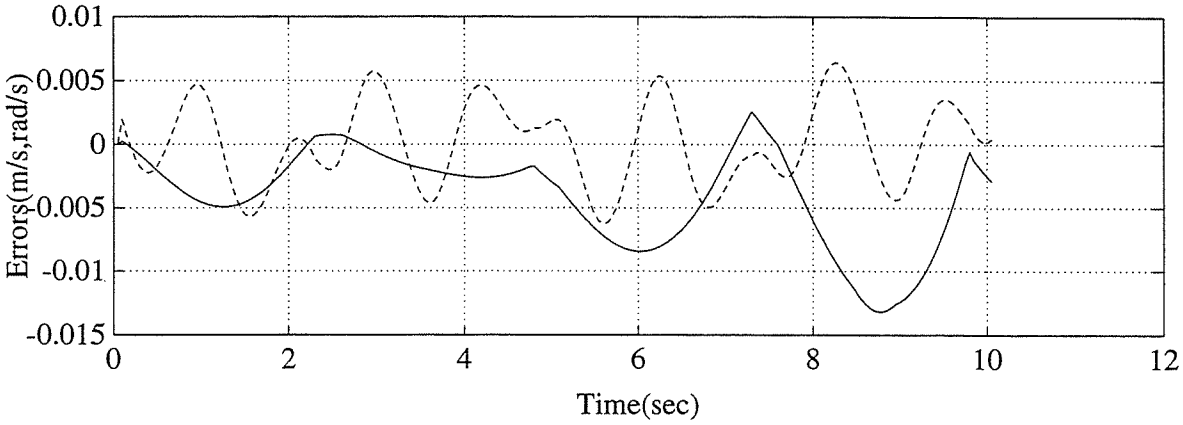

(a). Tracking errors, solid: linear speed, dotted: angular speed.

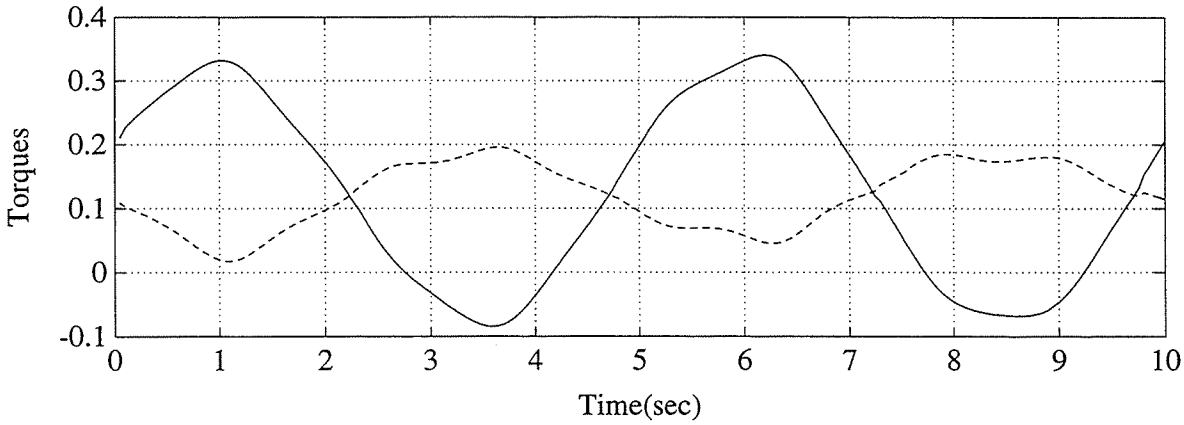

(b). Smooth control inputs, solid: left wheel torque, dotted: right wheel torque.

Figure 6-8. *Smooth control inputs and resulting control performances when including the uncertainties in the external forces, such that* $P_x = \hat{P}_x(1+0.1\sin(\pi t))$, $P_y = \hat{P}_y(1+0.1\sin(2\pi t))$, *and* $M_P = \hat{M}_P(1+0.1\sin(1.5\pi t))$; λ*=[20 0; 0 20],* η*=[0.1; 0.1],* Φ*=0.8.*

Chapter 7. TMR Position Tracking System

Mechanical linkage is selected for the *TMR Position Tracking System* as explained in the Chapter 2. The joint angles of the linkage is measured with optical encoders installed on its joints. The positions of the TMR platforms including angular position are obtained with these joint angles and linkage parameters. This kinematic equation is derived in Section 1. Section 2 also includes error analysis of the linkage due to some uncertainties.

7-1. Postures of Each Robots

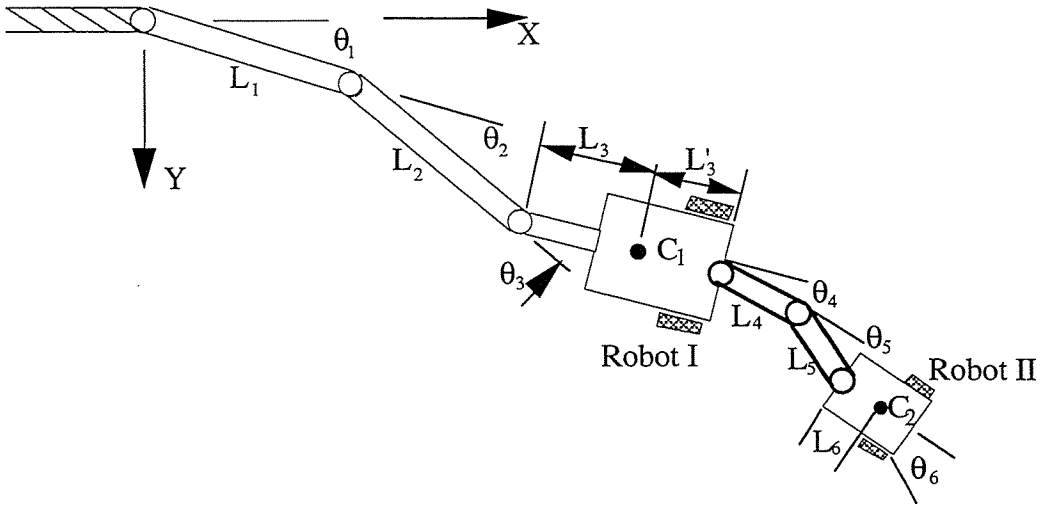

Figure 7-1. *Coordinate systems and parameters for the TMR position tracking.*

The position of the control point C_1 on the robot I are

$$X_{C_1} = L_1 \cos\theta_1 + L_2 \cos(\theta_1 + \theta_2) + L_3 \cos(\theta_1 + \theta_2 + \theta_3) \qquad (7\text{-}1\text{-a})$$

$$Y_{C_1} = L_1 \sin\theta_1 + L_2 \sin(\theta_1 + \theta_2) + L_3 \sin(\theta_1 + \theta_2 + \theta_3) \qquad (7\text{-}1\text{-b})$$

in the global coordinate system. And the angular displacement of the robot I is simply the sum of each joint angles,

$$\psi_{C_1} = \theta_1 + \theta_2 + \theta_3 \qquad (7\text{-}1\text{-c})$$

Similarly, we can represent the position of the point C_2 and angular position of the robot II using the position and angular position of the robot I as

$$X_{C_2} = X_{C_1} + L_3' \cos\psi_{C_1} + L_4 \cos(\psi_{C_1} + \theta_4) + L_5 \cos(\psi_{C_1} + \theta_4 + \theta_5) + L_6 \cos(\psi_{C_1} + \theta_4 + \theta_5 + \theta_6) \quad (7\text{-}2\text{-a})$$

$$Y_{C_2} = Y_{C_1} + L_3' \sin\psi_{C_1} + L_4 \sin(\psi_{C_1} + \theta_4) + L_5 \sin(\psi_{C_1} + \theta_4 + \theta_5) + L_6 \sin(\psi_{C_1} + \theta_4 + \theta_5 + \theta_6) \quad (7\text{-}2\text{-b})$$

$$\psi_{C_1} = \psi_{C_1} + \theta_4 + \theta_5 + \theta_6 \quad (7\text{-}2\text{-c})$$

The linear and angular velocity of each robots can be obtained from the time history of the posture (7-1) and (7-2) by differentiating them in terms of time. These current posture and their differentiation are supplied to the automatic control law to generate appropriate control commands.

7-2. Error Analysis in Position Sensing

In order to properly size and design the linkage, one must understand the general bias or systematic errors. These errors include items such as calibration errors, deformation errors, and limitations of sensor resolution. In this section, the limitations imposed by system resolution will be examined.

In the error analysis, we will consider only the first two links, since the remaining part has relatively short distance compare to the first two. The following kinematic equations represent the (x, y) location of the third joint that is on the robot I (see Figure 7-2) as a function of θ_1 and θ_2, and are represented as

$$x = l_1 \cos(\theta_1) + l_2 \cos(\theta_1 + \theta_2) \quad (7\text{-}3)$$

$$y = l_1 \sin(\theta_1) + l_2 \sin(\theta_1 + \theta_2) \quad (7\text{-}4)$$

where, $x, y =$ the end effector position,

$\theta_1, \theta_2 =$ link angles, and

$l_1, l_2 =$ link lengths.

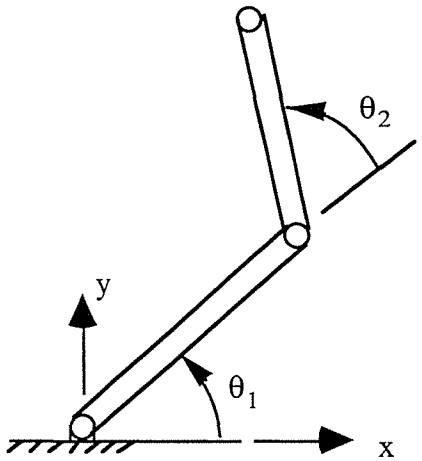

Figure 7-2. *Planar Two Bar Linkage (Redrawn from Winters, 1992).*

The error equations are represented as

$$x_{error} = -l_1 \sin(\theta_1)\delta\theta_1 + \delta l_1 \cos(\theta_1) - l_2 \sin(\theta_1 + \theta_2)(\delta\theta_1 + \delta\theta_2) + \delta l_2 \cos(\theta_1 + \theta_2) \tag{7-5}$$

$$y_{error} = l_1 \cos(\theta_1)\delta\theta_1 + \delta l_1 \sin(\theta_1) + l_2 \cos(\theta_1 + \theta_2)(\delta\theta_1 + \delta\theta_2) + \delta l_2 \sin(\theta_1 + \theta_2) \tag{7-6}$$

if the uncertainty values for the joint angle and the link length are included (Winters, 1992). The angle uncertainty $\delta\theta$ can contain the errors due to the limitation of the sensor resolution and the deflection in x-y plane. The link length uncertainty δl can contain the errors due to the thermo-mechanical deformation, the joint displacement.

To simplify the equations, the case

$$l = l_1 = l_2, \delta\theta = \delta\theta_1 = \delta\theta_2, \delta l = \delta l_1 = \delta l_2$$

will be considered, which still contains the maximum error. And the following notations will be used,

$$s_1 = \sin\theta_1, c_1 = \cos\theta_1, s_{12} = \sin(\theta_1 + \theta_2), c_{12} = \cos(\theta_1 + \theta_2).$$

Then,

$$x_{error} = -ls_1\delta\theta + \delta lc_1 - 2l\delta\theta s_{12} + \delta lc_{12}$$
$$y_{error} = lc_1\delta\theta + \delta ls_1 + 2l\delta\theta c_{12} + \delta ls_{12}. \quad (7\text{-}7)$$

The total error can be defined as following,

$$Error^2 = x_{error}^2 + y_{error}^2. \quad (7\text{-}8)$$

In order to find the maximum error, the partial derivatives of (7-8) will be evaluated.

$$\frac{\partial(Error^2)}{\partial\theta_1} = 2x_{error}\frac{\partial x_{error}}{\partial\theta_1} + 2y_{error}\frac{\partial y_{error}}{\partial\theta_1} \quad (7\text{-}9)$$

$$\frac{\partial x_{error}}{\partial\theta_1} = -lc_1\delta\theta - \delta ls_1 - 2l\delta\theta c_{12} - \delta ls_{12} = -y_{error}$$
$$\frac{\partial y_{error}}{\partial\theta_1} = -ls_1\delta\theta + \delta lc_1 - 2l\delta\theta s_{12} + \delta lc_{12} = x_{error}. \quad (7\text{-}10)$$

Plugging (7-10) into (7-9), then

$$\frac{\partial(Error^2)}{\partial\theta_1} = -2x_{error}y_{error} + 2y_{error}x_{error} = 0. \quad (7\text{-}11)$$

From this equation, we can conclude that the maximum error will occur no matter what the θ_1 is.

Similarly,

$$\frac{\partial(Error^2)}{\partial\theta_2} = 2x_{error}\frac{\partial x_{error}}{\partial\theta_2} + 2y_{error}\frac{\partial y_{error}}{\partial\theta_2} \quad (7\text{-}12)$$

$$\frac{\partial x_{error}}{\partial\theta_2} = -2l\delta\theta c_{12} - \delta ls_{12}$$
$$\frac{\partial y_{error}}{\partial\theta_2} = -2l\delta\theta s_{12} + \delta lc_{12} \quad (7\text{-}13)$$

$$x_{error}\frac{\partial x_{error}}{\partial \theta_2}+y_{error}\frac{\partial y_{error}}{\partial \theta_2}=2l^2(\delta\theta)^2(s_1c_{12}-c_1s_{12})+l\delta l\delta\theta(s_1s_{12}+c_1c_{12}) \\ -2l\delta l\delta\theta(s_1s_{12}+c_1c_{12})+(\delta l)^2(s_1c_{12}-c_1s_{12}). \tag{7-14}$$

Recall the following trigonometric relationships,

$$\sin(\theta_1-(\theta_1+\theta_2))=\sin(-\theta_2)=(s_1c_{12}-c_1s_{12}) \\ \cos(\theta_1-(\theta_1+\theta_2))=\cos(-\theta_2)=(c_1c_{12}+s_1s_{12}) \tag{7-15}$$

$$\frac{1}{2}\frac{\partial(Error^2)}{\partial\theta_2}=-2l^2(\delta\theta)^2s_2+l\delta l\delta\theta c_2-2l\delta l\delta\theta c_2+(\delta l)^2s_2 \\ =-(2l^2(\delta\theta)^2+(\delta l)^2)\sin\theta_2-2l\delta l\delta\theta\cos\theta_2=0. \tag{7-16}$$

Solving this equation,

$$\theta_2=\tan^{-1}\left(\frac{-2l\delta l\delta\theta}{2(l\delta\theta)^2+(\delta l)^2}\right). \tag{7-17}$$

Consequently, the error will be maximum when the θ_2 satisfies the equation (7-17).

The following special cases are presented to illustrate the above relationships as examples.

Case i. Consider just angle uncertainty error.

We can choose $\theta_1=0$. From the equation (7-17), $\theta_2=0$.

So, we can get the error from (7-7), (7-8),

$$Error = 3l\delta\theta$$

Case ii. $\delta\theta=2\pi/10000$, $\delta l=2mm$, $l=1000mm$.

We can choose $\theta_1=0$. From the equation (7-17), $\theta_2=-27.7$.

The error is 4.4mm. The following pictures show the error distribution and its contour in terms of θ_1, θ_2.

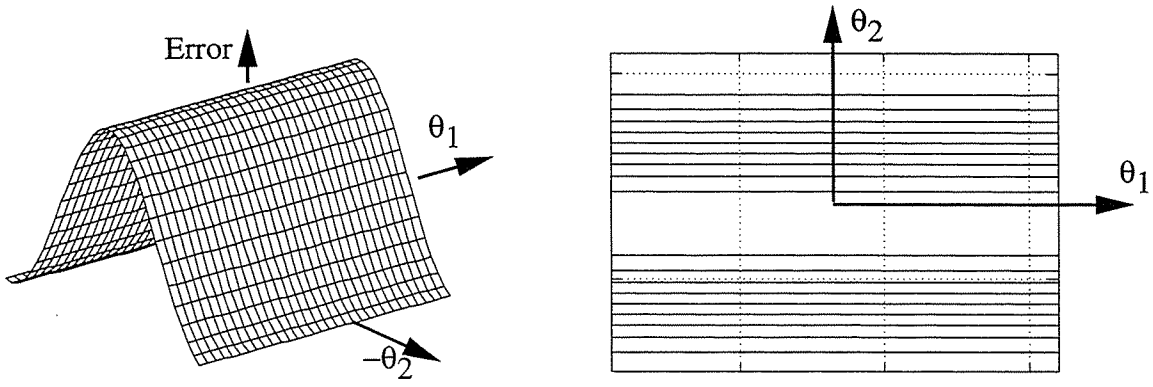

Figure 7-3. *The error distribution and its contour in terms of* θ_1, θ_1, $\delta\theta=2\pi/10000$, $\delta l=2mm$, $l=1000mm$..

The resolution of the encoder used for the linkage joint angle measurement is 10,000 pulses per revolution. From the case i, the error due to the encoder resolution is $3l\delta\theta$. The length of the linkage bar is 1066.8mm. So, the error due to the sensor resolution becomes 2mm, which is very small. This amount of error is allowed for highway maintenance operations.

Chapter 8. TMR Controller

8-1. System Overview

The TMR controller hardware is optimally designed and fabricated in order to implement the developed control algorithm including the Automatic Trajectory Tracking Control and the Manual Control with Joystick. The details of the TMR controller structure design and fabrication are included in this Chapter.

The TMR consists of multiple differentially steered wheeled mobile robots tethered together through a mechanical linkage and each mobile robot has two driving wheels which are driven by Brushless DC motors. Accordingly, the TMR controller should have as many node axis motor controllers as the number of the total driving wheels. Furthermore, the control algorithm for the TMR is multiple input/output. Due to these facts, the communication capability between each node is very important when designing the TMR controller. The Flexible Servo Controller has most of the necessary circuitry for designing any servo controller. It also has very flexible communication functions, either parallel or serial, so that the states of any nodes can be taken by another node controller at any instant by merely reading memory. This makes it very flexible and capable of implementing any type of modern control algorithm. A servo motor controller has been built using the FSC and the TMR controller has been assembled with it, which has been successfully implemented as a MIMO nonlinear controller. From this research, we have confirmed the flexibility and versatility of the FSC for a servo controller. Furthermore, we can easily design and fabricate a multi-axis motion controller using the FSC.

The control system hardware for the mid-sized robot has been built as a part of the whole TMR control system hardware. Because the control system hardware for the full-sized robot is almost same as the one for the mid-sized robot except power requirement, the successful and reliable control achievement of this system promises the success of the whole control system hardware. The system configuration is shown in Figure 8-1. The

80486 based PC takes the role of main robot controller. The purpose of this computer is to supervise the whole control system. The Automatic Trajectory Tracking Control, the Robust Velocity Control and the Supervisory Control System are in this computer. The TMR Position Tracking System is also hooked up this computer through encoder interface boards. And the Laser Range Sensor is also connected to this computer through image processing board and DSP board. The servo motor controllers are connected to this computer through bus interface circuit.

The servo motor controller drives the brushless DC (BLDC) motor that is coupled to the corresponding driving wheel. Here, the difference between two terminologies, the Flexible Servo Controller (FSC) and the servo motor controller, is needed to be clarified. The FSC is a ASIC (Application Specific Integrated Circuit) chip developed for servo control applications. And the servo motor controller is a servo motor control board designed and fabricated with the FSC chip as a main part of the board. The following sections describe the details of its components, control algorithm for the brushless DC motor and some control performance results.

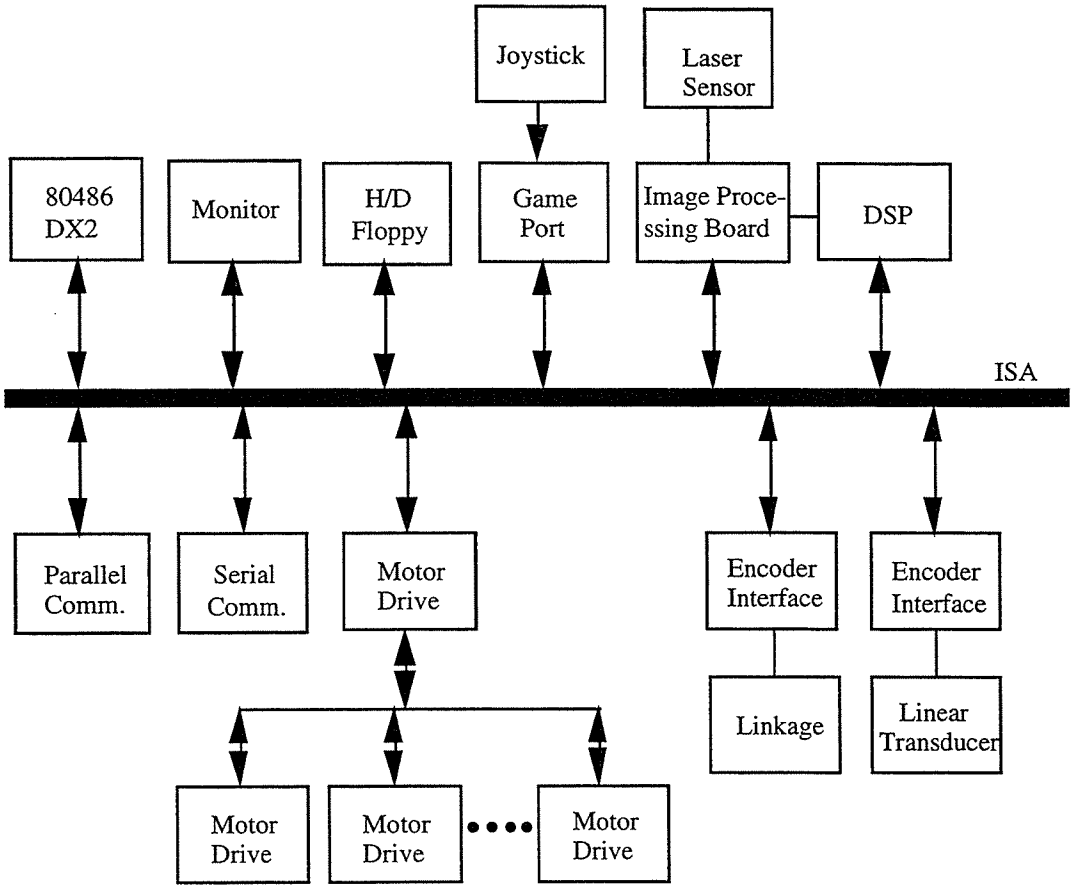

Figure 8-1. *The TMR control system hardware architecture.*

8-2. Flexible Servo Controller Architecture

The FSC is used to develop the servo motor controller which is one of core components of the entire TMR controller. The FSC has been designed by de Schepper and Yamazaki et. al., 1988, 1989, 1990. But there has no research that tested its functionality and performance. This research is the first effort to develop a dedicated embedded servo motor controller with the FSC chip. Accordingly, the development of the servo motor controller contributes the successful implementation of the TMR controller as well as the evaluation of the FSC itself. This section contains the brief explanation of the FSC architecture for smooth transition to the detail design of the servo motor controller.

Recent automated machines are typically electro-mechanical systems, which are commonly referred to as *Mechatronics Systems*. The electronics part of the Mechatronics System is a microprocessor based control system, the *Mechatronics Controller* and these are used as CNC machine tool controllers, robot controllers and other industrial process controllers. Such controllers utilize advanced micro-electronics, and thus, the essential technologies required in the mechatronics control system are:

1. Digital servo control, and
2. Programmable sequence control.

For a reliable and cost effective system, the hardware configuration should be optimized and the number of the hardware components should be minimized without losing functional flexibility and versatility. The mechatronics controller should also be flexible for the user or mechatronics system designer such that they can infuse their own engineering knowledge and experience into the controller, and thus develop an application specific mechatronics controller easily.

The most popular actuator for a mechatronics system is an electric motor. These motors can be conventional DC servo motors, AC synchronous (Brushless DC) servo motors, or AC induction motors. Most of the commercially available motors must be

accompanied by an electric servo amplifier to perform servo control. The currently available servo amplifiers mostly employ analog or analog-digital combined circuit technology. Recently, synchronous AC servo motors and induction type AC servo motors have become increasingly popular due to their maintenance free and cost effective features. The AC synchronous or Brushless DC motors are mainly used for the feed-drive system in mechatronics systems, and AC induction motors are commonly employed for spindle drive systems.

As shown in Figure 8-2, the structure of a current servo controller is based on a multi-loop feedback system, and the controller in each loop uses conventional feedback with feed forward algorithms. Since it is possible to represent all necessary control actions by logical and numerical equations, a flexible system has been proposed to integrate the total control processing into the software by utilizing a highly integrated microprocessor. The aim was to reduce the number of hardware components required while concurrently eliminating the need for analog signal processing. The term *flexible* implies that the system incorporates the following features :

1. Flexibility in connection to various types of servo motors,
2. Flexibility in configuring the axis motion control (single axis, multi-axis, master/slave),
3. Flexibility in control hardware interfacing (parallel, serial, bus, LAN),
4. Flexibility in implementation of various control algorithms (conventional FB, modern control, etc.),
5. Flexibility in constructing the dedicated controller depending upon the engineering ability, and
6. Flexibility in redesigning the future FSC-ASIC for dedicated application.

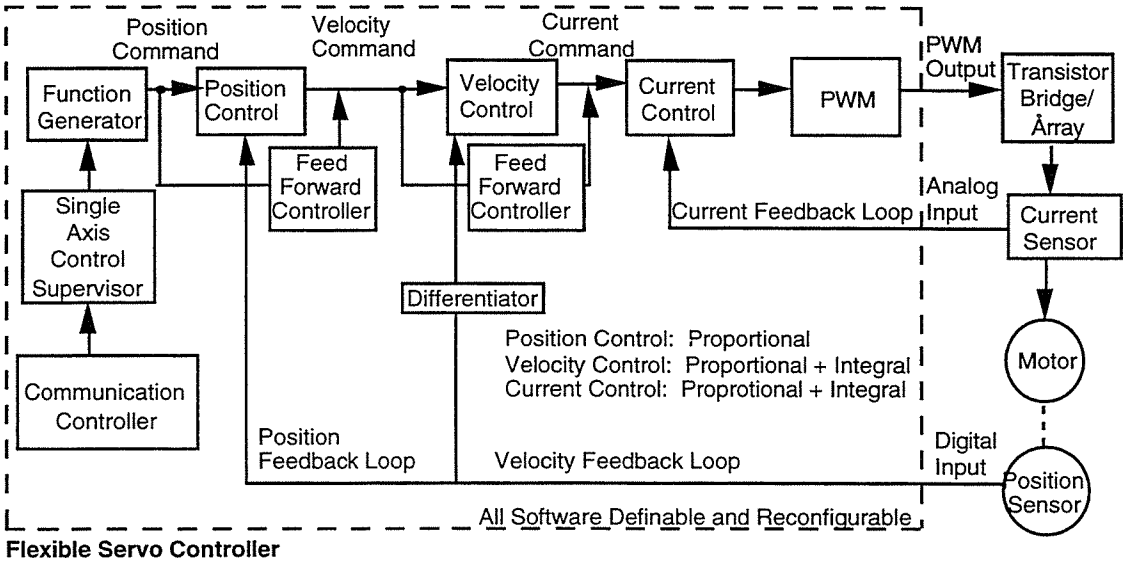

Figure 8-2. *General configuration of a servo motor controller. (Redrawn from Schepper, 1988.)*

The main part of the hardware of the Flexible Servo Controller is a highly integrated microprocessor specially designed for industrial control purposes. In addition to the regular functions available in the general processor, this integrated hardware should have the following functions:

1. High speed processing for control calculation,
2. A/D conversion to receive the current signal,
3. Pulse Width Modulation (PWM) to generate the transistor switching pulses, and
4. High speed data communication to receive commands and to send status from/to upward supervisory control.

In order to verify the feasibility of the proposed concept, the highly integrated FSC-ASIC was previously developed. Figure 8-3 shows the architecture of the FSC chip. The analog-digital mixed chip was designed by using the silicon compilation technique and fabricated using a 1.3 micron design rule. The digital part of the chip holds about two

hundred thousand transistors. The features of the FSC chip are as follows (Yamazaki, et al., 1990)[22]:

1. The single accumulator and all registers contain **16 bit integers.**
2. The ALU contains **a hardware multiplier, a hardware divider, a 16 bit barrel shifter, signed integer overflow protection and a hardware sine generator** to assure fast servo control processing.
3. On powering up the application program can be uploaded from the host CPU or from the outside EPROM via a special upload port into a **512 words long on-chip program RAM.**
4. **A PWM generator** which can drive the pre drivers of AC/BLDC motor (6 signals) is integrated.
5. **An Up-Down Counter** for the encoder signals has been extended to 32 bits for high precision applications.
6. The **on-chip program ROM** contains a 512 words long servo control library of frequently used routines. These routines can be called from the uploaded application program. In this way the application program can be written very compactly.
7. The **execution cycle** has been brought to 100 nanoseconds (FSP-2 : 200ns).
8. A **448 X 16 bits data RAM** has been provided allowing the processing of more complicated algorithms.
9. The **integration of analog circuit** is one of high-tech. features of the FSC 3 channels of A/D converter: 10 bit, 1 channel of D/A converter: 8 bit
10. **High speed serial communication** has been integrated in the form of a hardware digital signal processor communicating with FSC's CPU via dual port RAM.
11. The **parallel communication** with the Host CPU has been implemented in the form of dual port RAM. In this way all control registers used by FSC can be

scanned by Host CPU, which results in fast, easy and user friendly programming and debugging environment.

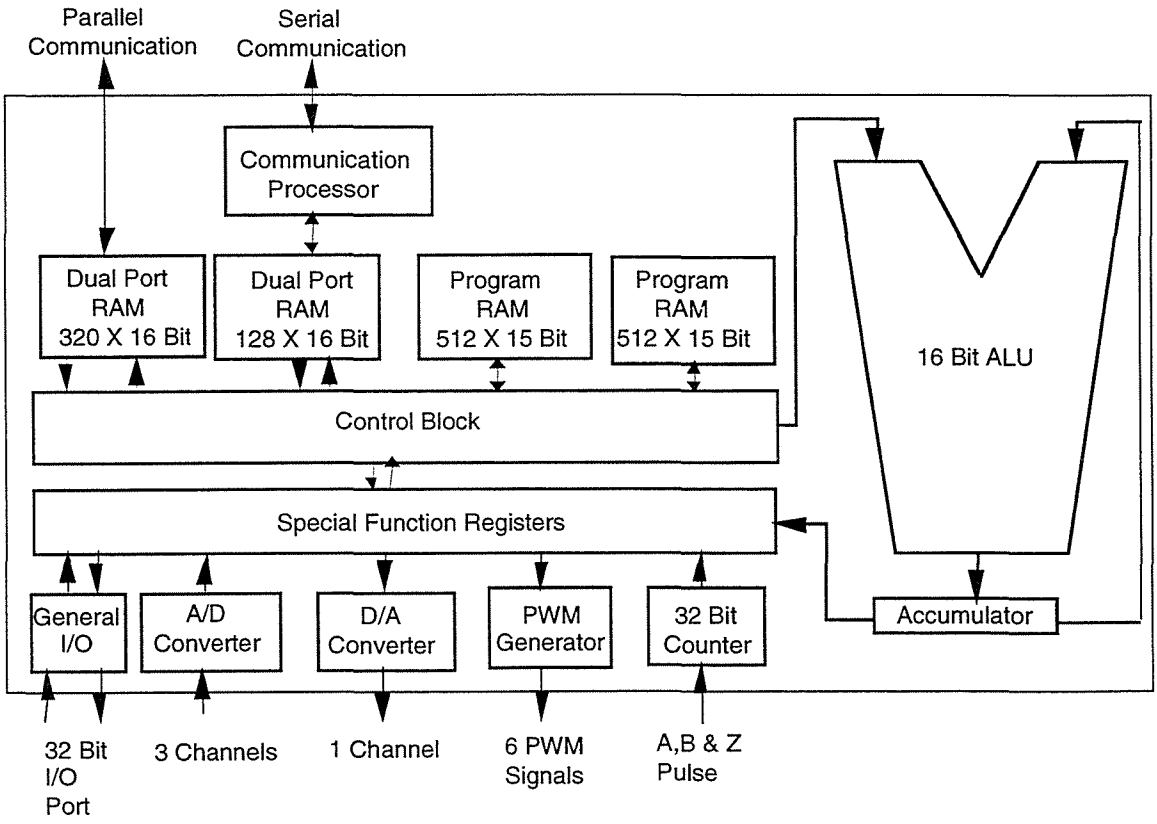

Figure 8-3. *The architecture of FSC. (Redrawn from Schepper et al., 1990.)*

8-3. Servo Motor Controller Design with FSC

The purpose of this section is to discuss the design and fabrication of the servo motor controller with the FSC. There have been no papers to discuss the development of any embedded servo controller utilizing the advantages of the FSC. The functionality and performance of the FSC itself therefore have not been proved yet. This research is the first effort to evaluate and utilize its advantages for developing an advanced servo controller.

The FSC has the characteristics that it can be applied to three types of motors, DC, Brushless DC and AC motors, with same hardware merely by changing software inside. Consequently, any types of motors can be controlled with the FSC if appropriate control program is transferred to the controller. The FSC is fully programmable, so that any advanced modern control algorithms can be imported for motor control.

The servo motor controller is expected to has the following features in order to be applied to the TMR control system that is a multi-axis nonlinear multi-input multi-output:

1. High reliability due to the compact hardware,
2. High flexibility,
3. Easy adjustment for desired control characteristics, and
4. Transparency to the end user.

The Figure 8-4 shows the block diagram of the servo motor controller board. The necessary components for the servo motor controller are invertor and its pre-driver, program ROM, serial communication peripherals, interface to the 80486 computer, power circuits, and so on. The following sections contain the detail discussion of each components.

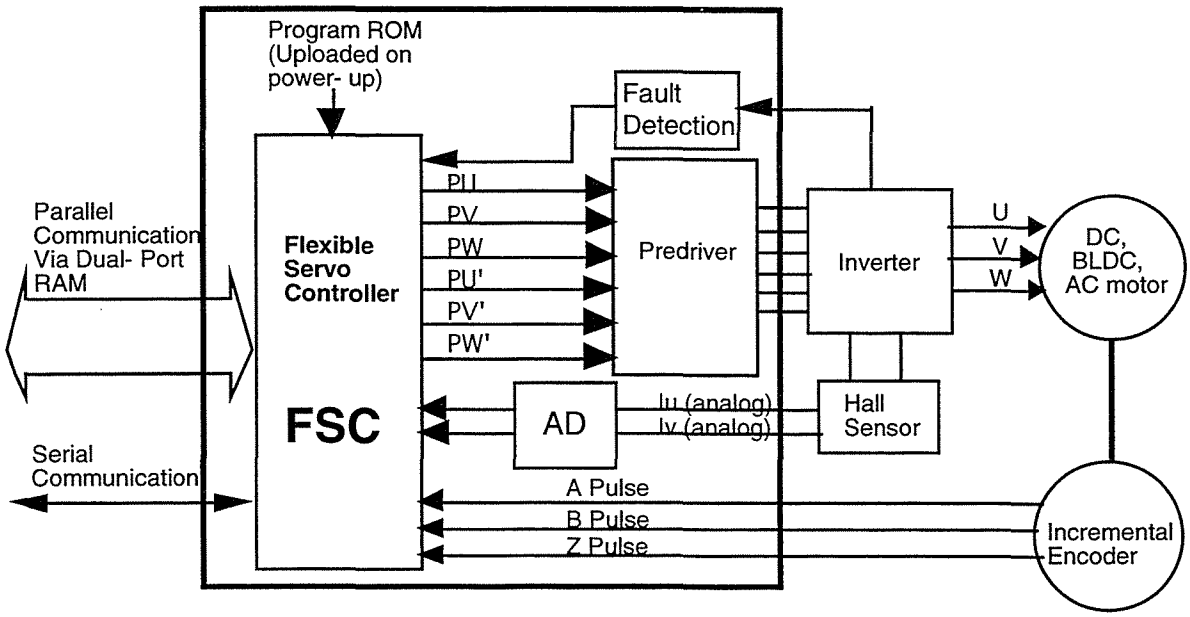

Figure 8-4. *The block diagram of servo motor control board equipped with the FSC.*

8-3-1. Bus Interface to AT-Bus over Dual Port RAM

The FSC has dual-port RAM (Random Access Memory) for serial and parallel communications. The dual-port RAM has 2 port that can be read from 2 directions. The read timings of each ports are different, so that timing interference can be easily avoided. But writing to the dual-port RAM can be done from just one direction. The FSC data memory consists of 16 bit 448 word resisters that are dual-port RAM shown in the Figure 8-5. There are 4 sub-regions, CPUW_RAM, CPUR_RAM, SEND_REGS, and REC_REGS in the data memory. Control variables are easily accessed by external host CPU through the CPUW_RAM and CPUR_RAM registers. And the SEND_REGS and REC_REGS are used for the serial communication.

The communication between the FSC and the main controller is performed through the dual-port RAM, CPUW_RAM and CPUR_RAM registers. The first 0 to FFH[1] address block is assigned to communicate with the main controller and the second 100H to

[1]H represents hex-decimal number.

1BFH address block is assigned to communicate with other FSC servo motor controllers through optical fiber serial link.

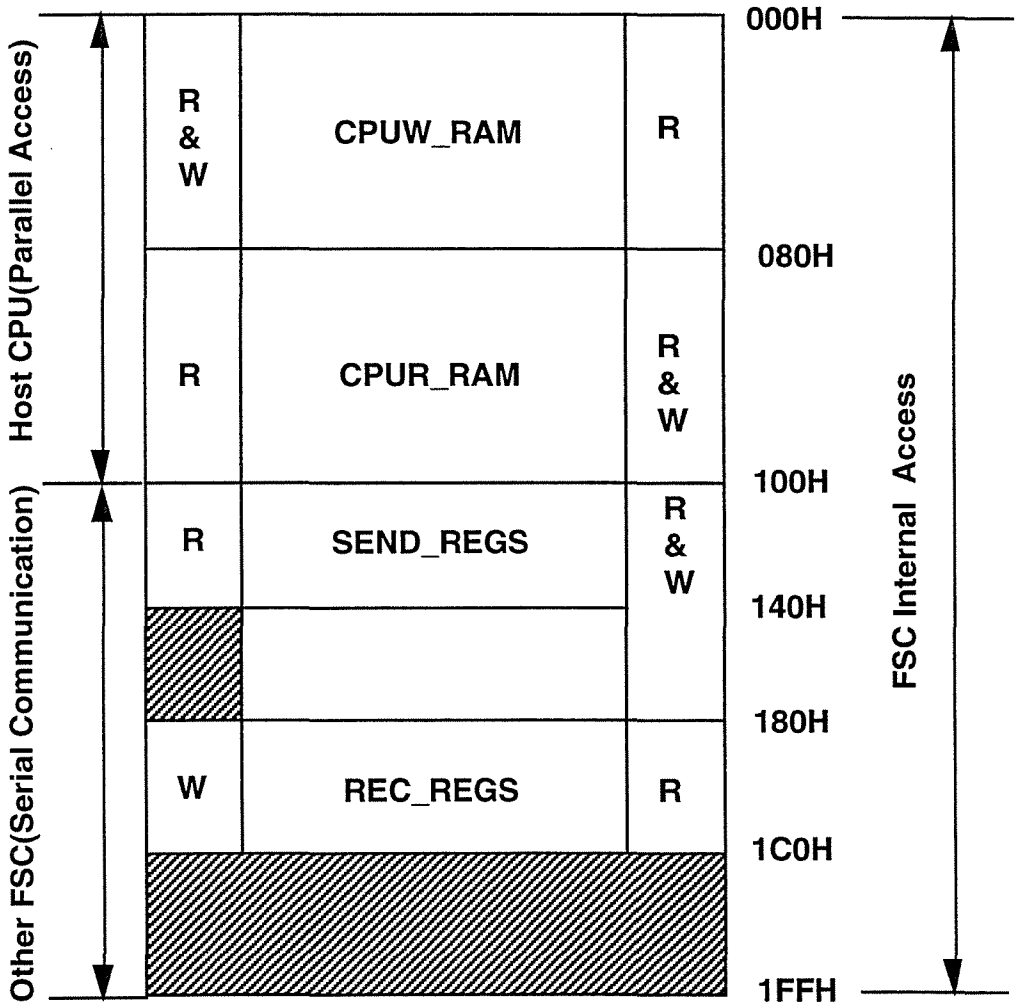

***Figure 8-5**. Memory map of FSC dual-port RAM.*

The timing chart for host interface is shown in the Figure 8-6. X_CS that is a chip select signal is decoded from the address signals. Hence, its timing is identical to the ADDRESS.

READ CYCLE: ADDRESS and X_RD are set by the host. When the data on the bus set by the FSC is stable, the data can be read by the host.

t1: data stable time after address stable, max. one FSC cycle.

t2: data stable time after X_RD stable, max. a few 10 nanosecond.

t3: data remaining stable time after address unstable, min. 0 sec., max. half FSC cycle.

t4: data stable time length, n cycle, such that n cycles < address stable < n+1 cycles.

WRITE CYCLE: ADDRESS and DATA are set by the host. When both are stable, the write cycle can be started by setting X_WR to 0. To assure proper operation, the address and data should be kept stable until X_WR is set back to 1.

t5 and t6: address and data stable time before X_WR, a few 10 nanoseconds is enough.

t7: X_WR stable length, at least 1 FSC cycle.

t8: address and data stable time after X_WR unstable, min. a few 10 nanoseconds.

READ CYCLE

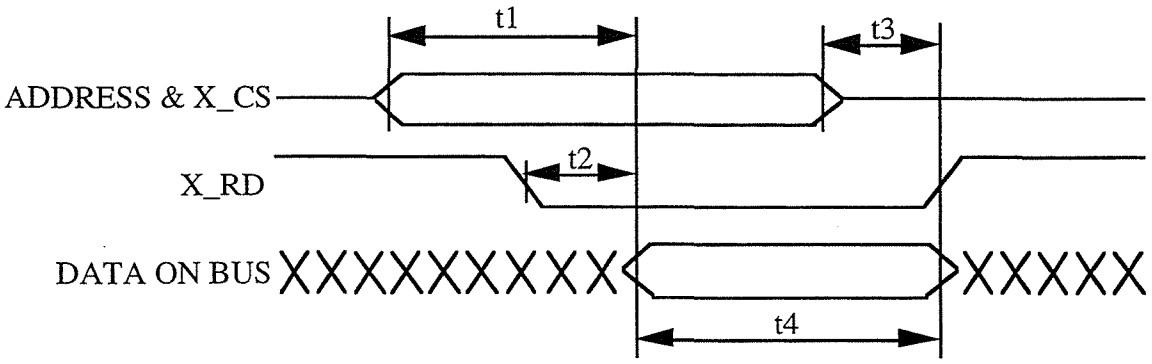

WRITE CYCLE

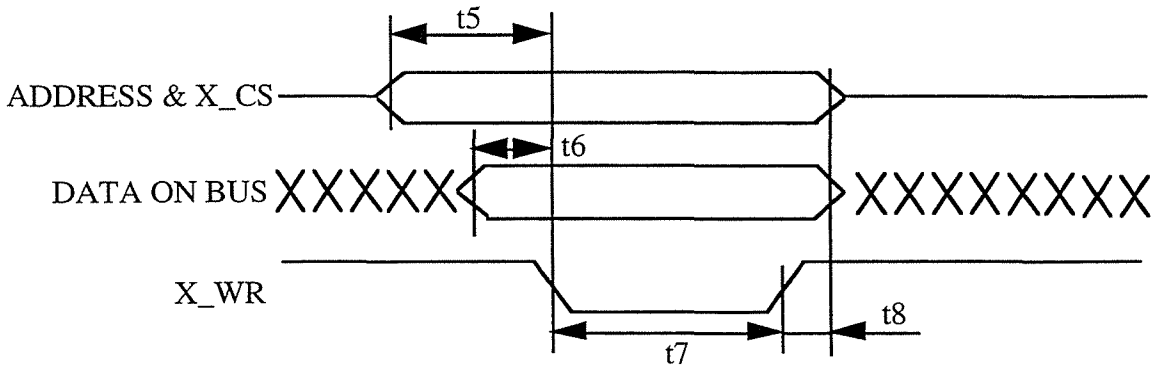

Figure 8-6. *Timing chart for host interface.*

The servo motor controller board is designed to have 2 jumper connectors which have address bus, data bus, and control bus of the FSC dual-port RAM for host computer bus connection. And the board also has micro switches and some jumpers for test purpose. Detail circuit drawing is shown in the Appendix.

The host is considered to be a slow micro-controller (or its expansion bus speed is slow) in order to read and write data to the dual-port RAM of the FSC without any special handshake or synchronization. But read or write cycle for the IBM AT-BUS takes about 3 clock cycle when 16 bit data transfer is being used, which is faster than FSC's. In order to

solve this timing problem, one wait state is put during AT_BUS read write cycle. This setting can be done by modifying CMOS set up table. The dual-port RAM is 16 bit, so that 16 bit transfer of AT-BUS is used instead of 8 bit transfer which is normally being used. We can save lots of data transfer time which is very big CPU burden when we try to achieve high speed control sampling time since the 16 bit transfer time is much faster than the 8 bit transfer

The FSC dual-port RAM has 256 address space, 0H to FFH, for host communication. The address space 0 to FFH is too big to assign I/O space inside the IBM ISA-BUS I/O space. There is not such a big unused block in the IBM I/O space. In order to solve this problem, the following trick is utilized. The first 10 address lines (A0 - A9) are decoded to have address space 320H ~ 32FH and then the remaining 6 address lines (A10 - A15) are hooked up to the dual-port RAM. The following table shows the address line connections between the ISA Bus and the FSC dual-port RAM. For example, the I/O address B324H (=1011,0011,0010,0100 binary) must be chosen in order to access the address B2H (=1011,0010 binary) in the FSC dual-port memory.

ISA Bus	*FSC*
A1	ADDR0
A2	ADDR1
A10	ADDR2
A11	ADDR3
A12	ADDR4
A13	ADDR5
A14	ADDR6
A15	ADDR7

8-3-2. Serial Communication Network

The TMR for the crack sealing operation consists of total 4 driving wheels which require corresponding 4 motor controllers. The control timing and communication must be precisely synchronized in order to get better control performance. The FSC has a communication processor which can perform serial communication. Its communication speed is up to 5 M baud rate, which is enough to achieve precise synchronization. Serial communication network is designed with optical fibers and related receivers and transmitters to connect these communication processors of each servo motor control boards. So, the servo motor controller board is design to be equipped with these optical fiber transmitters and receivers. Since each motor control boards take charge of communications each others, the main controller, 80486 computer, only needs to communicate with the first motor controller board. The CPU burden of the main controller, therefore, can be lessened. In this section, the communication method will be discussed.

The "virtual multi-port memory" method (VMP) has been proposed to cope better with the requirements of a servo motor control systems by Schepper (1990), in which standard protocols can still be used in slightly simplified form. The basic concept of the VMP method is that all control CPUs (masters and slaves) are virtually connected to a common multi port memory. In this way the control CPUs communicate with each other by simply reading and writing a multi port memory, which results in a minimum overhead of the control CPUs. But the multi-port memory can not be physically realized with only normal memory circuits. The circuit that performs an equivalent operation to a multi-port memory should therefore be developed. A kind of the multi-port memory can be realized with dual-port memory and a communication processor as an intermediate agency that transmits communication data either way. This is not real multi-port memory which does not exist but a virtual multi-port memory. All control CPUs are connected to a dual port memory each other side by side. The secondary side of the dual port memory is connected

with a communication processor which is hooked up to the communication processors of other nodes by means of a serial line. The task of this communication processor is to transfer the contents of the dual port memories in all nodes so that the control CPUs are accessing virtually a multi port memory. This task is very simple so that it can easily be realized with a specially constructed hardware circuit (communication signal processor) as is the case of the FSC implementation. The VMP method has actually been integrated in the FSC chip in the form of an ASIC peripheral signal processor. Figure 8-7 shows the block diagram of the communication hardware. The communication processor is in fact made up of two processors; one receive processor and one send processor. The receive processor is always listening even when its own node is sending. When its own node is sending data, the sent data is received back at the end of the ring in order to allow the control CPUs to check whether its data has been sent properly or not. Communication control logic extracts the address token from the received data and decides when the send processor should start to transmit. At that time the ring is broken inside the ASIC.

A region in the SEND_REGS and the REC_REGS can be selected by setting the corresponding bit of the region status register. The region status register is 8 bits as shown in the Figure 8-8. Each bit of the region status register corresponds each 8 by 8 region in the SEND_REGS and the REC_REGS. The 8 bit number that represents the ownership of each regions can be written to the region status register with the instruction, *wrreg*.

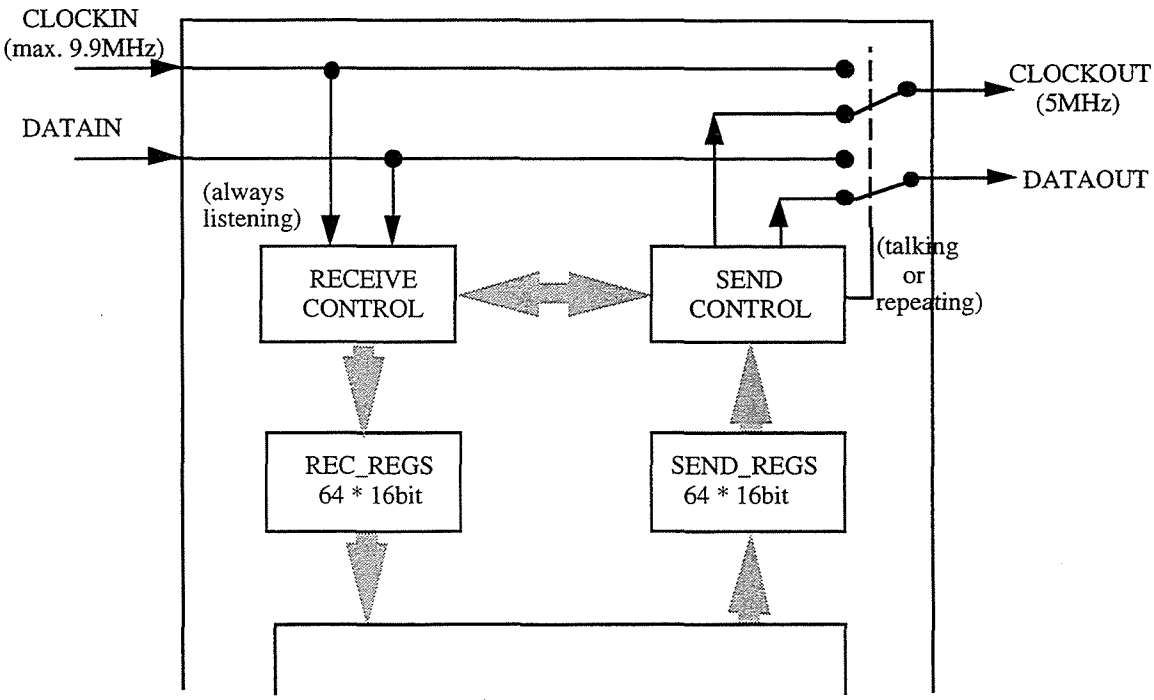

Figure 8-7. *Block diagram of serial communication processor. (Redrawn from Schepper, 1990.)*

Optical fiber transmitters and receivers are provided on the servo motor controller boards for the serial communication link. The maximum transfer speed through the selected optical fiber is 5 M bit per second due to the limit of the FSC communication processor, 5 M baud rate. The detail circuit diagram for the optical communication link is shown in the Appendix.

REGION_STATUS register

7	6	5	4	3	2	1	0

SEND_REGS

REGION #0 8 WORDS
REGION #1 8 WORDS
REGION #2 8 WORDS
REGION #3 8 WORDS
REGION #4 8 WORDS
REGION #5 8 WORDS
REGION #6 8 WORDS
REGION #7 8 WORDS

REC_REGS

REGION #0 8 WORDS
REGION #1 8 WORDS
REGION #2 8 WORDS
REGION #3 8 WORDS
REGION #4 8 WORDS
REGION #5 8 WORDS
REGION #6 8 WORDS
REGION #7 8 WORDS

Figure 8-8. *REGION_STATUS register and corresponding regions inside SEND_REGS and REC_REGS.*

8-3-3. User Program Uploading

A user developed program can be uploaded from the host CPU or from an externally supplied ROM. When the pin UPL is high, the FSC tries to read a user program via the dual port RAM that is interfaced to the host CPU. The register 01H in the dual-port RAM contains one instruction word and the register 02H contains its address to be stored. The

FSC responds to the host CPU by writing the program address to the register 8bH. The host CPU can thus check whether the contents of 8bH and 02H are same before writing a new code to 01H and the new address to 02H in order to confirm right transformation of the program code. If the pin UPL is 0, then the user program is uploaded from the external ROM at power on or at reset. And the program in the external ROM should be stored following the format shown in the Figure 8-9. There should be 2 bytes of 0FFH right after the end of the program to indicate the end of program. The file format follows the Intel hexa file format. The Figure 8-10 shows the program memory map of the FSC. The internal ROM contains the built in subroutines that represent some basic I/O commands and some servo specific functions, for example, PI (Proportional and Integral) control routine, PWM calculation routines, etc. The internal ROM can not be altered. The internal RAM which starts from the address 200H loads the user program from the external ROM or from the host CPU depending on the UPL pin status. The user program should therefore start from the address 200H and have 2 bytes of 0FFH at the end of the program.

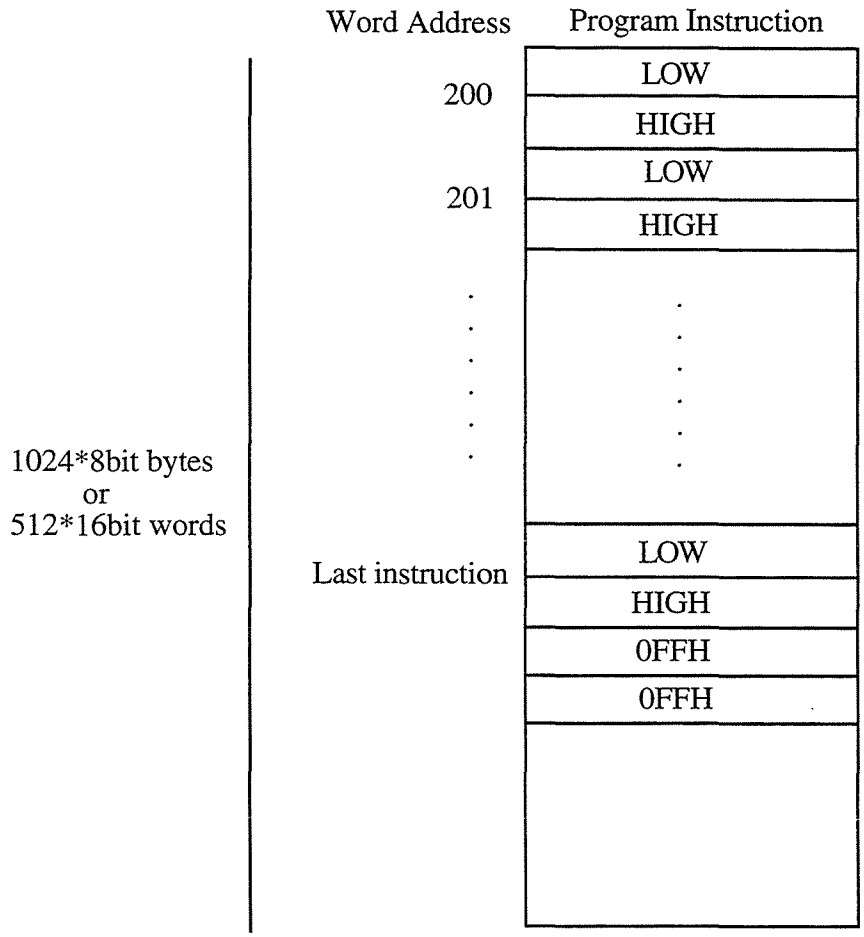

Figure 8-9. *Program format to be stored in the external ROM.*

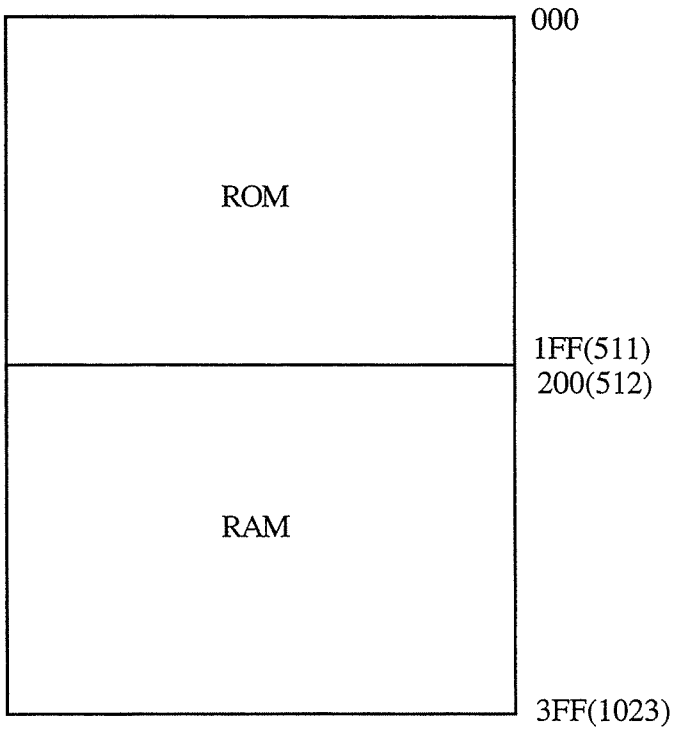

***Figure 8-10**. Program memory map of the FSC, 1024 15 bit words.*

On the servo controller board, the program ROM is provided to load a user program. The Figure 8-11 shows the connection of the external ROM to the FSC. The data lines of the ROM are hooked up to the lower byte of the input port 2 of the FSC. The 10 lines of the output port is utilized as the address lines of the ROM. A jumper is placed on the board for the UPL pin. The UPL pin can be low or high by proper jumper setting. The detail circuit diagram is shown in the Appendix.

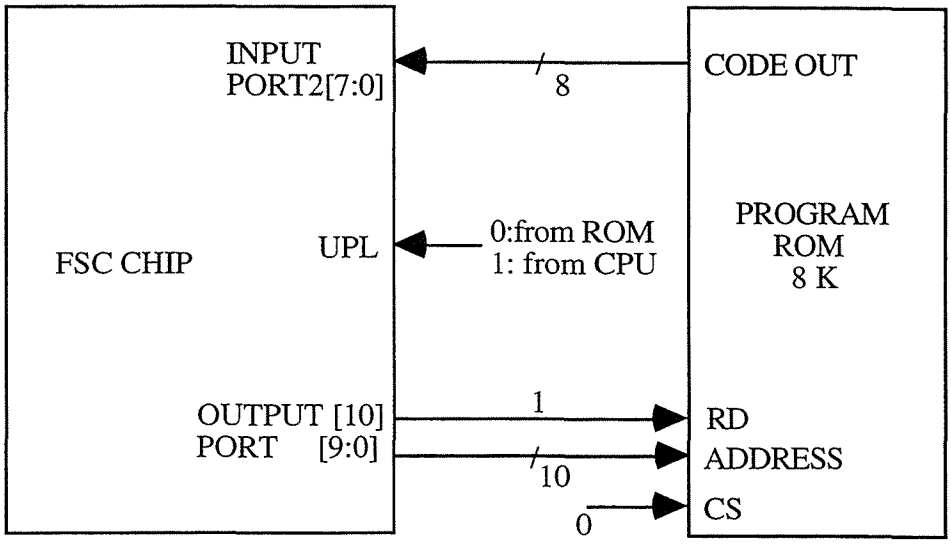

Figure 8-11. *Connection diagram of the external ROM to the FSC.*

8-3-4. Pulse Width Modulation

Most of modern servo motor controllers, even analog controllers, use switching power transistors driven by Pulse Width Modulation (PWM) signals in order to amplify and supply the amplified voltage to motor. The PWM signal can be considered as digital signals and it may be one of the biggest reason that the current servo motor controllers are able to be more and more digitalized.

Figure 8-12 shows a simple configuration for power transistor switching. When a digital on-off signal is applied to the gate of the transistor, the voltage at S follows similar curve but:

1. delayed (parameter on time T_{on} and off time T_{off}),
2. distorted (parameter rise time T_r and falling time T_f), and
3. amplified (according to voltage V_{dc}).

These time constants are inherent characteristics of transistor.

A more practical configuration is depicted in Figure 8-13 where the purpose is to generate a certain line voltage on point L. Transistor T and $\overline{T}$ are repeatedly switched on

and off respectively and when this is done at high frequency it can be considered as equivalent to the mean value of the voltage or equal to:

$$\text{voltage} = V_{dc} * \text{duty}(T). \tag{8-1}$$

The important thing in this configuration however is that two power transistors are connected in series and therefore a delay time should be applied in order to prevent current spike. Those spike currents would flow when the transistor T is not completely turned off and $\overline{T}$ is already turned on to some extent. During this short time, it forms short circuit that has small resistance but very big voltage resulting in very high current spike that breaks the transistors in a microsecond. A delay time,

$$\begin{aligned} T_{delay} &> T_{on} + T_r \\ T_{delay} &> T_{off} + T_f \end{aligned} \tag{8-2}$$

should be used in order to avoid this very dangerous phenomenon. The bigger number should be chosen among the 2 numbers.

On the other hand, the delay time may not be chosen too big because the voltage on point L is not exactly known or controllable during the delay time. It is the direct cause of very annoying non-linearity. The purpose of the PWM is to generate a voltage on an impedance like a coil or a motor amateur. For big duty differences, the average voltage on the impedance varies linearly with the duty difference. When the duty difference becomes uncontrollable and results in a non-linear voltage-duty characteristic, it directly influences on the control performance of the current loop.

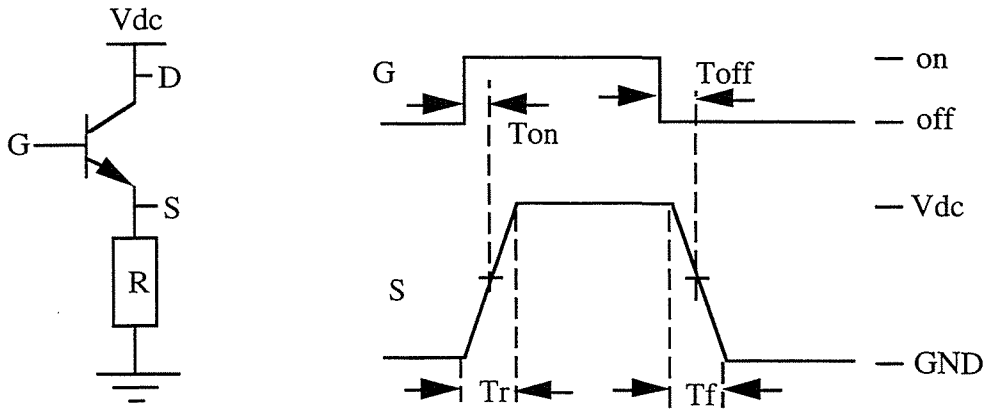

Figure 8-12. *Simple configuration of Pulse Width Modulation. (Redrawn from Sechpper, 1990.)*

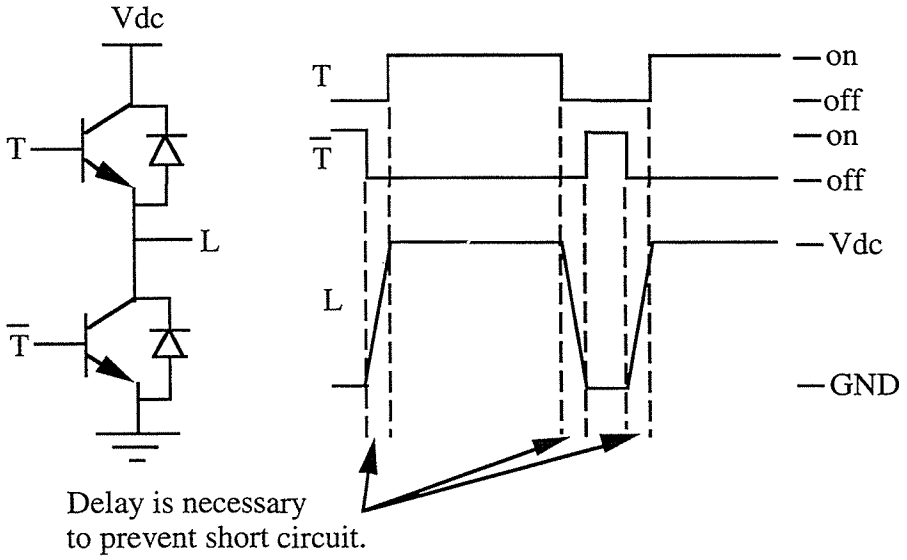

Figure 8-13. *Line voltage generation with the series of two transistors. (Redrawn from Sechpper, 1990.)*

There are four parameters to be set, PWM basic period or basic frequency, delay time, duty resolution, and switching method. There are four reasons to choose the PWM frequency as high as possible (Schepper, 1990):

1. The linear characteristics of voltage versus duty are only obtained if the PWM period is much smaller than the electrical time constant of the motor.

2. Aiming at small ripple, the PWM period T should be as small as possible.
3. The PWM frequency should be taken higher than the sensitivity of the human ears which is about 16 kHz max in order to avoid annoying noise.
4. The PWM period can be seen as one part of the phase delay of the current loop causing instability when increasing the control gains.

There are however 3 reasons to choose small PWM frequency (Schepper, 1990):

1. The transistor loss in the form of switching dissipation is proportional to the switching frequency and should therefore be taken as small as possible.
2. As the PWM frequency increases, total delay time also increases. This means uncontrollability and also non-linearity for small current increases to some extent.
3. If the PWM period is too small, the resolution on the duty also decreases. If the clock cycles for peripheral circuits with the present IC technologies are about 10 MHz, then a maximum 9 bit resolution is available for a PWM frequency of 20 kHz.

The delay time is generally given in specification sheet of transistor. The delay time is direct cause of non-linearity for small current and should be chosen as small as possible. Experiments and simulations have shown that 4 or 5 bit resolution are enough for PWM duty (Schepper, 1990). The reason is that the gains of the control algorithms become bigger and bigger as the performance of controller increases. Accordingly, the controller approaches more and more to the theoretically optimal "bang-bang" controller which has 1 bit output resolution (ON-OFF) in principle.

An AC synchronous motor (BLDC motor) can be thought of as 3 impedances connected with each other in a delta form like in the Figure 8-14. Three transistor pairs are tied together to generate 3 line voltages such that the phase voltages (voltages over the impedances) are varying in the manner that each voltages are 120 degrees shifted sinusoidal waves. The double sided switching method is practically impossible to be use for the

BLDC motor. The single sided and symmetric switching method are more appropriate. The following Table 8-1 shows that care should be taken when generating sinusoidal phase voltages. In order to make 100% use of the voltage source, 120 degree shifted sinusoidal line voltages should be adopted.

The following equations (8-3) and (8-4) show how to find out the appropriate counter number for PWM frequency and delay. The servo controller boards is designed to have the PWM signal lines from the FSC. These lines go to the pre driving circuit in order to drive the signals up the level which the power transistor can be controlled with.

$$frequency[counter\ number] = \frac{FFFF \times PWM\ freq[Hz]}{clock\ freq[Hz]} \tag{8-3}$$

$$delay[counter\ number] = \frac{FFFF \times delay[\mu \sec]}{period[\mu \sec]} \tag{8-4}$$

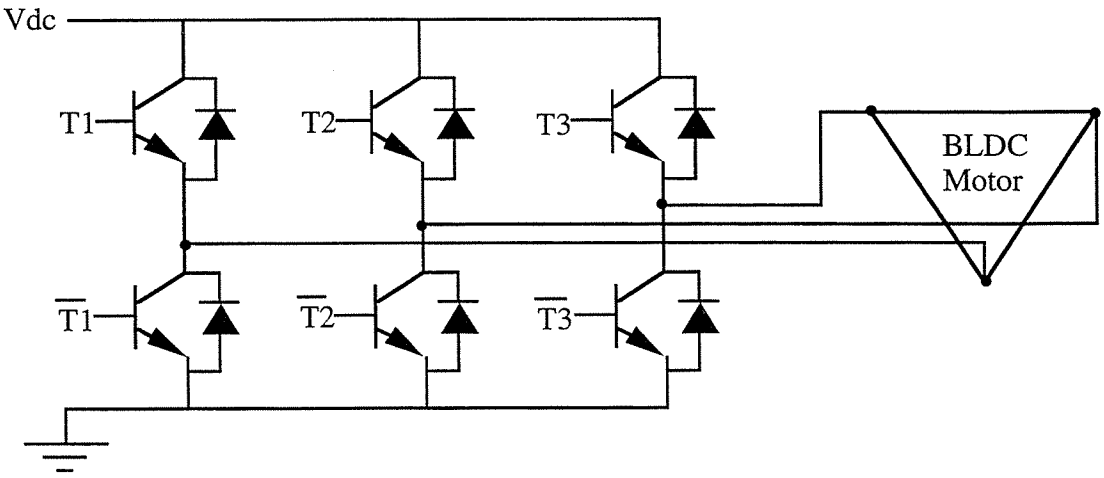

Figure 8-14. *Power transistor array and PWM configuration for AC synchronous motor.*

LINE VOLTAGE to PHASE VOLTAGE TRANSFORMATION:

phase voltage u = V_{dc} • (duty T_2 - duty T_1)

phase voltage v = V_{dc} • (duty T_3 - duty T_2)

phase voltage w = V_{dc} • (duty T_1 - duty T_3)

SINUSOIDAL LINE VOLTAGES give REDUCED PHASE VOLTAGES:

duty T_1 = 50% + 50% • sin θ

duty T_2 = 50% + 50% • sin (θ+120)

duty T_3 = 50% + 50% • sin (θ+240)

↓

phase voltage u = 86% • V_{dc} • cos(θ+60)

phase voltage v = 86% • V_{dc} • cos(θ+180)

phase voltage w = 86% • V_{dc} • cos(θ+300)

where 86% = $\sqrt{3}/2$.

SHIFTED SINUSOIDAL LINE VOLTAGES give FULL SCALE PHASE VOLTAGE:

for θ = 210 to 330:

duty T_1 = 0%

duty T_2 = 58% • [sin(θ+120) - sinθ]

duty T_3 = 58% • [sin(θ+240) - sinθ]

for θ = 330 to 90:

duty T_1 = 58% • [sinθ – sin(θ+120)]

duty T_2 = 0%

duty T_3 = 58% • [sin(θ+240) - sin(θ+120)]

for θ = 90 to 210:

duty T_1 = 58% • [sinθ – sin(θ+240)]

duty T_2 = 58% • [sin(θ+120) - sin(θ+240)]

duty T_3 = 0%

↓

phase voltage u = V_{dc} • cos(θ+60)

phase voltage v = V_{dc} • cos(θ+180)

phase voltage w = V_{dc} • cos(θ+300)

,where 58% = $1/\sqrt{3}$.

Table 8-1. *Generating sinusoidal phase voltages. (Redrawn from Schepper, 1990.)*

8-3-5. Power Transistor and Its Predriving Circuit

An intelligent power module has been chosen for the invertor circuit. This module has 6 Insulated Gate Bipolar Transistors (IGBT) which form 3 phase inverting circuit like the Figure 8-14 and a protection circuit inside which covers over current, over temperature, wrong control signals, and low or over voltage of gate control signals. This module also has one IGBT for break circuit. The protection function makes the motor controller more reliable. The fault signal from the protection circuit of the module is hooked up to the PWM reset pin of the FSC and to the relay that cuts off the circuit breakers of 3 phase 220 V lines.

This IGBT module requires at least 15 V gate signal to turn it on and off. The FSC generates PWM signals but these are not high enough to drive the IGBT's. The pre driving circuit amplifies 5 V PWM signals to 15 V. High speed switching of high power causes terrible noise problem. The controller logic circuit side is electrically isolated from the power circuit side using high speed opto isolators and the 15 V powers that are supplied to the IGBT's through the opto-isolators are totally isolated using a transformer. The pre driving circuit is shown in the Appendix .

8-3-6. Printed Circuit Board Design and Fabrication

The designed circuit has been fabricated on the Printed Circuit Board (PCB). The 4 layer board whose inner two layers are ground and +5 V power was selected in order to reduce noise problem. The developed circuit board is driven with 20 MHz clock, so 4 layer is necessary due to the capacitive noise problem.

The circuit was drawn using the PCB CAD software, OrCAD. And then the output file which is GERBER format was sent out to a PCB manufacturer. The circuit drawing with the OrCAD is shown in the Appendix . And the board layout and the traces of the topside and the bottom side are shown in the Appendix . The following picture shows the fabricated PCB. The Figure 8-15 shows the assembled servo motor controller. The big chip around center of the board is the FSC chip. All peripheral circuits including the PCB

and the power circuits are designed and built for the TMR controller. The Figure 8-16 shows the TMR controller. Two separate servo motor controller are placed right on the 80486 rack mount industrial PC.

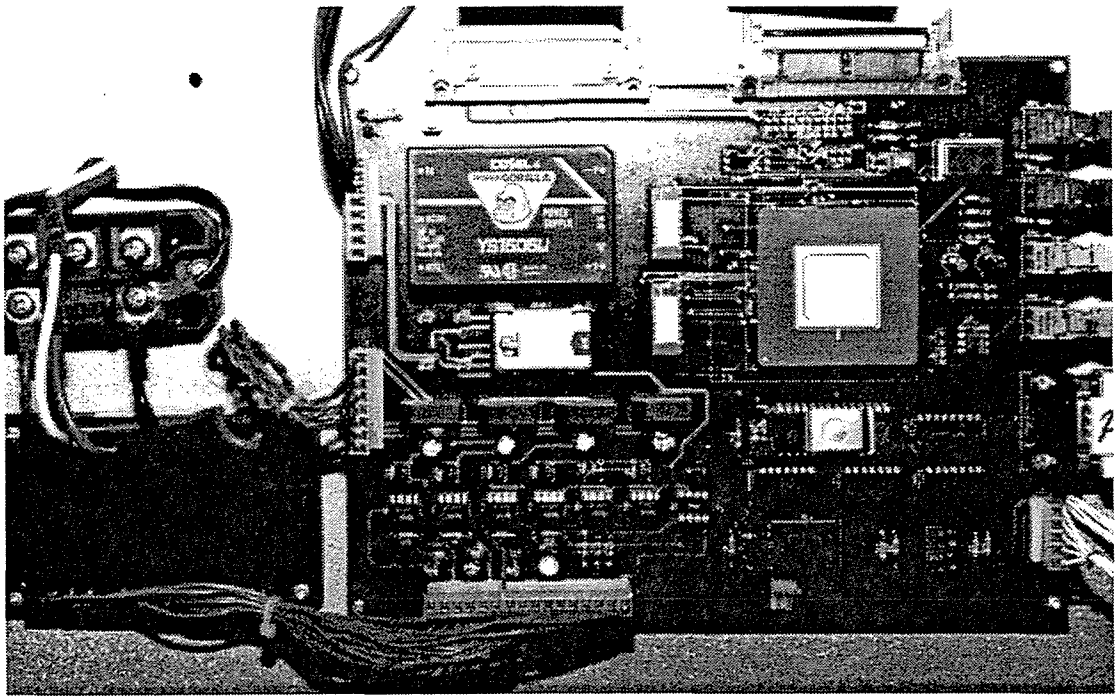

Figure 8-15. *The servo motor controller board equipped with the FSC.*

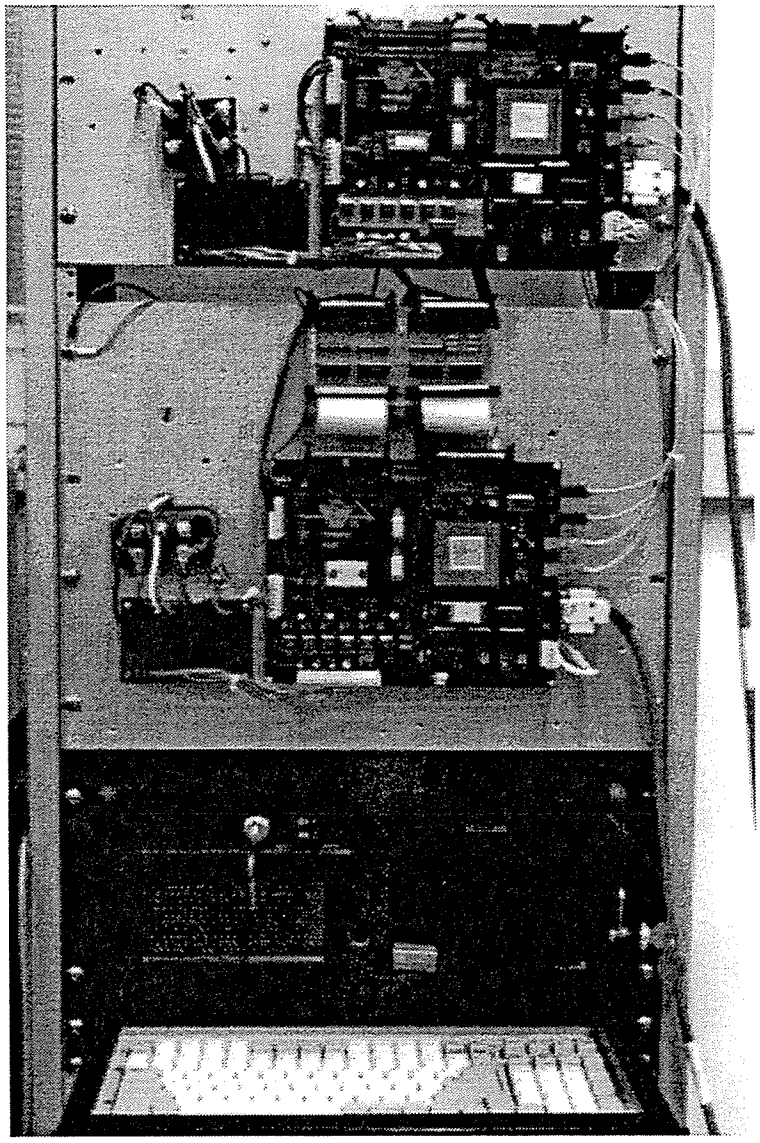

Figure 8-16. *Front view of the TMR controller.*

8-4. BLDC Motor Control

The structure of the BLDC motor is opposite to DC motor, in the sense that its rotor contains permanent magnet and its stator contains manipulative electric coil. A mathematical model can be obtained applying d-q motor model. Figure 8-17 shows the d-q motor model of the BLDC motor. The following equations (8-5) are the voltage-current relations driven from the Figure 8-17. And the equation (8-6) is the current-torque relation (Dote and Kinoshita, 1990):

$$\begin{bmatrix} V_{ds} \\ V_{qs} \end{bmatrix} = \left(R_s + j\omega L_s\right)\begin{bmatrix} I_{ds} \\ I_{qs} \end{bmatrix} + \omega_m \begin{bmatrix} L_s I_{qs} \\ -\left(L_s I_{ds} + \Phi_m\right) \end{bmatrix} \tag{8-5}$$

$$T_{sr} = \frac{3}{4} \times (number\ of\ poles) \times \Phi_m I_{qs} = J\dot{\omega}_m + B\omega_m + T_l \tag{8-6}$$

where the subscript s represents stator and

R_s is the armature resistance,

L_s is the armature inductance,

J is the motor moment of inertia,

Φ_m is the magnetic flux of the permanent magnet,

ω_m is the angular velocity of the motor,

B is the angular coefficient of viscous friction,

V_{ds}, V_{qs}, I_{ds}, I_{qs} are *d, q* axis voltage and currents,

T_l is the load torque.

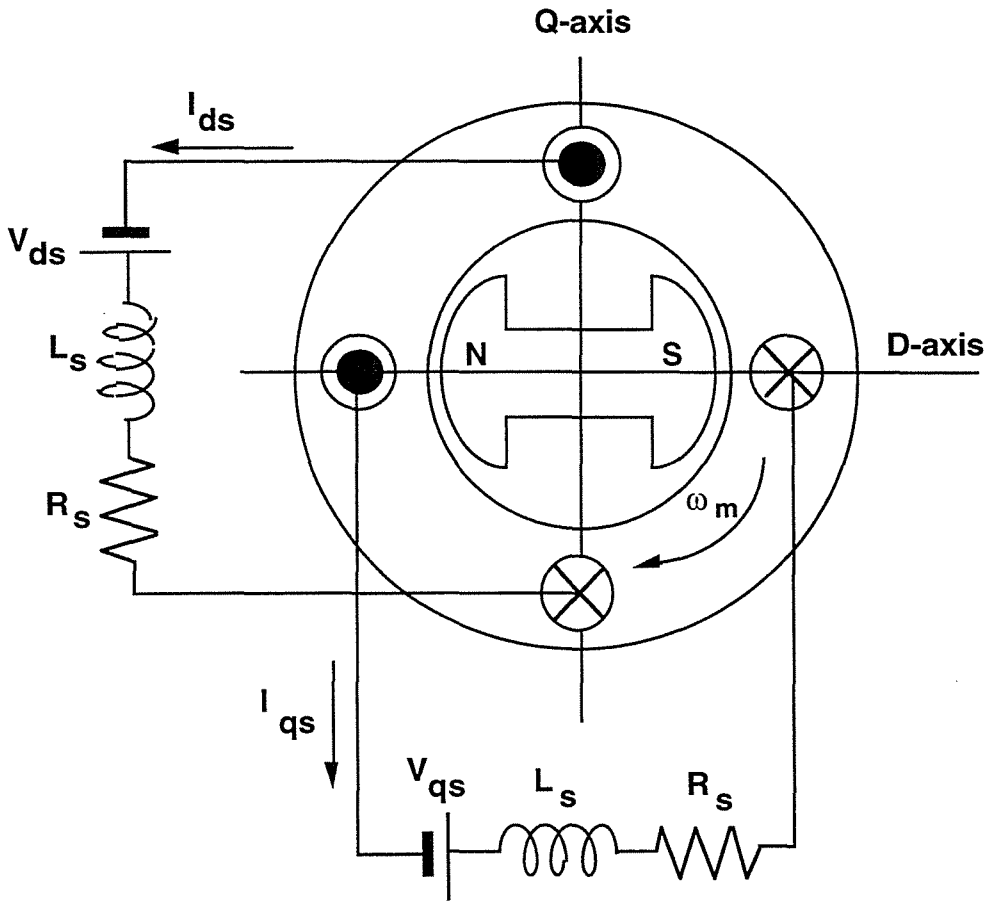

Figure 8-17. *The d-q motor model of BLDC motor. (Redrawn from Schepper, 1990.)*

I_{ds} is controlled to be zero. Then, BLDC motor control problem becomes DC motor control one. I_{qs} becomes the current of the motor.

The currents I_{ds}, I_{qs} are derived by transformation from the detected currents, I_u, I_v, and I_w which are the phase currents. Also, the manipulative voltages V_{ds} and V_{qs} are applied after transformation to the phase line voltages V_u, V_v, and V_w. The transformation equations can be easily derived by considering that the u, v, and w phases should contain 3 phase AC voltage and 3 phase AC currents, which means that those voltages and currents can be described by three 120 degree shifted sine or cosine curves. If cosine curves are used to describe the transformation from the q-axis to the u, v, and w phase then sine curves should be used for the d-axis.

As the (u,v,w) plane contains 3 degree of freedom and the (d,q) plane 2 degree of freedom, an additional factor m is needed to determine the transformation one by one. The third constraint that can be used is the constraint of invariant power transformation,

$$V_u I_u + V_v I_v + V_w I_w = V_q I_q + V_d I_d. \tag{8-7}$$

The factor m can then be determined as $\sqrt{2/3}$. This proportional factor is however only of mathematical importance because in a real controller this factor is completely absorbed into other control gains. For the voltage transformation m will be included in the voltage PWM gains, and for the current transformation m is integrated in the gains of current detection and the gains of the control law. The final transformation equation is given as

$$\begin{bmatrix} u \\ v \\ w \end{bmatrix} = \sqrt{\frac{2}{3}} \begin{bmatrix} \cos\theta & \sin\theta \\ \cos(\theta+120) & \sin(\theta+120) \\ \cos(\theta+240) & \sin(\theta+240) \end{bmatrix} \begin{bmatrix} q \\ d \end{bmatrix}. \tag{8-8}$$

There are two ways to connect the windings of a 3 phase motor: the star and the delta configuration. Despite of the fact that the most of BLDC and AC induction motors adopt the delta winding configuration for practical reasons, it is mathematically possible and more convenient to assume the windings as star configuration. An important property of the star configuration is that the line currents behave like

$$I_u + I_v + I_w = 0. \tag{8-9}$$

With this property and the intrinsic property of 3 phase AC voltages,

$$V_u + V_v + V_w = 0, \tag{8-10}$$

the above transformation equations can be rewritten in the form,

$$\begin{bmatrix} u \\ v \end{bmatrix} = \sqrt{\frac{2}{3}} \begin{bmatrix} \cos\theta & \sin\theta \\ \cos(\theta+120) & \sin(\theta+120) \end{bmatrix} \begin{bmatrix} q \\ d \end{bmatrix}$$

$$w = -u - v \tag{8-11}$$

or

$$\sqrt{2}\begin{bmatrix} \sin(\theta+120) & -\sin\theta \\ -\cos(\theta+120) & \cos\theta \end{bmatrix} = \begin{bmatrix} q \\ d \end{bmatrix}. \tag{8-12}$$

This form is better suited for software implementation due to higher execution speed.

Figure 8-18 shows the control block diagram. There are two different variables to be controlled, velocity, and current depending on the TMR control algorithm. If the final command input to the actuator (BLDC motor in our case) is velocity of driving wheel, the variable to be controlled should be velocity of the motor. However, if it is the torque of the driving wheel, then the variable to be controlled should be current which is proportional to the motor torque. So, the motor control consists of two control loops, current control loop, and velocity control loop, which forms multi-loop control system. Since the electric time constant of a motor is much faster than its mechanical time constant, the command following of the inner loop, that is current loop, is so fast that it does not affect the outer loop control performance. Also, the velocity loop can be skipped in the case that the control command of the TMR control algorithm is motor torque.

There are two corresponding sensors to each control loops: the hall effect sensor to measure current and the incremental encoder to measure motor velocity through differentiation. The voltage output that is finally supplied to the motor is amplified using Pulse Width Modulation (PWM) circuit.

The Proportional and Integral (PI) control algorithm is applied to both control loops. The current controller controls the current in R-L circuit and compensates the back voltage which is proportional to motor velocity. This back voltage can be considered as a slow disturbance compared to the current behavior and can thus be completely compensated by

using integral control action. Similarly, velocity disturbance due to load inertia, frictional force, etc., can be compensated by using integral control.

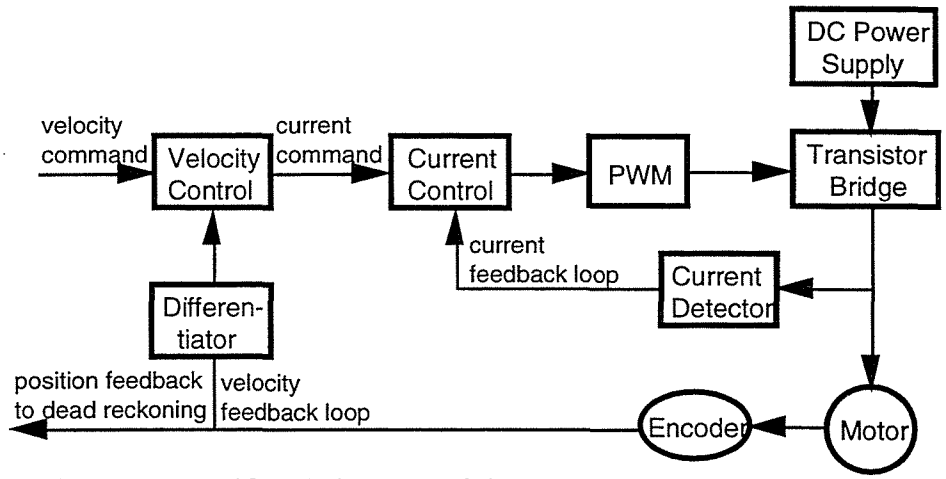

Figure 8-18. *The control block diagram of the motor speed and current control.*

An additional advantage of the multi-loop feedback control formulation is that the different control loops can be executed with different sampling times according to the dynamic behavior of their controlled variables. This dynamic behavior can be quantified in terms of the natural frequencies of the controller variables. Typical servo motors(200W to 1.5 kW) have the following frequencies,

- current: 500 Hz to 1000 Hz,
- position & velocity: 0.1 Hz to 10 Hz.

This fact leads obviously to different sampling times for the different loops. The position and velocity loop do not have to be executed with the same speed as the current loop.

These natural frequencies give only a upper limit for the sampling times. For performance reasons and technical limitations, the sampling times are chosen as followings:

- current loop: 50 micro-second,
- velocity loop: 500 micro-second.

A flow chart and execution scheme of the control software is given in the Figure 8-19. After initialization procedure, the different control loops are scheduled by polling the timer of the FSC. Then, the human interface processing is executed with the lowest priority to give the chances to set control parameters. The control parameters can be changed any time during control sampling by the virtue of the dual-port communication method. The flow charts of the different control loops are also given in the Figure 8-20, 21. The human interface allows the user to interfere freely. Control gains can be changed, variables can be displayed continuously, etc.

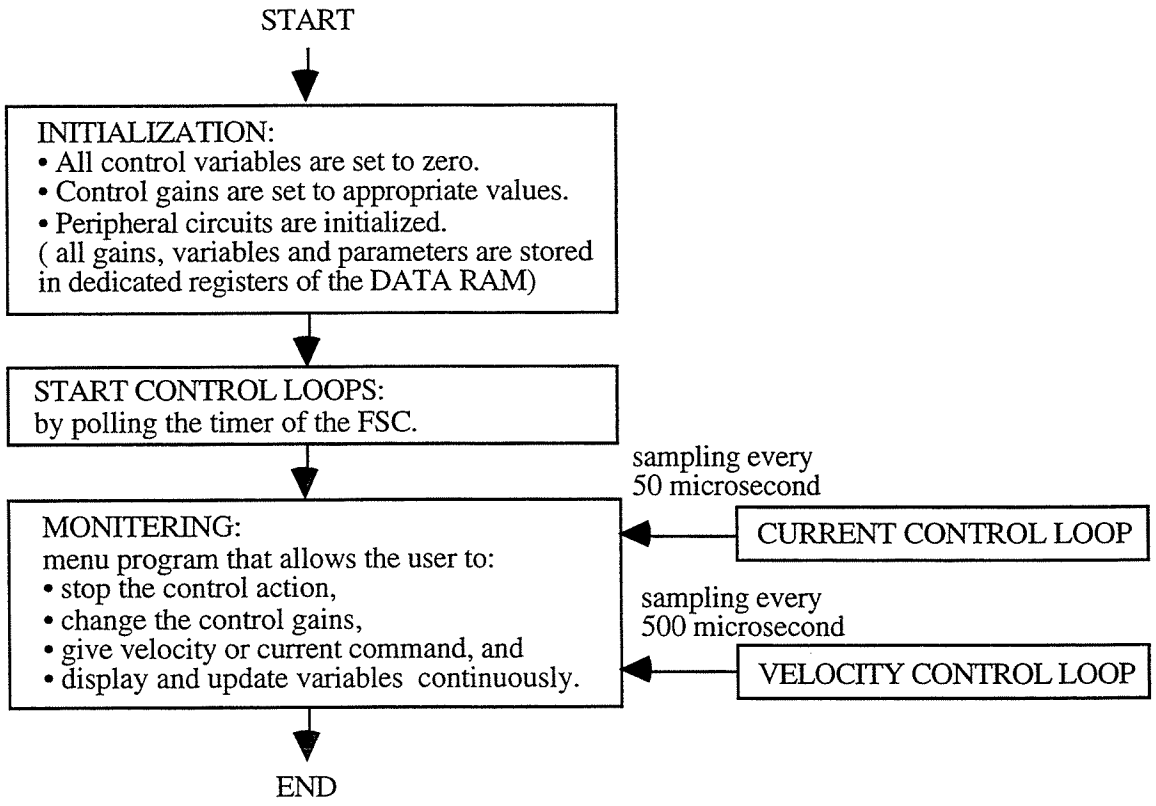

Figure 8-19. *Flowchart of the control software.*

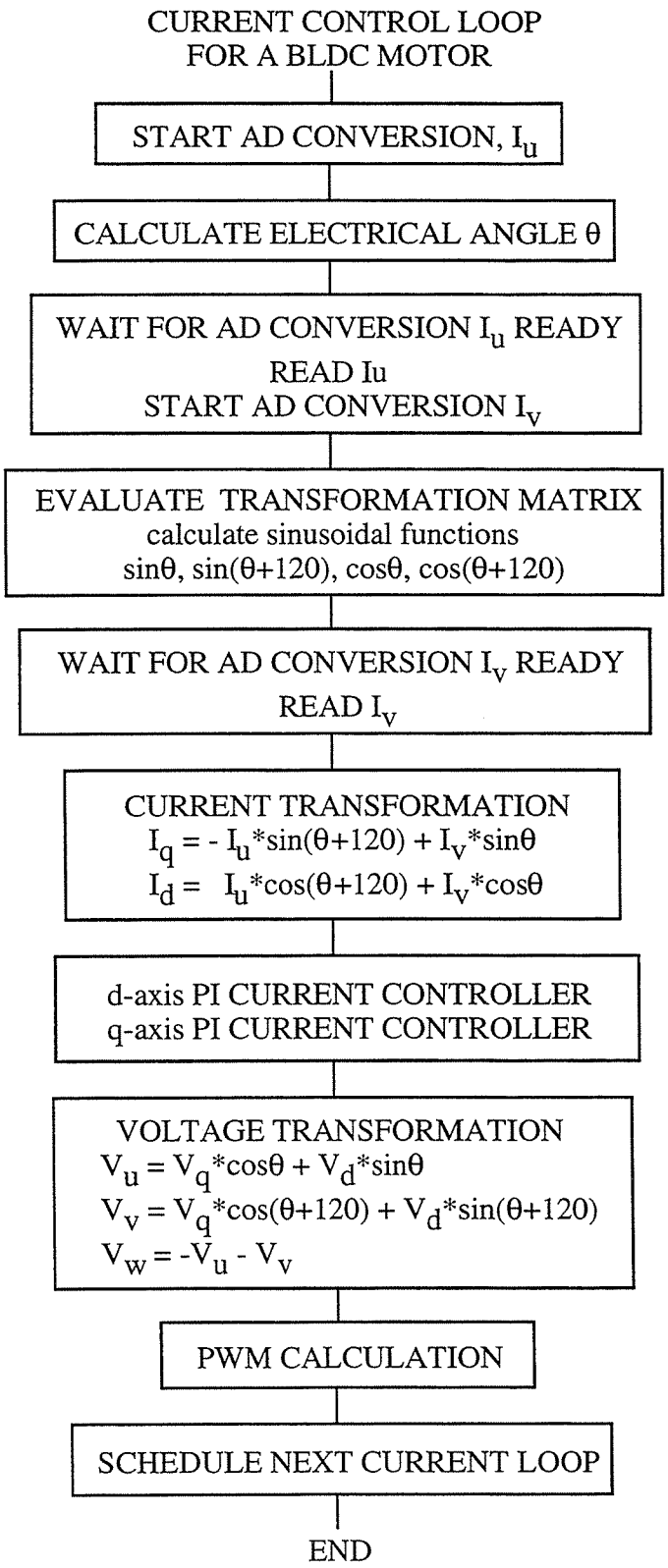

Figure 8-20. *Flowchart of the current control software for BLDC motor.*

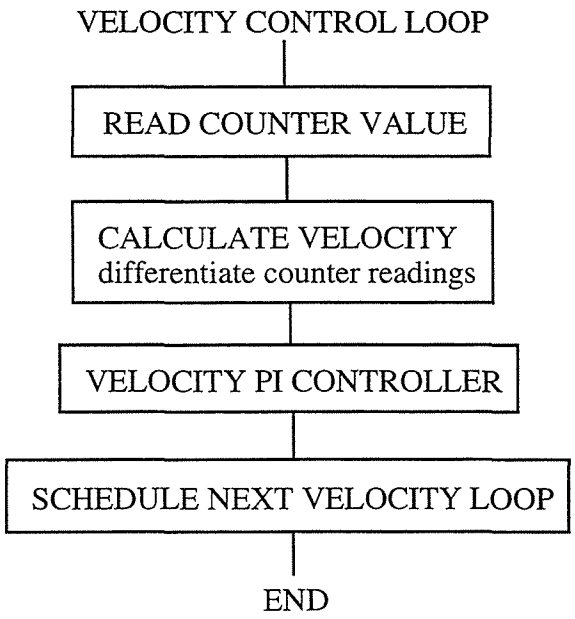

Figure 8-21. *Flowchart of the velocity control software for BLDC motor.*

The following Figure 8-22 shows one example of time response. The first figure is the time response of current control when I_{qs} reference is 500 in A/D converter number that corresponds to 0.95 A in physical value. And remember that I_{ds} is always controlled to zero. The unit of x-axis is micro second. The second figure shows the time response of velocity control when there is no external load except the motor rotor inertia. The reference velocity is 1000 RPM. And the velocity PI control gains are 20000 and 1500 respectively.

The Figure 8-23 shows speed responses of the TMR platform not just bear motor when giving each wheels motor commands in rpm. The linear velocity and angular velocity are taken from the TMR position tracking system. The drive wheel motors are facing each other, so that the signs of the velocity commands should be opposite in order to get straight line motion.

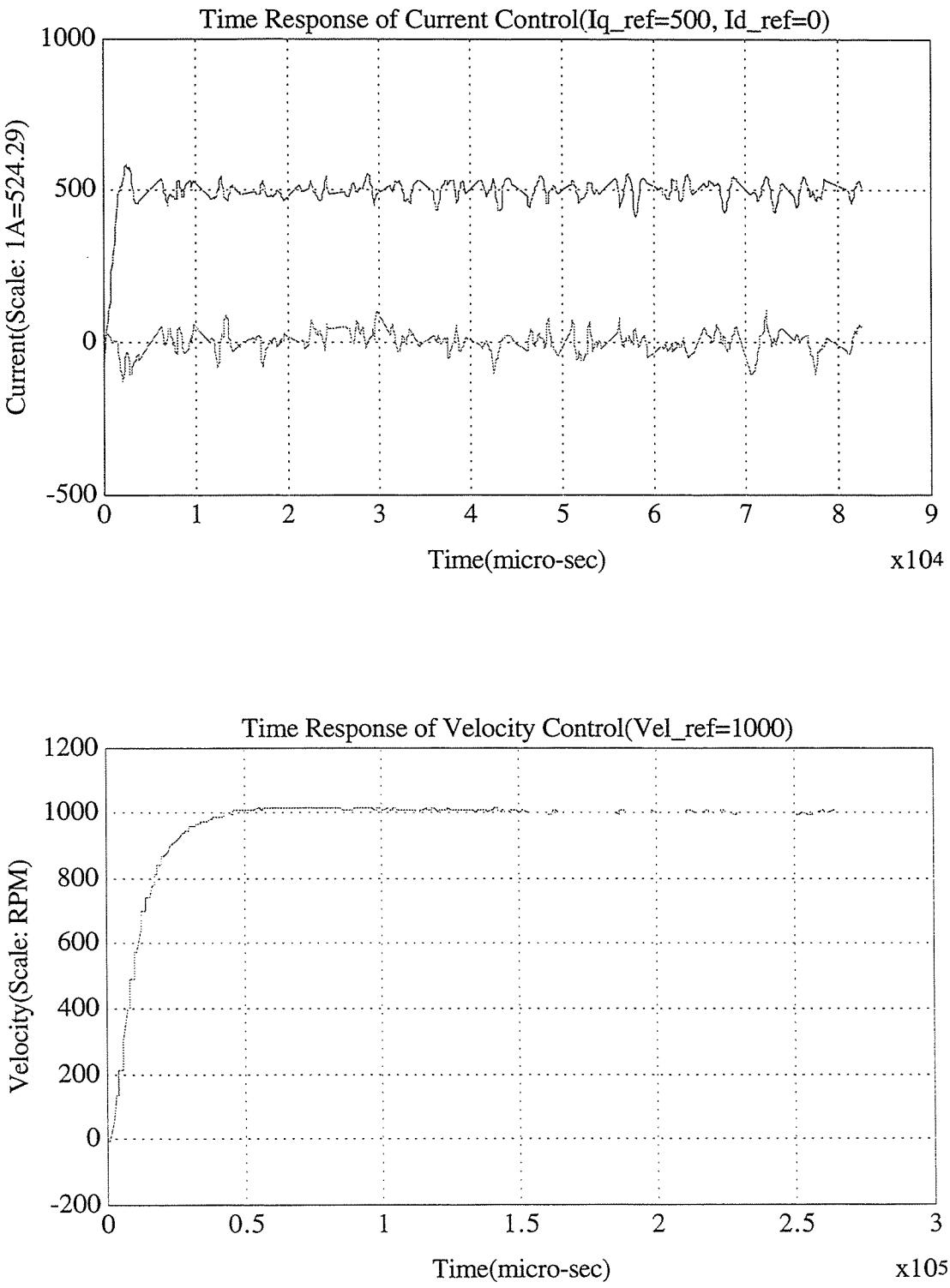

Figure 8-22. *Experimental results of brushless DC motor control.*

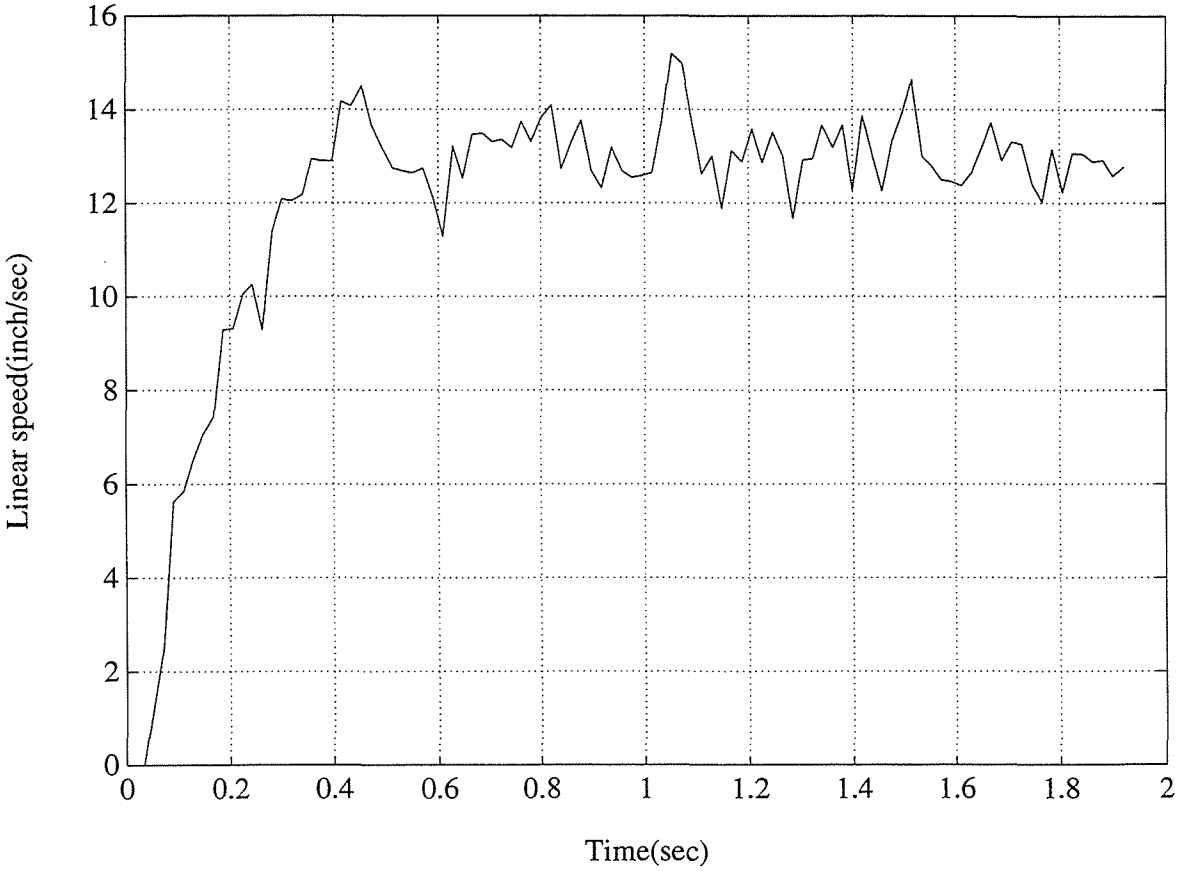

Figure 8-23 (a). Linear velocity response, left wheel motor speed: 100 rpm, right wheel speed: -100 rpm, K_P=20000, K_I=1500.

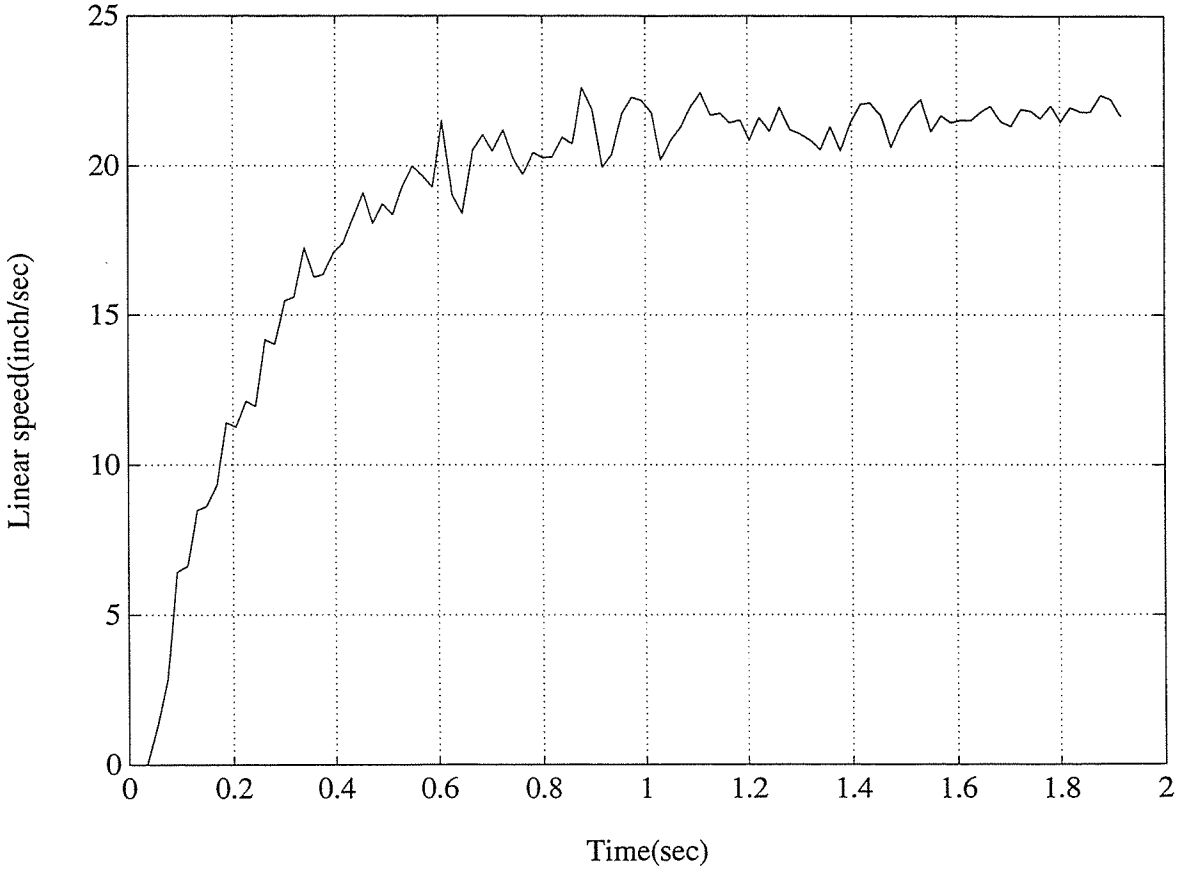

Figure 8-23 (b). Linear velocity response, left wheel motor speed: 200 rpm, right wheel speed: -200 rpm, K_P=20000, K_I=1500.

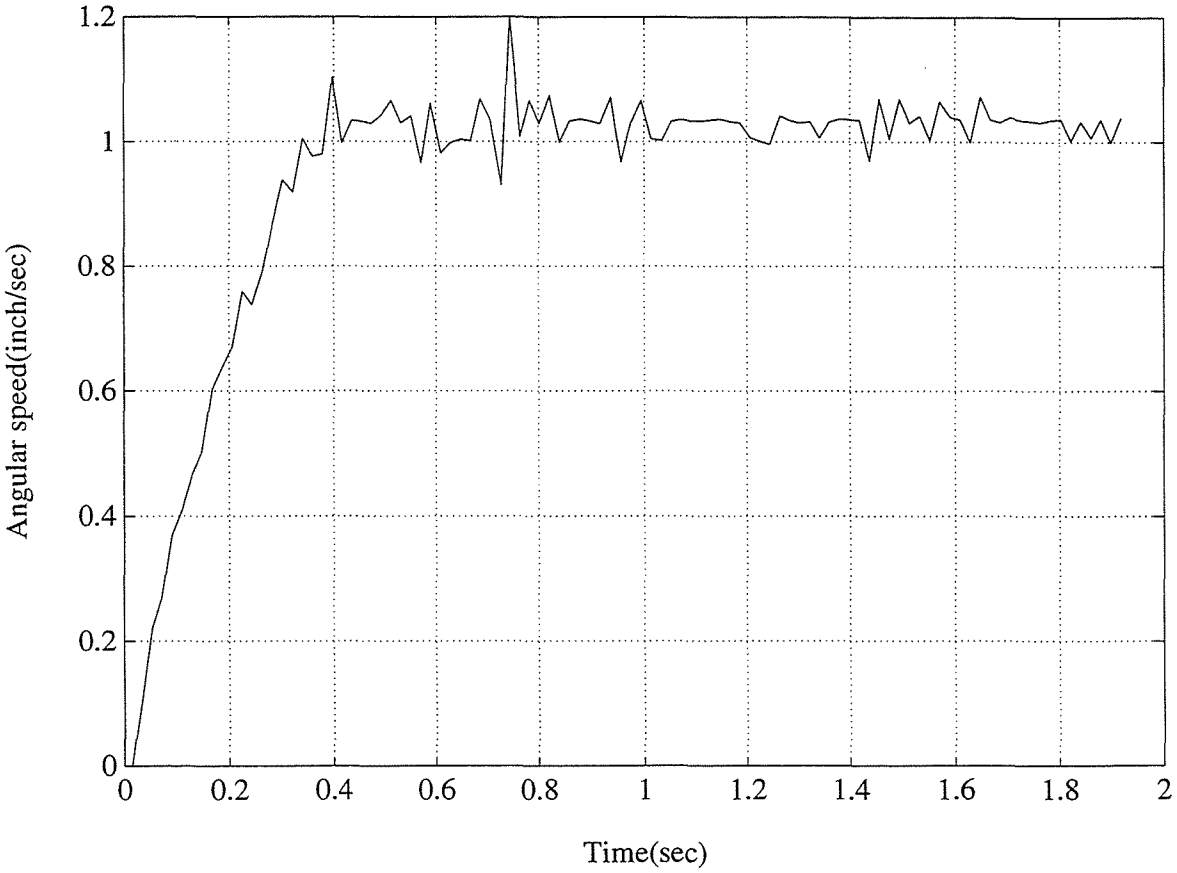

Figure 8-23 (c). Angular velocity response, left wheel motor speed: -100 rpm, right wheel speed: -100 rpm, K_P=20000, K_I=1500.

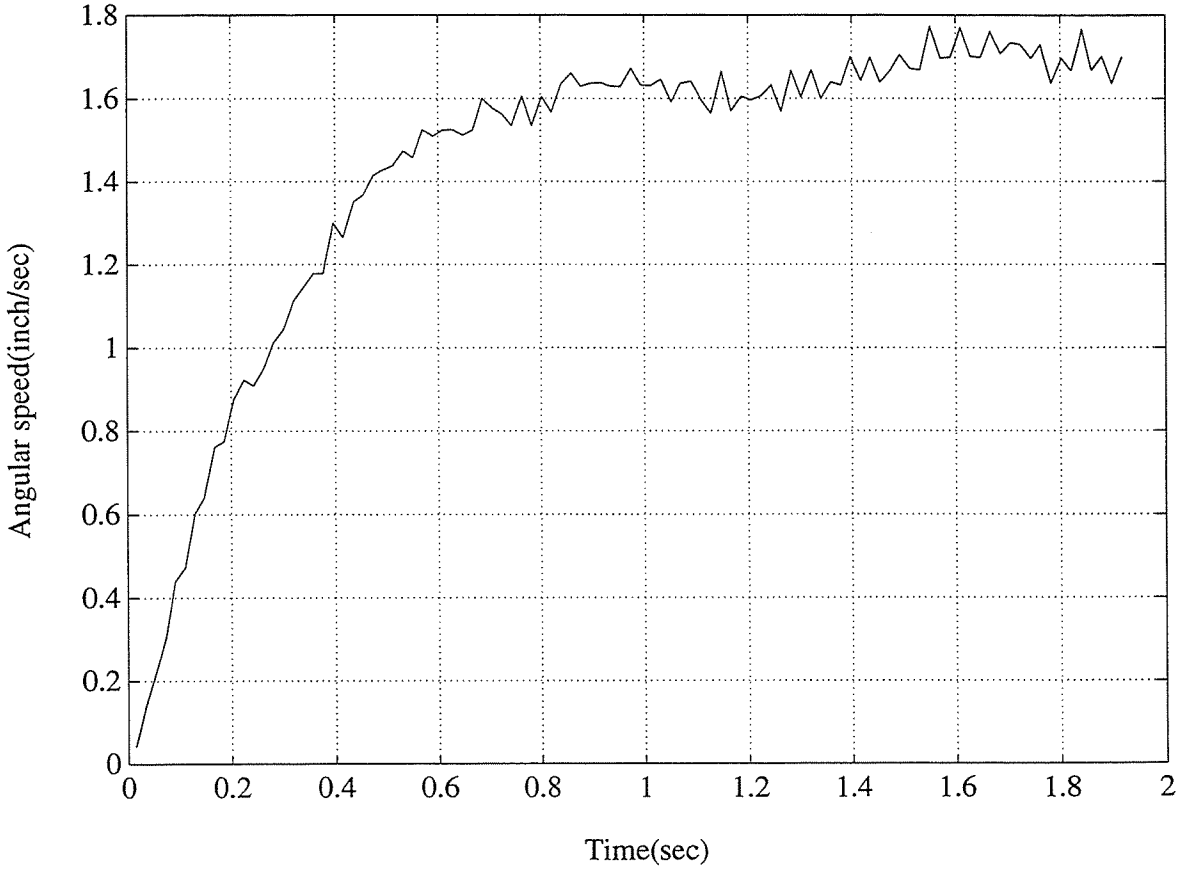

Figure 8-23 (d). Angular velocity response, left wheel motor speed: -200 rpm, right wheel speed: -200 rpm, K_P=20000, K_I=1500.

Figure 8-23. *Velocity responses of the TMR platform when giving motor velocity commands.*

Chapter 9. Conclusions

The purpose of this thesis was to develop the most appropriate control system for the Tethered Mobile Robot. The development involved control system architecture, tracking control algorithms, and controller hardware for their implementations.

Three different control modes, *Manual Control with Joystick, Automatic Trajectory Tracking Control, and Robust Velocity Control,* were proposed for most of highway maintenance operations after exploring their requirements. Most of highway maintenance operations which require positioning equipment within close proximity to a support vehicle could be automated with these control modes.

Manual Control with Joystick mode was designed to be performed by human operator with a joystick. This control mode can be used for the cases when the operator needs to manually place the TMR at a specific position or to make the TMR trace a path manually.

Automatic Trajectory Tracking Control mode was provided for the case that the TMR should automatically track a specific reference path without any manual operations. The reference path for this mode could be generated either from pre-defined table in disk file form or from a real time sensor, which formed a sensor based real time navigation problem. The roadway sign stenciling, for example, could use this control mode with a sequence of pre-defined reference path commands to follow a pre-defined roadway sign. Also, this control mode could be used for the crack sealing operation to track the crack on pavement surface with the laser range sensor.

Many of highway maintenance operations require very robust control systems which are to external force disturbances that are hard to estimate. The routing process for the crack sealing operation is a good example. The routing force is difficult to predict and also severely fluctuating during the process. *Robust Velocity Control* mode was provided to

surmount these difficulties. This control mode was developed with dynamic model of the TMR.

A new non-linear path tracking control algorithm for a 2 DOF differentially steered mobile robot was derived for the *Automatic Trajectory Tracking Control* and its exponential stability was proved in this thesis. One difficulty of non-holonomic mobile robot control problem arose from non-square nature of its equations of motion. A new idea was proposed to overcome this inherent problem and an exponentially stable non-linear control law was successfully derived using feedback linearization technique. This approach was simple, systematic, and unique compare to other existing research papers about mobile robot guidance control. The stability for a non-linear system usually does not guarantee its robustness to uncertainties. The stability, performance, and robustness of the developed algorithm against parametric uncertainty and unmodeled dynamics was explored through simulations. This control law was implemented with the TMR platform and the developed controller. Both of tracking control with reference table and tracking control with the laser range sensor were tested. From the simulations and experiments, it was concluded that this stable non-linear control algorithm would be more appropriate to the applications to highway maintenance operations than the control algorithms developed for general purpose mobile robots.

In the TMR control, the biggest concerns were the non-linear terms due to centrifugal force and routing force that was very hard to estimate. Fortunately, we could figure out the upper and lower bounds of the fluctuating routing force using an appropriate experimental method. Therefore, the robust control using the sliding mode technique was one of the most appropriate to the TMR control problem. No papers have not been found concerning the sliding mode control issue for wheeled mobile robot even though much research has been conducted about wheeled mobile robot control. In this research, the sliding mode control for wheeled mobile robot was formulated and this was a unique control strategy for

the TMR and general wheeled mobile robot. From simulations with TMR parameter close to real situation, it was concluded that the developed control law could be one of best solution for harsh operations such as crack routing process.

The TMR controller was optimally designed using 80486 CPU and the motor controller equipped with the Flexible Servo Controller, in order to implement the developed control algorithms. The motor controller was the most important part in the TMR controller hardware. The motor controller board was designed with the Flexible Servo Controller (FSC) chip and fabricated using the Printed Circuit Board CAD software. This servo motor controller was the first application of the FSC chip. The TMR controller was designed to have unique feature utilizing the advantages of the servo motor controller board equipped with the FSC. The PI control law was implemented with this controller and optimum gains were determined through experiments. The functionality and performance of this TMR controller were proved through motor control experiments and TMR control experiments. The current control loop sampling time was 50 micro-second including current vector calculations and A to D conversion, etc.

The contribution of this research in academic and also practical point of view can be summarized as followings.

1. Optimum control system architecture for the TMR was developed including software and hardware to accomodate most of possible processes of highway maintenance operations.
2. New approach to derive a non-linear stable tracking control law for non-holonomic mobile robot was created. This idea simplified derivation of a non-linear stable tracking control law for non-holonomic mobile robot.
3. Robust sliding mode control was formulated for the TMR and its robustness and performance were proved through simulations. This can be easily extended to general mobile robot control problem.

4. New servo motor controller equipped with the FSC was designed and fabricated. This servo motor controller was the first application using the FSC chip.
5. The TMR controller was designed and fabricated with the servo motor controller. The TMR controller was designed to have unique feature utilizing the advantages of the servo motor controller board.
6. The functionality and performance of all necessary control algorithms and hardware were shown through actual demonstration.

REFERENCES

Alexander, J.C. and Maddocks, J.H., "On the Kinematics of Wheeled Mobile Robots," Autonomous Robot Vehicle (I.J. Cox and G.T. Wilfong, eds), pp. 5-24, Springer-Verlag, 1990.

Banta, L.E., "A Self Tuning Navigation Algorithm," IEEE Int. Conf. on Robotics and Automation, pp. 1313-1314, 1988.

Baumgartner, E.T. and Skaar, S.B., "An Autonomous Vision-Based Mobile Robot," IEEE Trans. Automatic Control, Vol. 39, No. 3, pp. 493-502, Mar. 1994.

Borenstein, J., "A Model-Reference Adaptive Controller for a Differential-Drive Mobile Robot," Proc. IEEE Int. Conference on Robotics and Automation, pp. 3091-3096, 1994.

Borenstein, J., "The CLAPPER: A Dual-drive Mobile Robot with Internal Correction of Dead-reckoning Errors," Proc. IEEE Int. Conference on Robotics and Automation, pp. 3085-3090, 1994.

Boyden, F.D. and Velinsky, S.A., "Dynamic Modeling of Wheeled Mobile Robots for High Load Applications," Proc. IEEE Int. Conf. on Robotics and Automation, pp. 3071-3078, 1994.

Boyden, F.D. and Velinsky, S.A., "Limitations of Kinematic Models for Wheeled Mobile Robots," Advances in Robot Kinematics and Computational Geometry (J. Lenarčič & B. Ravani, eds.), Kluwer Academic Publishers, Dordrecht, Netherlands, pp. 151-160, 1994.

Canudas, C. de Wit and Roskam, R., "Path Following of a 2-DOF Wheeled Mobile Robot under Path and Input Torque Constraints," Proc. IEEE Int. Conference on Robotics and Automation, pp. 1142-1147, 1991.

Cho, D., Kato, Y., and Spilman, D., "Sliding Mode and Classical Controllers in Magnetic Levitation Systems," IEEE Control Systems Magazine, Vol. 13, No. 1, pp. 42-48, Feb. 1993.

Cox, I.J. and Wilfong, G.T., Autonomous Robot Vehicle, Springer-Verlag, 1990.

Dote, Y. and Kinoshita, S., Brushless Servo motors Fundamentals and Applications, Oxford Science Publications, 1990.

Gentile, A. and Mangialardi, L., "Comparisons between Different Mobile Robot Configurations," 3rd Int. Workshop on Advances in Robot Kinematics, 1992.

Hong, D., Yamazaki, K., and Velinsky, S.A., "S-cube: Super Servo System for Intelligent Motion Control for Mechatronics Systems," Intelligent Automation and Soft Computing (M. Jamshidi, C.C. Nguyen, R. Lumia, and J. Yuh, eds.), Vol. 1, TSI Press, pp. 505-510, 1994.

Jo, B.R., Ahn, H.W., and Youn, M.J., "Multi-Variable Sliding Mode Control of Quantum Boost SRC," IEEE Trans. Control Systems Technology, Vol. 2, No. 2, pp. 148-150, June 1994.

Kanayama, Y., Kimura, Y., Miyazaki, F., and Noguchi, T., "A Stable Tracking Control Method for an Autonomous Mobile Robot," Proc. IEEE Conference on Robotics and Automation, pp. 13-18, 1990.

Kanayama, Y. and Krahn, G., "Two dimensional Transformations and Its Application to Vehicle Motion Control and Analysis," Proc. IEEE Conference on Robotics and Automation, pp. 384-389, 1993.

Kanayama, Y., Nilipour, A., and Lelm, C., "A Locomotion Control Method For Autonomous Vehicles," Proc. IEEE Conference on Robotics and Automation, pp. 1315-1317, 1988.

Khoukhi, A., "Constrained Dynamic Navigation for a Mobile Robot," Artificial Intelligence and Information Control Systems of Robots-89 (edited by Ivan Plander), pp. 335-344, 1989.

Kirschke, K.R. and Velinsky, S.A., "Histogram-Based Approach for Automated Pavement Crack Sensing," J. of Transportation Engineering, 118(5), pp. 700-710, 1992.

Kochekali, H. and Velinsky, S.A., "Adaptation of Wheeled Mobile Robots to Highway Maintenance Operations," AHMCT Research Report, 1994.

Krulewich, D.A. and Velinsky, S.A., "Development of a High Resolution Sensing System for Automated Crack Sealing Machinery," Interim Report SHRP of H-107A, Strategic Highway Research Program, National Research Council, Washington, D.C.

Kumar, V., and Waldron, K.J., "Actively Coordinated Vehicle Systems," Journal of Mechanisms, Transmissions and Automation in Design, pp. 223-231, June 1989.

Laumond, J.P., "Controllability of a Multibody Mobile Robot," IEEE Tran. Robotics and Automation, vol 9, No. 6, pp. 723-731, 1993.

Lin, W.C. and Chin, Y.-K., "Analysis of Variable-Structure Control on Vehicle Wheel-Slip Regulation," Advanced Automotive Technologies-1989 (edited by A.M. Karmel, E.H. Law, S.R. Velinsky), pp. 397-411, 1989.

Muir, P.F. and Neuman, C.P., "Kinematic modeling of wheeled mobile robots," J. Robotics Systems, 4(2), pp. 281-280, 1987.

Petrov, P.P., "Robust Trajectory Tracking Algorithms For A Wheeled Mobile Robot," IEEE International Conf. on Industrial Electronics, Control & Instrumentation, pp. 1071-1074, 1991.

Pin, F.G. and Killough, S.M., "A New Family of Omnidirectional and Holonomic Wheeled Platforms for Mobile Robots," IEEE Trans. Robotics and Automation, Vol.10, No. 4, pp. 480-489, Aug. 1994.

Reister, D.B. and Unseren, M.A., "Position and Constraint Force Control of a Vehicle with Two or More Streerable Drive Wheels," IEEE Tran. Robotics and Automation, vol 9, No. 6, pp. 723-731, 1993.

Salichs, M.A., Puente, E.A., Gachet, D., and Moreno, "Trajectory Tracking for a Mobile Robot - An Application to Contour following," IEEE International Conf. on Industrial Electronics, Control & Instrumentation, pp. 1067-1070, 1991.

Samson, C. and Ait-Abderrahim, K., "Feedback Control of a Nonholonomic Wheeled Cart in Cartesian Space," Proc. IEEE Int. conference on Robotics and Automation, pp. 1136-1141, 1991.

Schepper, F de., Yamazaki, K., Imai, M., and Satou, J., "Application of ASIC-Technology to Mechatronics Control: Development of the Flexible Servo Peripheral Chip," Annals of the CIRP, Vol. 37(1), pp. 329-332, 1988.

Schepper, F. de, "A Study on Flexible and Integrated Servo Controller for Actuators in Mechatronics Systems," Ph.D. Thesis, Toyohashi University of Technology, Japan, 1990.

Schepper, F. de and Yamazaki, K., "Development of an Asic Performing High Speed Current Loop Processing of Servo Motor Control for Mechatronics Applications," Annals of the CIRP, Vol. 38(1), pp. 355-358, 1989.

Schepper, F. de, Yamazaki, K., and Nakagami, H., "Development of a Perfect One-Chip Flexible Servo Controller by Silicon Compilation," Annals of the CIRP, Vol. 39(1), pp. 371-374, 1990.

Slotine, J.-J.E. and Li, W., Applied Nonlinear Control, Prentice Hall, 1991.

Slotine, J.-J.E., "Tracking Control of Nonlinear Systems Using Sliding Surfaces," Ph.D. dissertation, Dep. Aero. and Astro., M.I.T., Cambridge, May 1983.

Slotine, J.-J.E., "The Robust Control of Robot Manipulators," Int. J. Robotics Res., vol. 4, No. 2,1985.

Sϕrdalen, O.J., and de Wit, C.C., "Exponential Control Law for a Mobile Robot: Extension to Path Following," IEEE Trans. Robotics and Automation, Vol.9, No. 6, pp. 837-841, Dec. 1993.

Sreenivasan, S.V., Dutta, P.K., and Waldron, K.J., "The Wheeled Actively Articulated Vehicle (WAAV): An Advanced Off-Road Mobility Concept," Advances in Robot Kinematics and Computational Geometry (J. Lenarčič & B. Ravani, eds.), Kluwer Academic Publishers, Dordrecht, Netherlands, pp. 141-150, 1994.

Su, C.-Y. and Leung, T.-P., "A Sliding Mode Controller with Bound Estimation for Robot Manipulators," IEEE Trans. Robotics and Automation, Vol.9, No. 2, pp. 208-214, April 1993.

Tsumura, T., Fujiwara, N., Shirakawa, T., and Hashimoto, M., "An Experimental System for Automatic Guidance of Robot Vehicle, following the route in Memory," Proceedings 11th International Symposium on Industry Robots, pp. 187-193, 1981.

Velinsky, S.A., "Heavy Vehicle System for Automated Pavement Crack Sealing," Heavy Vehicle Systems, Special Series of the International Journal of Vehicle Design, Vol.1, No.1, pp. 114-128, 1993.

Velinsky, S.A., "Fabrication and Testing of Maintenance Equipment Used for Pavement Surface Repairs," Final Report of SHRP H-107A, National Research Council Strategic Highway Research Program, Washington DC, 1993.

Velinsky, S.A. and Kirschke, K.R., "Design Considerations for Automated Pavement Crack Sealing Machinery," Proceedings of the Second ASCE International Conference on Applications of Advanced Technologies in Transportation Engineering, pp. 76-80., 1991.

West, M. and Asada, H., "Design of Holonomic Omnidirectional Vehicle," Proc. IEEE Int. Conf. Robotics and Automation, pp. 97-103, May 1992.

White, W. A., "Development of Robotic Positioning Devices for the Automated Sealing of Cracks," M.S. Thesis, Univ. California, Davis, 1994.

Winters, S.E., "Development of Tethered Mobile Robot," M.S. Thesis, University of California, Davis, 1992.

Winters, S.E., Hong, D., Velinsky, S.A., and Yamazaki, K., "A New Robotic System Concept for Automating Highway Maintenance Operations," Proc. of SPACE '94-ASCE Conference on Robotics for Challenging Environments, pp. 374-382, 1994

Yoerger, D.R. and Slotine, J.-J.E., "Robust Trajectory Control of Underwater Vehicles," IEEE Journal of Oceanic Engr, Vol. OE-10, No. 4, pp. 462-470, Oct. 1985.

Zhang, Y. and Velinsky, S.A., "On the Tracking Control of Differentially Steered Wheeled Mobile Robots," submitted for publication, 1994.

Zhao, Y. and BeMent, S.L., "Kinematics, Dynamics and Control of Wheeled Mobile Robots," Proc. IEEE Int. Conf. on Robotics and Automation, pp. 91-96, 1992.

APPENDICES

SUBCIRCUIT CONNECTIONS

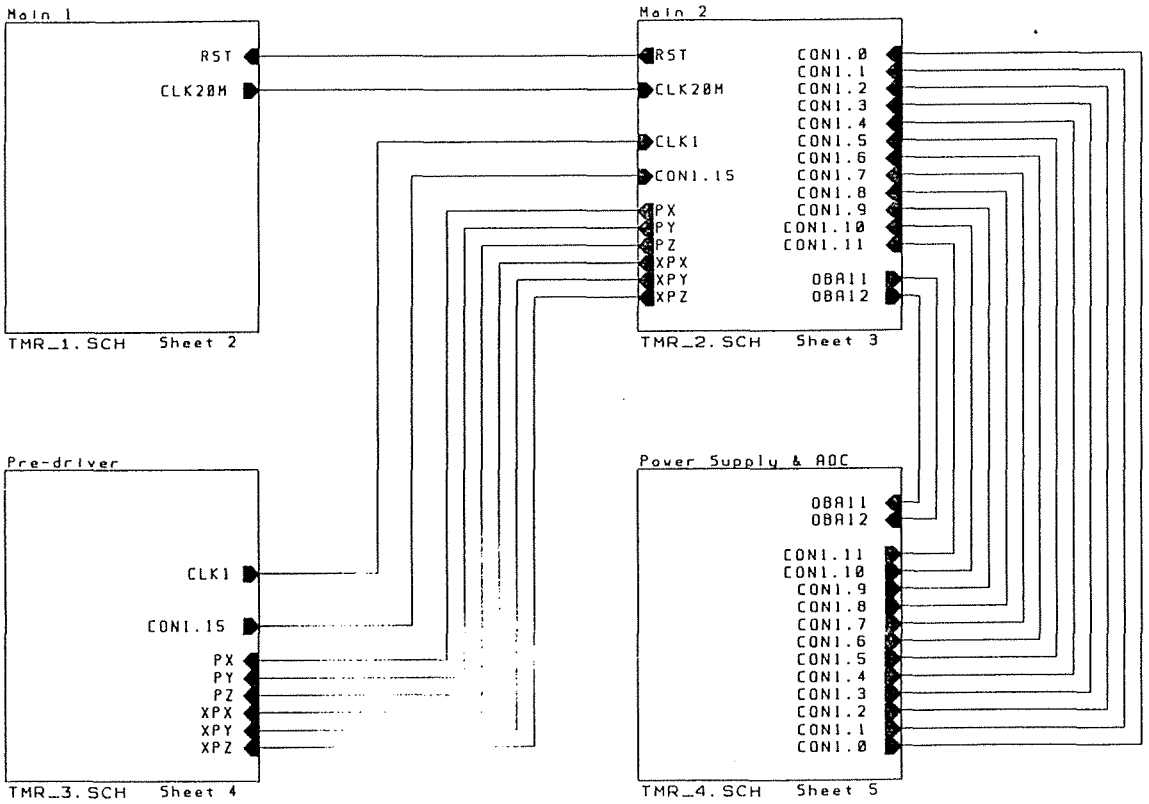

University of California, Davis		
Size A	Document Number TETHERED MOBILE ROBOT	REV A
Date: January 23, 1994	Sheet 1 of 5